الجمهورية الجزائرية الديمقراطية الشعبية
DEMOCRATIC AND POPULAR ALGERIAN REPUBLIC
وزارة التعليم العالي والبحث العلمي
MINISTRY OF HIGHER EDUCATION AND SCIENTIFIC RESEARCH
جامعة الشهيد حمه لخضر الوادي
ECHAHID HAMMA LAKHDAR UNIVERSITY OF EL-OUED
كلية التكنولوجيا
Faculty of Technology
قسم الهندسة الكهربائية
Department of Electrical Engineering

Master 's Thesis

In order to obtain an Academic Master's diploma in Technology

Specialty: Telecommunications Systems

Title

Performance analysis of FSO Communications in desert environments

Presented by:

DAHMRI Abderrahim
BELAID Mebarek

Jury Members:

President: Dr.TINEDERT Imad Eddine	**MCA**	**El-Oued University**
Examiner: Dr.Prof. KAHELIL Abd Ellatif	**Pr**	**El-Oued University**
Supervisor: Dr. HADJADJI Narimane	**MCA**	**El-Oued University**

University year: 2025/2026

بسم الله الرحمن الرحيم

Acknowledgments

First and foremost, I am deeply grateful to the Almighty for granting me the resilience and wisdom to successfully navigate this journey of knowledge and growth.

I extend my heartfelt thanks and appreciation to my supervisor, HADJADJI Narimane, for her exceptional guidance, patience, and boundless support. Her insightful feedback and continuous encouragement were essential to the success of this research.

I would also like to acknowledge all the faculty members and mentors who contributed to my academic development, as well as everyone who supported me, near or far, throughout this transformative experience. I truly cherish this milestone, which I hope will serve as a fruitful contribution to the field of wired and wireless telecommunication systems.

Dedication

To my esteemed teachers, who were like a laser beam in the darkness of research, piercing through the fog of questions to lead me to the clarity of knowledge.

To those who taught me that light, even in the heart of sandstorms, can carry the message if we learn to steer it well.

And to my family, my steadfast support when the Sirocco winds blow, and my abundant shade when the heat of the road intensifies.

To those who planted patience in me before I knew the meaning of simulation, and sustained me with prayers before I was ever sustained by cables.

To my teachers and my family, together,
I dedicate this work, which would never have seen the light were it not for the light of their knowledge and the warmth of their hearts.

Abstract

This thesis tackles the issue of high-speed digitalization in the desert environment specially in our country. The key argument is that Free-Space Optical (FSO) communication may offer significant capacity (112 Gbps) and be cheaper than fiber in theory, but reliability failure in desert region is a serious concern because of its warm climate. The main constraining factor is not the technology as such, but the environment: severe thermal scintillation, damaging sandstorms driven by Sirocco, and complex aerosol behaviour owing to the combination of airborne dust and agricultural humidity.

The study tackles this issue in two sequenced phases. The first stage is diagnostic: performance analysis of a single input single output system under diverse atmospheric scenarios to benchmark channel degradation against an established baseline. The second stage is solution-oriented represented by the proposal and performance evaluation of a multiple-input multiple-output (MIMO) architecture under specific atmospheric scenarios and a rigorous comparison to the single link to arrive at clear conclusions.

With respect to Bit Error Rate (BER) and Q-Factor limits relative to Forward Error Correction (FEC), the performance of proposed MIMO-FSO system remains well above the SISO link performance. Essentially, the MIMO configuration allows for a sufficient link margin during extreme dust-storm conditions, which bridges the connectivity gap. The MIMO-FSO configuration is confirmed to the powerful engineering solution for high-speed.

Keywords: Free-Space Optics (FSO), MIMO Systems, Atmospheric Attenuation, Dust Storms, bit error rate, Forward Error Correction (FEC).

الملخص

تتناول هذه الأطروحة مسألة التحول الرقمي عالي السرعة في البيئة الصحراوية، وخاصة في بلدنا. وتتمثل الحجة الرئيسية في أن الاتصالات الضوئية في الفضاء الحر (FSO) قد توفر سعة كبيرة (112 جيجابت في الثانية) وتكون أرخص من الألياف الضوئية نظريًا، إلا أن فشل الموثوقية في المناطق الصحراوية يمثل مصدر قلق بالغ نظرًا لمناخها الحار. ولا يكمن العامل المُعيق الرئيسي في التكنولوجيا بحد ذاتها، بل في البيئة: التذبذب الحراري الشديد الذي يتجاوز 45° درجة مئوية، والعواصف الرملية المدمرة التي تغذيها (رياح السيروكو)، وسلوك الهباء الجوي المعقد نتيجة لتفاعل الغبار المحمول جوًا مع الرطوبة الزراعية.

تتناول الدراسة هذه المسألة على مرحلتين متتاليتين. المرحلة الأولى تشخيصية: تحليل أداء نظام أحادي المدخلات والمخرجات في ظل سيناريوهات جوية متنوعة لتقييم تدهور القناة مقارنةً بخط أساس مُحدد. أما المرحلة الثانية فهي موجهة نحو الحلول، وتتمثل في اقتراح وتقييم أداء بنية متعددة المدخلات والمخرجات (MIMO) في ظل أربعة سيناريوهات جوية محددة، ومقارنة دقيقة بالوصلة الأحادية للوصول إلى استنتاجات واضحة.

فيما يتعلق بمعدل خطأ البت (BER) وحدود عامل الجودة (Q) بالنسبة لتصحيح الخطأ الأمامي (FEC)، يظل أداء نظام MIMO-FSO المقترح أعلى بكثير من أداء وصلة SISO. في الأساس، يتيح تكوين MIMO هامش أمان كافيًا للوصلة خلال ظروف العواصف الترابية الشديدة، مما يسد فجوة الاتصال. وقد ثبت أن تكوين MIMO-FSO حل هندسي فعال للاتصالات عالية السرعة في المناطق الصحراوية الجافة، ويراعي تمامًا الظروف المناخية للصحراء الجزائرية.

الكلمات المفتاحية: البصريات في الفضاء الحر (FSO)، أنظمة MIMO، التوهين الجوي، العواصف الترابية، معدل خطأ البت، تصحيح الخطأ الأمامي (FEC).

Résumé:

Cette thèse aborde la problématique de la numérisation à haut débit en milieu désertique, et plus particulièrement dans notre pays. L'argument principal est que la communication optique en espace libre (FSO) offre une capacité importante (112 Gbit/s) et peut, en théorie, s'avérer moins coûteuse que la fibre optique. Cependant, la fiabilité de cette communication en zone désertique, en raison de son climat chaud, constitue une préoccupation majeure. Le principal facteur limitant n'est pas la technologie elle-même, mais l'environnement : scintillation thermique intense au-delà de 45 °C, tempêtes de sable destructrices provoquées par le sirocco et comportement complexe des aérosols dû à la combinaison de poussières atmosphériques et d'humidité agricole.

L'étude aborde cette problématique en deux phases séquentielles. La première phase est diagnostique : analyse des performances d'un système à entrée et sortie uniques (SIP/SIO) sous différents scénarios atmosphériques afin d'évaluer la dégradation du canal par rapport à une référence établie. La seconde phase est axée sur la recherche de solutions : proposition et évaluation des performances d'une architecture à entrées et sorties multiples (MIMO) sous quatre scénarios atmosphériques spécifiques, et comparaison rigoureuse avec la liaison unique afin de tirer des conclusions claires

En ce qui concerne le taux d'erreur binaire (TEB) et les limites du facteur Q par rapport à la correction d'erreurs sans voie de retour (FEC), les performances du système MIMO-FSO proposé restent nettement supérieures à celles d'une liaison SISO. La configuration MIMO assure une marge de liaison suffisante même lors de tempêtes de poussière extrêmes, comblant ainsi le déficit de connectivité. La configuration MIMO-FSO s'avère être une solution technique performante pour les communications à haut débit.

Mots-clés : Optique en espace libre (FSO), Systèmes MIMO, Atténuation atmosphérique, Tempêtes de poussière, Taux d'erreur binaire, Correction d'erreurs sans voie de retour (FEC).

Table of Contents

LIST OF FIGURES

LIST OF TABLES

LIST OF ABBREVIATIONS

5G	Fifth Generation
BER	Bit Error Rate
CAGR	Compound Annual Growth Rate
DP-16QAM	Dual-Polarization 16-Quadrature Amplitude Modulation
DSP	Digital Signal Processing
EMI	Electromagnetic Interference
FEC	Forward Error Correction
FSO:	Free-Space Optics / Free-Space Optical
HD-FEC	Hard-Decision Forward Error Correction
IM	Intensity Modulation
LAN	Local Area Network
LD	Laser Diode
LED	Light-Emitting Diode
LoS	Line-of-Sight
MAN	Metropolitan Area Network
MIMO	Multiple-Input Multiple-Output
MZM	Mach-Zehnder Modulator
OOK	On-Off Keying
NASA	National Aeronautics and Space Administration
PDF	Probability Density Function
PIN	Positive-Intrinsic-Negative (Diode)
PPM	Pulse Position Modulation
Q-Factor / Q Factor	Quality Factor
QAM	Quadrature Amplitude Modulation
RF	Radio Frequency
Rx	Receiver
SD-FEC	Soft-Decision Forward Error Correction
SISO	Single-Input Single-Output
SNR	Signal-to-Noise Ratio
Tx	Transmitter
VCSEL	Vertical-Cavity Surface-Emitting Laser

General Introduction

General Introduction

Free-Space Optical communication has emerged as a high-speed, secure wireless alternative with ultra-wide bandwidth. However, its efficiency degrades significantly in arid environments, such as the El Oued region in Algeria, due to severe atmospheric impairments including dust, sandstorms, and optical turbulence. To address these challenges, this thesis designs and simulates an advanced 112 Gb/s FSO system utilizing Dual-Polarization 16-QAM and coherent detection at 1550 nm via **OptiSystem.**

Through an empirical comparative study, the research evaluates a conventional SISO-FSO system across seven distinct desert meteorological scenarios, and contrasts it with a MIMO architecture operating under four critical weather conditions. The findings demonstrate that MIMO configurations provide substantial diversity gains, serving as a highly effective engineering solution to mitigate desert-induced signal attenuation.

The thesis is organized into three main chapters:

- **Chapter 1** reviews the core fundamentals of FSO technology and the physical mechanisms of atmospheric attenuation.
- **Chapter 2** focuses on the mathematical modeling of desert-specific impairments using the Beer-Lambert law and robust statistical frameworks (Log-normal, Gamma-Gamma, and K-distribution).
- **Chapter 3** presents the simulation results, critically comparing the SISO and MIMO setups based on SNR and BER metrics, followed by concluding remarks and future recommendations.

Chapter 1

Introduction and Fundamentals

1.1 Introduction

Free-Space Optical communication represents a fundamental evolution in wireless infrastructure; it transmits data via modulated optical beams using lasers or LEDs, with the air acting as the transmission medium, thereby eliminating the need for fiber or copper cabling. These links are unguided, which allows for faster deployment and operation without expensive licenses, while offering immunity to electromagnetic interference, high capacity, and very low latency[1]. As a result, their applications are expanding to include last-mile connectivity, cellular backhaul, and secure satellite-to-ground communications [2]. However, atmospheric phenomena severely degrade their reliability, particularly in arid regions such as the El Oued province in Algeria, where attenuation ranges from moderate fog (15–25 dB/km) to intense dust storms (exceeding 50 dB/km) [3]. Accurately quantifying these effects is therefore a technical necessity for building robust FSO networks, and achieving a Bit Error Rate (BER) of 10^{-9} or less in harsh desert environments remains a major technical challenge despite its importance as a performance benchmark.

Figure 1.1 illustrates the anticipated exponential growth of FSO technology, with the market valued at approximately 1.4 billion USD in 2024 and projected to leap to 27.2 billion by 2035, at a Compound Annual Growth Rate (CAGR) of 31.6% between 2025 and 2035. This growth is driven by the increasing demand for high bandwidth and faster, more cost-effective alternatives to fiber.

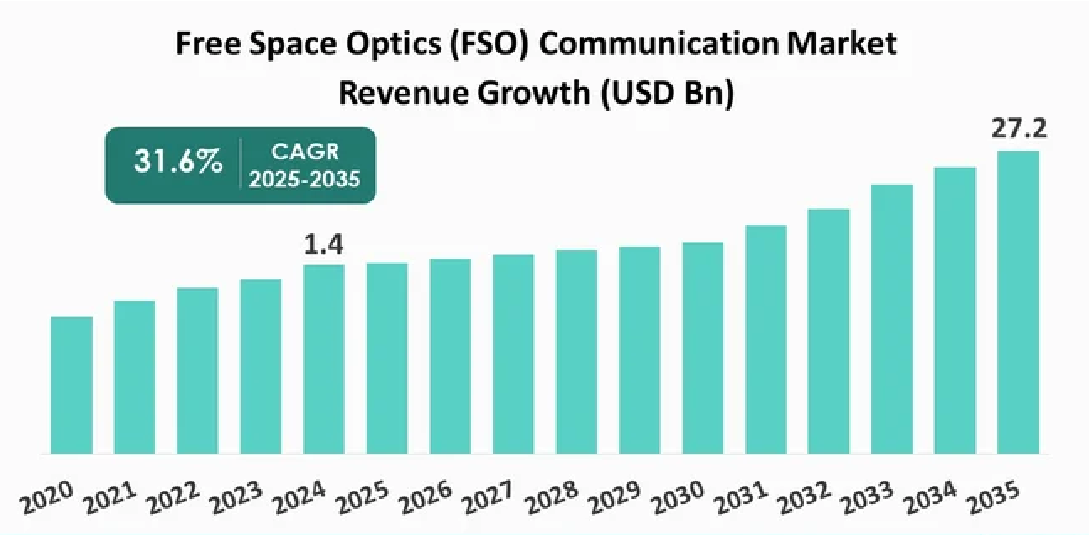

Figure 1.1: *Prediction of the growth of FSO technology [4].*

The year 2025 is adopted as the starting point for the simulations in this research due to its pivotal significance in the market's growth trajectory, ensuring that the results remain both current and strategically valuable for industry.

1.2 Background and Motivation

With the rapid advancements in the world of communications and the increasing need for high-speed internet, new technologies have emerged that can provide high speeds without requiring complex infrastructure. Among these technologies is free-space optical communication, which relies on transmitting data using laser beams through the air between two points [5]. This technology is similar to optical fiber communication in terms of speed, but it does not require laying cables underground.

In Algeria, there is a clear trend towards improving digital infrastructure and providing high-speed connectivity across various regions. However, in some southern areas, such as the city of El Oued, laying optical fiber becomes difficult and costly due to the desert environment and vast distances. Additionally, the El Oued region is seeing a growth in both agricultural and urban development. This increase creates an urgent need for a stronger communications network to power essential digital services, from education and commerce to the connectivity required by public institutions and facilities.

For this reason, FSO technology can be considered a suitable solution, as it can connect buildings or institutions quickly and easily without the need for trenching or laying long cables [6].

Moreover, El Oued's unique geography, which includes both open urban areas and large deserts, makes it a great place to test this technology. The city's buildings are very close together, and the roofs are very high, which makes it easy to set up both short- and medium-range optical wireless communications. These characteristics render El Oued an exemplary case study for examining FSO applications in arduous desert settings [7].

By utilizing local meteorological data from 2025, this study models the optical channel through Beer-Lambert’s law and the gamma-gamma distribution. These models allow us to simulate atmospheric turbulence using OptiSystem software. Ultimately, this research provides a technical roadmap for reliable connectivity in harsh desert environments. Our goal is to bridge the digital divide by offering telecommunications engineers in the region a robust, last-mile solution.

1.3 Problem Statement

The atmospheric conditions in El Oued represent a complex environment free space optical communication systems, as weather conditions change rapidly and directly affect the quality of the optical signal during propagation.

During the summer, temperatures can exceed 45°C, causing strong air turbulence represented by the parameter C_n^2. It leads to signal fluctuations and beam wander. In addition, sandstorms carrying fine dust particles pose another challenge which increasing light scattering and causing significant signal loss. The presence of a mixture of dust and localized humidity further complicates the atmospheric medium and affects signal propagation.

Another key challenge is the rapid variation in visibility. It can drop from around 10 km under clear conditions to less than 0.2 km during severe sandstorms. Therefore, designing an FSO network in this region requires a system capable of adapting to these variable conditions to maintain stable communication.

1.4 Research Methodology

This study employs an analytical approach and digital simulation to evaluate the performance of a Free-Space Optical (FSO) communication system under the specific climatic conditions of El Oued Province. The methodology consists of the following steps:

1.4.1 Data Acquisition and Local Environment Analysis

Our analysis is built on El Oued climate data recorded throughout 2025. We can accurately figure out how atmospheric circumstances affect optical propagation in a desert by looking at basic meteorological factors including temperature, horizontal visibility, and wind speed. This data serves as the foundation for evaluating system performance under localized weather conditions.

1.4.2 Mathematical Modeling and System Design

The simulation model is built using specialized software (OptiSystem) according to the following parameters:

- **Network Design:** Projecting the optical link design onto the city's urban plan, specifying the actual link distances between vital centers (such as the buildings of the University of Martyr Hamma Lakhdar of El Oued).
- **Channel Modeling:** Atmospheric conditions in the Algerian Sahara, including dust and sand particles, air turbulence, occasional humidity, and strong Sirocco winds, are incorporated to accurately represent the desert environment. These factors significantly affect the propagation by, scattering, absorption, and fading of optical signals, providing a realistic model of FSO link performance in desert conditions.

- **Application of Physical Laws:** The Beer–Lambert Law is used to estimate attenuation levels, and the Gamma-Gamma model is used to model atmospheric turbulence and thermal scintillation.

1.4.3 Comparative Analysis and Performance Evaluation

The methodology concludes with a comparative study to evaluate the system's performance under varying climatic scenarios, including:

- **The ideal scenario:** A clear summer day to measure the effect of heat only.
- **The critical scenario:** A moderate sandstorm to measure the effect of light scattering caused by dust.

The results are evaluated based on key performance indicators to ensure the reliability of the proposed system.

1.5 Significance of the Study

This study's significance is twofold, offering a valuable contribution to both academic research and the El Oued community. This work goes beyond theory to give a practical plan for Last-Mile connectivity by giving a strategic framework for telecommunications in dry areas. We suggest FSO network as a high-speed wireless alternative to regular optical fiber.

It is specifically made to bypass the logistical and topographical problems that come with desert terrain.

Furthermore, this study plays an important role in closing the digital divide across the Algerian Sahara. By introducing a high-speed, cost-effective solution, it provides a backbone for essential sectors like healthcare, education, and public administration. What sets this work apart is its evolution from a theoretical model into a professional-grade feasibility study. We achieved this by integrating localized, year-round meteorological data, focusing specifically on temperature and visibility sourced directly from local weather stations.

In the end, these results offer telecommunication specialist in the Wilaya a plan based on reliability. This makes it possible to set up strong optical links between important infrastructures without the need for expensive or disruptive trenching, even when facing the region's extreme desert climate.

1.6 Overview of Wireless Communication

1.6.1 Introduction

Wireless communication refers to the transmission of information over a distance without the use of physical conductors, relying instead on electromagnetic wave propagation through free space [8]. Traditionally, wireless systems have been dominated by Radio Frequency (RF) technologies due to their robustness, long transmission range, and ability to penetrate obstacles. RF-based communication has enabled the development of cellular networks, satellite systems, and wireless local area networks that form the backbone of modern connectivity.

However, the rapid growth of data-intensive services such as high-definition video streaming, cloud computing, and Internet of Things (IoT) applications has led to severe congestion of the RF spectrum. This phenomenon, which is referred as the spectrum crunch, this issue is pushing researchers toward alternative transmission media.

Optical Wireless Communication (OWC), which operates in the visible and infrared bands, has become a particularly strong candidate [9]. OWC and Free-Space Optical systems can send data at substantially greater speeds and with far better security than traditional RF installations because they use the large, unlicensed optical spectrum.

1.6.2 Types of Wireless Communication Systems

Communication systems are essential for transmitting information between people and devices over various distances. They have evolved significantly with the rapid advancement of digital technology and the growing need for fast and efficient data exchange. These systems vary depending on the distance they cover and the type of infrastructure used to transmit signals.

Generally, communication systems can be classified into three main types: short-range communication, long-range communication, and point-to-point communication. The choice of system depends on several factors, including the required distance, data transfer speed, cost, and the nature of the intended application.

- **Short-Range Communication**

Short-range communication systems, such as Wireless Local Area Networks (WLAN), are among the most widely used technologies today. They are used to connect devices within a limited area, such as homes, offices, or university campuses. These networks usually rely on the IEEE 802.11 standard, which defines how devices communicate wirelessly with access points. WLANs are easy to deploy, relatively low-cost compared to wired networks. Also, its provide sufficient data rates for applications such as internet browsing, file sharing, and other digital services within a local network. [13]

- **Long-Range Communication (Satellite)**

Long-range communication systems include satellite communication, which is used to transmit information over very long distances, often spanning thousands of kilometers. In this system, a signal transmit from a ground station to a satellite in orbit, which receives the signal and resent it to another ground station at a different location. This technology is particularly important for providing connectivity in remote or desert areas where building terrestrial networks is difficult. It is widely used for television broadcasting, satellite internet, and international communication. [10]

- **Point-to-Point Communication**

Point-to-point (ptp) communication refers to a dedicated direct link between two specific locations, where data travels directly from the sender to the receiver without being shared with other users. This type of system can be implemented using microwave links, optical fiber, or free-space optical communication. Point-to-point links are often used to connect buildings or institutions or to provide backhaul connections in communication networks, offering high data transfer speeds and reliable performance compared to some other systems. [11].

Next, we take a balanced look at wireless communication technology by examining both the strengths and the limitations.

1.6.3 Advantages of Wireless Communication

1. **Wireless Freedom**: No physical cables are required, allowing flexible setup.
2. **Rapid Deployment**: Wireless networks can be quickly expanded or installed.
3. **Global and remote coverage**: Enables connectivity in remote areas, battlefields, deserts, or regions where wiring is impractical.
4. **Cost-effectiveness**: Avoiding cables reduces costs in installation and maintenance.
5. **Mobility and portability**: Wireless networks are easy to move and reinstall elsewhere.
6. **Low maintenance**: ongoing maintenance is generally simpler and more affordable.
7. **Remote access**: Users can access the network from any location, enabling remote work.
8. **Easy network planning**: Software-based configuration of frequency, power, and other parameters simplifies network design.
9. **Scalability**: Can serve a large number of clients without major hardware upgrades [12].

1.6.4 Disadvantages of Wireless Communication

1. **Security risks**: Wireless networks are more vulnerable to hacking due to open-space transmission.

2. **Unreliability**: Performance can fluctuate because of interference or environmental factors.

3. **Interference**: Susceptible to signal interference from other devices or networks.

4. **Jamming**: Increased risk of intentional or accidental signal jamming.

5. **Limited bandwidth**: Bandwidth constraints may affect network performance.

6. **Impact of weather and environment**: the different distortions [12] can reducing signal strength.

1.7 Introduction to Free Space Optical communication

Free-space optical (FSO) communication is a promising technology for metropolitan and local area networks, especially as a solution to the last-mile access network problem. It offers high data rates, relatively low deployment costs, and fast installation. It makes it an attractive alternative to traditional wired and radio frequency communication systems.

However, the performance of FSO systems is strongly affected by atmospheric conditions. Aerosols such as fog, smoke, sand-dust particles, and water vapour can degrade signal quality due to scattering and absorption effects. Among these factors, sand-dust weather conditions are particularly harmful, as dust, particles can cause significant signal attenuation and even interrupt the optical link.

Therefore, studying the impact of sand-dust particles on FSO transmission is essential for reliable system design. Early research on laser propagation mainly used the Lambert-Beer law to analyze single scattering by spherical particles. This approach is limited because, in real atmospheric conditions, multiple scattering occurs as transmission distance increases and visibility decreases. To address this issue, several models and simulation methods, such as Mie theory and Monte Carlo techniques, were developed to better describe signal attenuation and pulse distortion.

Most of these studies assume that sand-dust particles are spherical. In reality, sand-dust particles have irregular and non-spherical shapes, which can lead to inaccurate results. More advanced methods have therefore been introduced to study light scattering by non-spherical particles.

In this work, the radiation propagation method and the small-angle approximation are used to analyze laser transmission characteristics in sand-dust atmospheric channels and to better understand the impact of sand-dust conditions on FSO system performance [13].

1.7.1 FSO Technology – Yesterday And Today

The history of FSO technology or atmospheric optical communication began not in the 90s and not in the 70s of the XX century, but many centuries earlier. This is the oldest long-distance communication technology known to us.

The principle of wireless optical communication originated in ancient times. The first systems of communication were sentry posts located around settlements on specially built towers or towers (Figure 1.2). When the enemy approached, an alarm fire lit up. Then the lights moved in a chain from post to post, and so the information about the enemy reached the key point. The Greeks improved the system somewhat by creating an optical flare telegraph in 450 BC. The 24 letters of the alphabet were decomposed into 5 lines. At night – torches, and during the day – signal flags indicated a specific letter. However, such an invention has not been widely used.

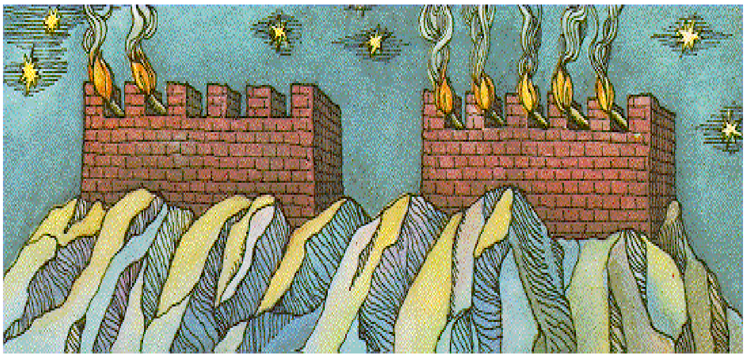

Figure 1.2: *Fire Beacons as a Primitive Model.*

The earliest research on data transmission technology, most similar to modern FSO equipment, was conducted at the end of the XIX century by Alexander Bell. Together with his assistant Sarah Or and colleague Charles Tainter, in 1880 he designed a photophone (seen in Figure 1.3), a device that allows you to transmit voice sounds using light rays. A line was installed between two buildings, the distance between the receiver and the transmitter was about 213 m.

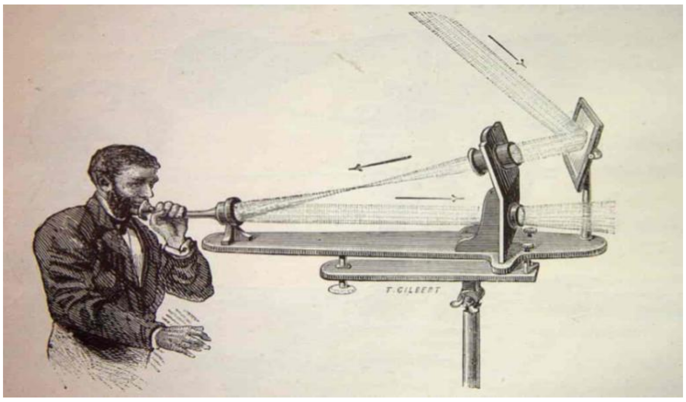

Figure 1.3: *Bell's demonstration of the "photophone" in 1880 [14].*

During the Great War, when wired communications were often damaged, the German command developed its own version of the optical telegraph, which was called Blinkgerät (literally – flashing device). The device operated at distances up to 4 km during the day and up to 8 km at night, a red filter was used to conceal information. Despite the fact that the first batches were put into service at the end of the war, the device was installed on a wide range of technical means, including airplanes, tanks, balloons.

Figure 1.4: *The optical telegraph.*

In the 1960s, with the discovery of the laser, the technology received a new impetus for development. It became possible to build communication systems that transmit, in addition to telephone, television signals, and subsequently computer signals. Laser systems did not take root: the slightest vibrations of the building from a passing dump truck or even the wind knocked the beam off course and the connection was lost.

The advent of automatic guidance and channel stabilization systems in the 1990s solved the problem. Along with the use of a modern element base, this made it possible already in the XXI century to create highly efficient systems comparable to the reliability of the channel with radio systems.

Figure 1.5: *Advanced FSO Transmitter with Beam Alignment Technology.*

In addition to ground communication, lasers are also used in the space environment. The most well-known in the media space is SpaceX's Starlink program, whose satellites have been equipped with laser terminals for communication in satellite groupings operating in low orbits since 2021(Figure 1.6). In Russia, these researches are included in the program of the state corporation “Roscosmos” under the name “Sphere”, and research is also conducted by a number of private space.

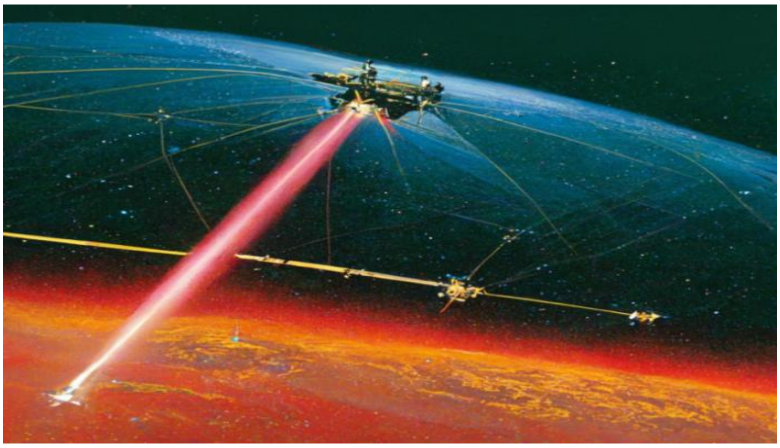

Figure 1.6: *Deep space laser communication.*

Free Space Optics is a wireless communication technology that uses tightly focused laser beams to transmit data through the atmosphere. FSO combines the high data rates of optical fiber with the flexibility and rapid deployment of wireless systems. As a result, it has gained increasing attention as a solution for last-mile access, metropolitan networks, and high-capacity backhaul links.

However, FSO performance is strongly dependent on atmospheric conditions. In desert regions such as El Oued region, sand-dust storms, high temperatures, and strong thermal turbulence pose significant challenges to reliable optical transmission [15].

1.7.2 Various Techniques for Generation FSO System

In Free Space Optics, modulation is the physical process of mapping digital binary data onto the characteristics of an optical carrier. Given the stochastic nature of the atmospheric channel in regions like El Oued, choosing an appropriate modulation scheme is vital to balance power efficiency, bandwidth requirements, and resistance to atmospheric turbulence.

1.7.2.1 Types of Modulation Techniques

In Free-Space Optical communication systems, modulation techniques have the main role in determining system performance, power efficiency, and spectral efficiency. Among the various modulation schemes proposed for optical wireless communication, On-Off Keying (OOK), Pulse Position Modulation (PPM), and Quadrature Amplitude Modulation (QAM) are widely used due to their suitability for different operational conditions and system requirements [16].

- **On-Off Keying (OOK)**

On-Off Keying is considered the simplest and most commonly implemented modulation technique in FSO systems. It belongs to the Intensity Modulation with Direct Detection (IM/DD) category, where data transmission is achieved by switching the optical signal on and off according to the binary input data as described in Figure 1.7. Due to its low implementation complexity, low cost, and ease of integration, OOK is widely used in short- and medium-distance FSO links. However, its performance can be significantly affected by atmospheric disturbances such as turbulence, attenuation, and scintillation [17].

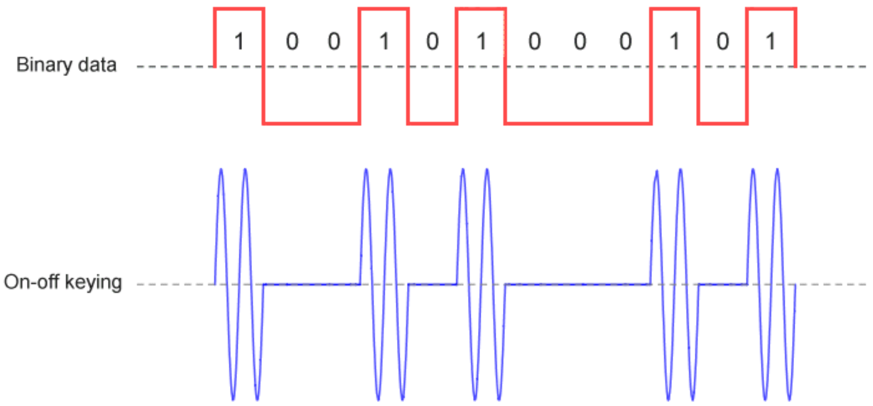

Figure 1.7: *Illustration of on-off keying modulation.*

- **Pulse Position Modulation (PPM)**

Pulse Position Modulation is another important modulation technique used in FSO communication systems. In this method, information is encoded in the position of a single optical pulse within a predefined symbol period divided into several time slots as mentioned in Figure 1.8. PPM is known for its high power efficiency, making it particularly suitable for long-distance FSO links. Nevertheless, this technique requires accurate synchronization between the transmitter and receiver and generally consumes more bandwidth compared to OOK [16].

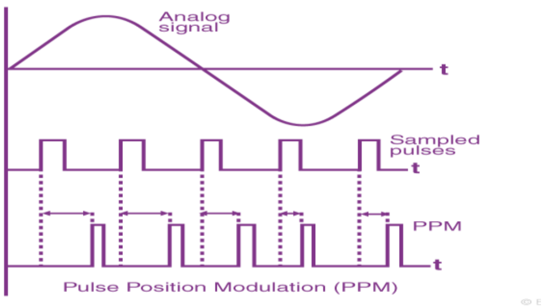

Figure 1.8: *Illustration of pulse position modulation (PPM).*

- **Quadrature Amplitude Modulation (QAM)**

Quadrature Amplitude Modulation is an advanced modulation scheme typically employed in coherent FSO systems. Unlike IM-based techniques, QAM transmits data by varying both the amplitude and phase of the optical carrier signal. This modulation relies on two orthogonal signal components known as the in-phase (I) and quadrature (Q) components.

Higher-order formats such as 16-QAM and 64-QAM (see Figure 1.9) enable higher data rates and improved spectral efficiency. However, QAM systems are more complex and more sensitive to atmospheric turbulence and phase distortions. It requires coherent detection and advanced digital signal processing techniques [17].

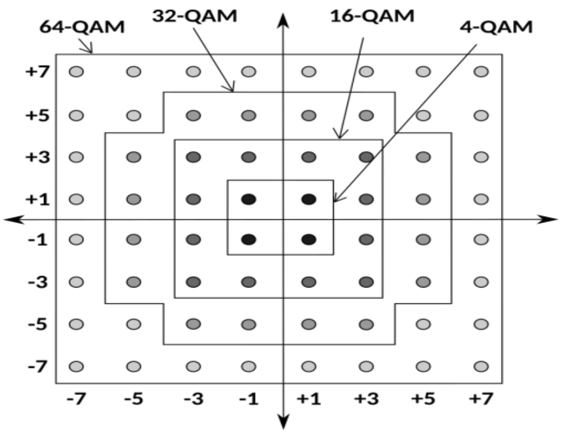

Figure 1.9: *Constellation of QAM (Quadratic Amplitude Modulation).*

1.7.2.2 Classification of Light Sources

The transmitter unit in free space optical communication systems fundamentally relies on optical sources capable of generating light beams with specific propagation characteristics through the atmosphere. These sources are technically classified into two mainly categories based on their coherence properties.

a. Incoherent Optical Sources

Incoherent sources produce optical radiation characterized by a lack of phase alignment and a relatively wide emission angle. The Light Emitting Diode (LED) is the most prominent example of this category.

LED technology is generally restricted to short-range optical wireless communication systems due to its cost-effectiveness and high reliability. However, high beam divergence and limited optical power render them suboptimal for long-distance FSO links. [17]

b. Coherent Light Sources

Coherent sources generate directional and phase-aligned optical beams, enhancing their efficacy in long-range propagation. Various types of lasers constitute the backbone of modern FSO systems.

b.1. Laser Diode (LD)

The Laser Diode is the predominant optical source in FSO architectures, characterized by a concentrated, narrow beam capable of long-distance propagation with minimal attenuation.

It typically operates within atmospheric transmission windows (e.g., 850 nm, 1310 nm, and 1550 nm) to mitigate signal loss. Also, using with minimal divergence angle for ultra-high data transmission rates. However, it requires high-precision alignment and exhibits sensitivity to atmospheric turbulence. [18]

b.2. Vertical-Cavity Surface-Emitting Laser (VCSEL)

The VCSEL represents an advanced generation of semiconductor lasers where light is emitted perpendicularly to the chip surface. This architecture facilitates fabrication and integration into laser arrays. [19]

It primarily have high power efficiency with thermal stability, and seamless integration with optical components. In addition, it utilized for short-to-medium range links.

1.7.3 Core Applications of FSO Technology in Saharan Environments

FSO communication systems are highly versatile (Figure 1.10), supporting applications that range from short-range links (<1 km) to long-range terrestrial and space-based communications. This technology provides a broadband solution, delivering high data rates without the need for physical cabling. It particularly suitable for connecting end users to the network backbone.

In short-range scenarios, FSO enables last-mile connectivity by linking various towers and buildings in urban areas. In contrast, the conventional fiber deployment is often impractical due to construction constraints and high trenching costs. Moreover, FSO systems can support point-to-point, point-to-multipoint, and broadband links, offering flexibility to meet diverse communication requirements. [21]

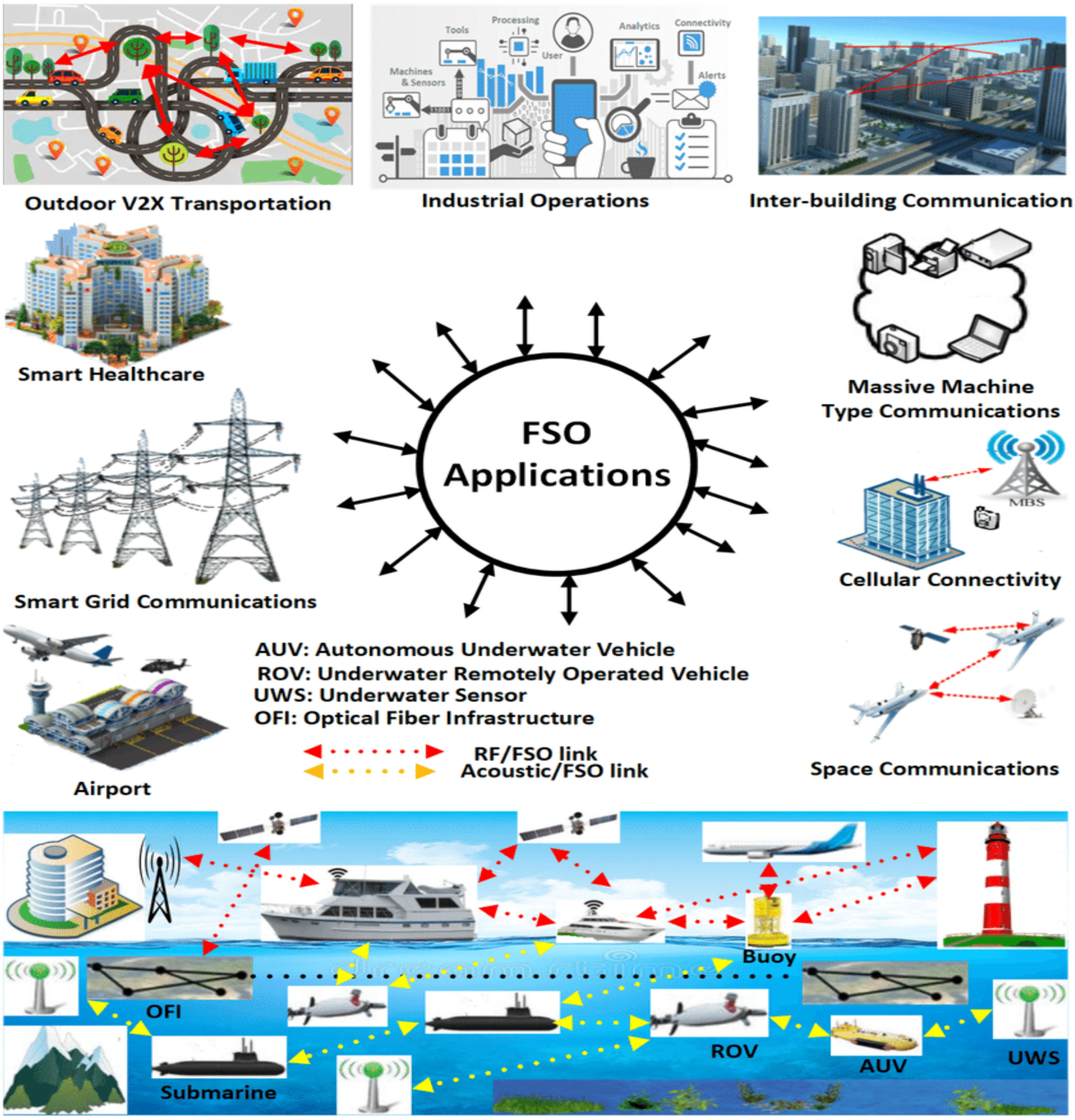

Figure 1.10: *A few applications of FSO systems connectivity [20].*

1.7.3.1 Last-Mile Access

The last-mile refers to the final leg of a telecommunications network that delivers services to end-users. In urban El Oued, providing this connectivity via traditional fiber optics is often obstructed by dense construction and the high cost of trenching in sandy soils. [21]

These units are typically installed on rooftops to provide last-mile connectivity, linking the primary fiber backbone directly to commercial and residential buildings. This approach enables the rapid rollout of gigabit-capacity links while completely bypassing the need for disruptive municipal excavation permits or ongoing physical cable maintenance.

1.7.3.2 Backhaul for 5G Towers in Remote Saharan Areas

As 5G networks expand into the desert to support industrial or residential growth, the backhaul (the link between the cell tower and the core network) becomes a significant bottleneck. [21]

High-power FSO transceivers act as a critical link, connecting remote base stations to the central network over distances of several kilometers. This technology delivers the ultra-low latency and massive throughput, often reaching 10 Gbps, required for peak 5G performance. In many ways, FSO outclasses traditional microwave links while avoiding the logistical nightmare of trying to lay optical fiber cables across the shifting dunes of a desert landscape.

1.7.3.3 Disaster Recovery and Infrastructure Resilience

Physical infrastructure in the Sahara is vulnerable to accidental fiber cuts during construction or displacement due to environmental factors.

Portable FSO terminals act as an essential emergency bridge to restore network access when a primary fiber link is severed. Since FSO operates within the unlicensed optical spectrum, these units can be deployed and aligned in just a few hours. This speed ensures that critical institution such as hospitals or government centers stay online while teams conduct physical repairs on the main infrastructure.

1.7.4 Advantages and Limitations of FSO Systems

The deployment of Free-Space Optical communication systems involves a careful trade-off between high performance and environmental sensitivity. In regions such as El Oued, atmospheric conditions play an essential role in determining system reliability and link stability. Among these, Sirocco winds, which carry fine dust and sand particles, are particularly significant in desert environments, as they can cause scattering and attenuation of the optical signal [22].

We now provide a comprehensive overview of the inherent advantages and technical challenges associated with this technology.

1.7.4.1 Advantages

- **High-Speed Full-Duplex Communication:** FSO systems can transmit simultaneous bi-directional data at gigabit-per-second rates over distances ranging from a few city blocks to several kilometers, providing fiber-like throughput.
- **License-Free Spectrum:** Operating in the near infrared to visible light spectrum, FSO systems avoid costly spectrum licensing. Power levels must comply with IEC60825-1 safety standards, but no frequency allocation fees are required.

- **Immunity to Electromagnetic Interference (EMI):** Because FSO relies on light rather than radio waves, it is unaffected by interference from power lines, cellular towers, or other radio frequency sources.
- **Rapid Deployment and Cost-Effectiveness:** Installation can be completed within days, particularly when units are mounted behind windows or on rooftops. FSO requires significantly less capital investment than comparable optical fiber networks, avoiding costly trenching and municipal permits while enabling service providers to start operations quickly.[23]

1.7.4.2 Limitations

- **Environmental Sensitivity:** Performance is heavily influenced by weather and atmospheric conditions. Dust from Sirocco winds can scatter the laser beam (Mie scattering). It reduce the link distance and throughput. Extreme heat can create thermal scintillation, causing the beam to fluctuate or wander, resulting in signal fading.
- **Line-of-Sight (LoS) Requirement:** Any obstruction, such as buildings, trees, or sand dunes, can fully interrupt the optical link. Elevated installation is often necessary to maintain a clear path.
- **Limited Range Compared to Fiber:** FSO is primarily suitable for LANs and MANs, as long-distance or transoceanic deployment is impractical, and performance declines under adverse environmental conditions.
- **Eye Safety Concerns:** FSO systems typically use 850 nm and 1550 nm wavelengths. The 1550 nm lasers are generally eye-safe, while 850 nm lasers may damage the retina if not carefully installed, requiring proper alignment and mounting to avoid exposure. [24].

1.8 Classification of FSO Networks

FSO systems are categorized based on their operational environment and the medium through which the optical beam propagates. In the context of the Algerian Sahara, these classifications determine the link budget and the necessary mitigation techniques for atmospheric interference.

1.8.1 Terrestrial FSO

This classification involves ground-to-ground communication, typically utilized within urban or industrial landscapes.

It focuses on horizontal or slanted links established between transceivers mounted on high-altitude structures, such as building rooftops or dedicated telecommunication towers as seen in Figure1.11.

FSO facilitates high-speed data transfer across dense urban environments or challenging sandy terrain. This makes it an ideal solution for linking university faculties or municipal offices where traditional cabling is blocked by infrastructure or geography.

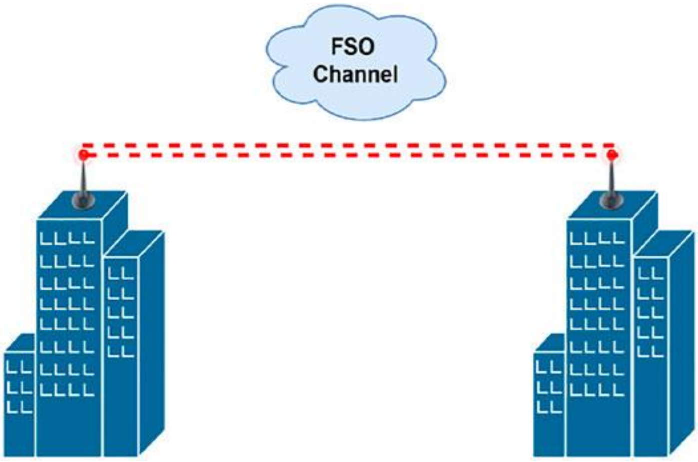

Figure 1.11: *Terrestrial FSO.*

1.8.2 Space and Satellite FSO

This involves optical communication beyond the Earth's atmosphere, where vacuum conditions eliminate the issues of dust and turbulence found in terrestrial links as described in Figure 1.12.

- **Inter-Satellite Links (ISL):** Data transmission between satellites in Low Earth Orbit (LEO) or Geostationary Orbit (GEO).
- **Deep Space Links:** Communication between ground stations and spacecraft or planetary probes.

Therefore, lack of atmospheric molecules allows for extremely long-distance communication with minimal signal divergence.

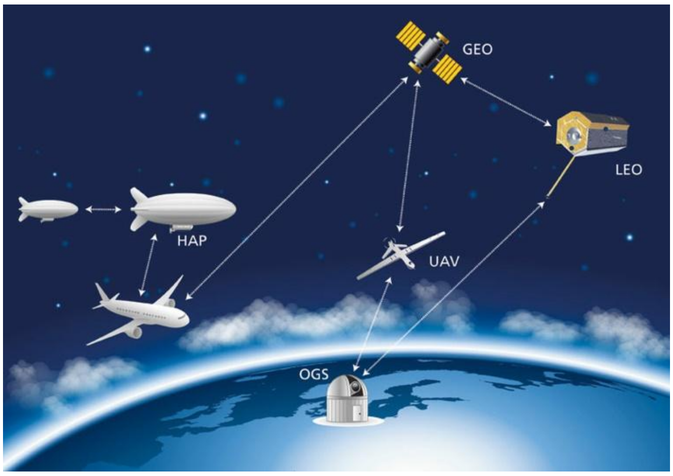

***Figure 1.12**: Space and Satellite FSO.*

1.8.3 Hybrid FSO/RF Networks

The hybrid configuration is a dual-layered architecture that integrates an FSO link with a backup Radio Frequency (RF) link (Figure 1.13).

While FSO provides superior bandwidth (10Gbps+), it is vulnerable to complete outage during intense Saharan sandstorms (Sirocco). The system employs a switching algorithm; during clear conditions, FSO carries the primary data load. If sensors detect high attenuation from dust or sand, the traffic reroute to the lower-frequency RF link (e.g., 60GHz or microwave). Ensures 99.999% network availability, combining the high speed of optics with the atmospheric penetration of radio waves.

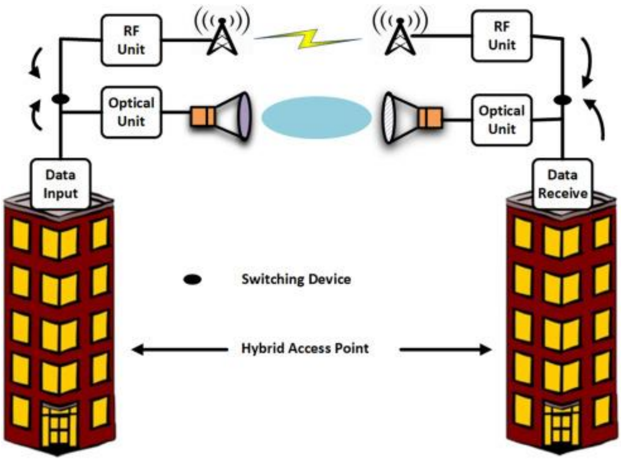

***Figure 1.13:** Hybrid FSO/RF.*

1.9 Network Topologies for FSO

In a desert city like El Oued, the main enemy of Free-Space Optics system is atmospheric attenuation, specifically from sandstorms and thermal shimmering (scintillation). Because this system requires a strict Line-of-Sight, the way you arrange your nodes determines whether your network stays online or goes dark during a storm.

Here is the four main topologies used how they fare in a desert environment:

1.9.1 Bus Topology

This configuration operates on a linear sequence of nodes connected via a single communication backbone. It represents a high-risk architecture for FSO. Since the integrity of the network depends on a singular path, any localized atmospheric obstruction or physical blockage (e.g., a sand plume) results in a catastrophic failure for all downstream nodes.

Generally avoided in critical desert infrastructure due to the lack of redundancy.

Figure 1.14: *Bus Topology [25].*

1.9.2 Ring Topology

In a ring architecture, each node is connected to two adjacent nodes, forming a closed loop for data transmission. It provides a primary backup path. If a single optical link is disrupted, the system can utilize a counter-rotating mechanism to redirect traffic. This is a conventional choice for Metropolitan Area Networks (MAN) where moderate redundancy is required.

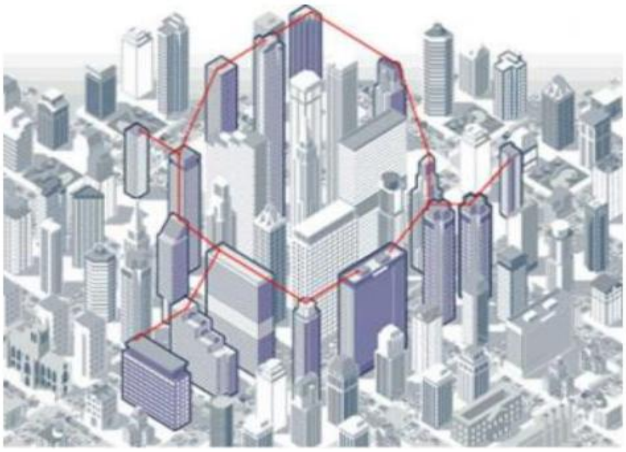

Figure 1.15: *Ring Topology.*

1.9.3 Star Topology

The star configuration utilizes a centralized hub to which all peripheral nodes are directly interfaced. This is highly efficient for localized deployment, such as a university campus (e.g., the University of El Oued). It allows for centralized management and simplified alignment.

The central hub constitutes a Single Point of Failure (SPoF). Environmental interference affecting the hub's transceivers results in a total network outage.

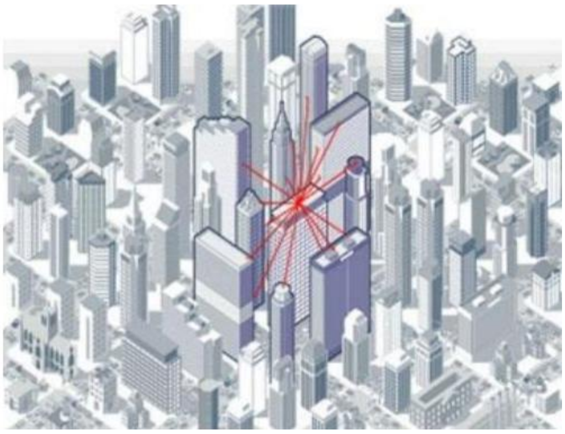

Figure 1.16: *Star Topology.*

1.9.4 Mesh Topology

The mesh architecture is characterized by a high degree of interconnection, where each node is linked to multiple others.

It is considered the most resilient topology for environments prone to sandstorms. The network employs dynamic rerouting protocols. If a specific optical path's Signal-to-Noise Ratio (SNR) drops below the operational threshold due to atmospheric attenuation, the data is autonomously rerouted through an alternative node.

Despite the increased complexity and hardware cost, Mesh topology ensures the highest link availability for city-wide FSO deployment.

Figure 1.17: *Mesh Topology [25].*

1.10 Conclusion

In conclusion, Free-Space Optical communication represents a promising solution to overcome traditional infrastructure obstacles in desert regions, particularly in the province of El Oued. The advantages offered by this technology such as high-speed data transfer, license-free operation, and rapid deployment render it the optimal choice for connecting vital institutions and areas amidst rapid urban expansion.

However, the successful exploitation of this technology in a harsh environment characterized by extreme temperatures and frequent sandstorms cannot be achieved without a profound understanding of the physical and mathematical principles governing the optical beam's path through the atmosphere. Transitioning from the awareness of the technology's importance to the engineering design phase necessitates a precise analysis of how the laser beam interacts with the molecules and particles suspended in the air.

Accordingly, next chapter will be dedicated to studying the principles of light propagation and the mathematical modeling of the optical channel.

Chapter 2

System Design and Atmospheric Challenges

2.1 Introduction

Free-space optical communication enables high-speed data transmission through the atmosphere without physical fiber, but deploying it in the harsh desert of El Oued Province presents unique challenges to signal integrity. This chapter establishes the theoretical foundation to address those challenges. It begins by selecting the most effective optical windows near-infrared (NIR) and short-wave infrared (SWIR) due to their superior ability to penetrate fine dust particles typical of the region's atmosphere. The chapter then revisits the Huygens-Fresnel principle and Gaussian beam optics, focusing on how extreme thermal gradients and low humidity affect propagation, and examines how heat rising from the desert floor generates scintillation that degrades signal quality, distinguishing between coherent and incoherent sources. A substantial part of the discussion analyzes the direct interaction between optical signals and the atmosphere: geometric diffraction losses, pointing errors caused by shifting winds, and statistical turbulence models (log-normal and gamma distributions) calibrated for hot climates. Empirical attenuation models are provided for local weather phenomena, including sandstorms (haboob), lowland winter fog, and dry heat haze. Finally, the chapter bridges theory and practice by proposing tailored mitigation strategies adaptive optics to correct beam wander and spatial diversity to counter uneven dust distribution equipping the reader with the tools to predict and maintain link reliability under the volatile conditions of the Algerian desert.

2.2 Principles of Optical Propagation in Free Space

To design an effective FSO link for the challenging environment of El Oued, we must first establish the physical laws governing the transmission of light. This begins with the electromagnetic spectrum, the fundamental map upon which all optical communication is based.

2.2.1 Electromagnetic spectrum and optical frequencies used in FSO

2.2.1.1 Overview of the electromagnetic spectrum

The electromagnetic spectrum represents the comprehensive continuum of electromagnetic radiation frequencies. It spans from the extremely low frequencies employed in modern radio communications to high-frequency gamma radiation, covering wavelengths that vary from thousands of kilometers to fractions of an atomic radius. The upper limit of wavelength is bounded only by the size of the universe, while the lower limit approaches the Planck length. Within this vast range, specific segments are heavily utilized for scientific spectroscopy, industrial manufacturing, and crucially, communication technologies [26][27].

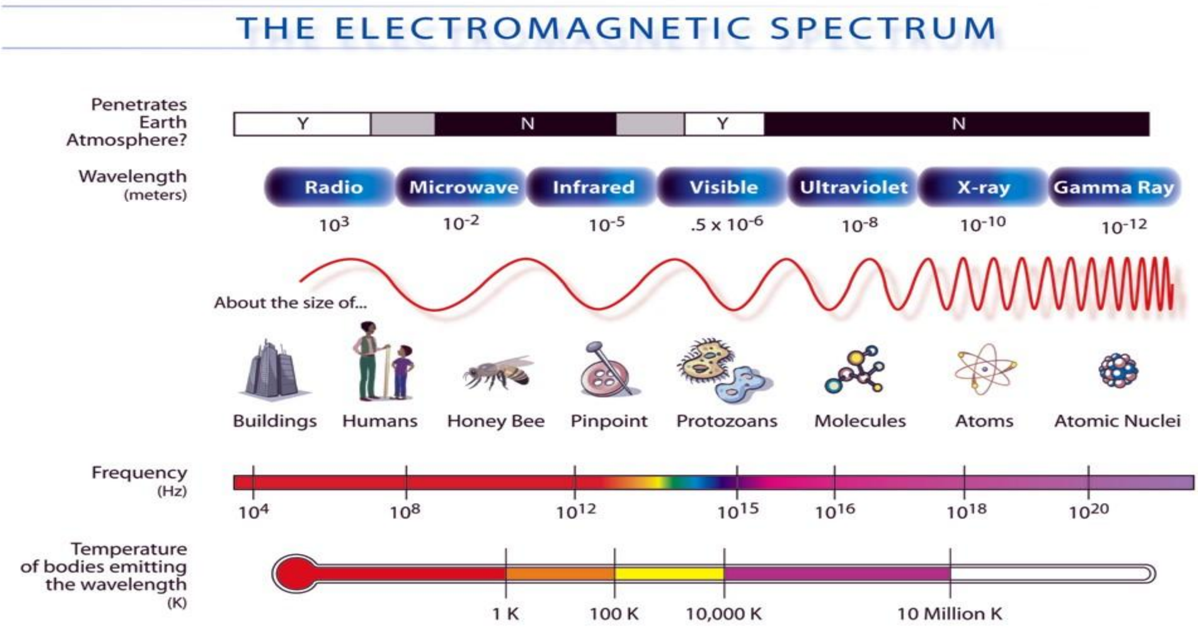

Figure 2.1: *The electromagnetic spectrum (Source: NASA, Public Domain).*

As illustrated in Figure 2.1, the spectrum can be quantified in terms of wavelength (λ), frequency (v), or photon energy. These properties are intrinsically linked; as frequency increases, so does the energy carried by the wave. The inverse relationship between wavelength and frequency is given by

$$c = \lambda . v \qquad (2.1)$$

Where c represents the speed of light in a vacuum. Furthermore, the energy (E) of a specific spectral component is directly proportional to its frequency, as described by Planck's relation:

$$E = h . v \qquad (2.2)$$

Here, h is Planck's constant (6.63×10^{-34} Joule seconds). While the standard unit for wavelength is the meter, in optical engineering, it is more practical to use microns (μm, 10^{-6} m) and nanometers (nm, 10^{-9} m). Frequency is measured in Hertz (Hz), representing one cycle of a sinusoidal wave per second, while energy is often expressed in electron volts (eV)

2.2.1.1.a Wavelength Selection Strategies

In the design of an FSO system, wavelength selection is a critical parameter that dictates link performance and detector sensitivity. This choice is rarely arbitrary; it is a complex trade-off between atmospheric attenuation (absorption and scattering), background noise levels, and the physical constraints of the hardware. Factors such as eye safety regulations, the cost of components, and the availability of off-the-shelf transmitters and receivers heavily influence the design process.

The International Commission on Illumination (CIE) classifies optical radiation into three primary bands: IR-A (700–1400 nm), IR-B (1400–3000 nm), and IR-C (3000 nm–1 mm). However, for telecommunications purposes, we categorize these into:

• **Near infrared (NIR):** Spanning 750 to 1450 nm. This is a low attenuation window historically used in optical fiber systems.

• **Short infrared (SIR):** Spanning 1400 to 3000 nm. Within this band, the 1530–1560 nm range is dominant for long-distance communication.

Commercially available FSO systems predominantly operate within these NIR and SIR ranges. This suggests a synergy with the mature fiber optic industry, allowing FSO designers to leverage readily available components [28].

2.2.1.1.b The two most distinct operational windows

• **The 850 nm window:** This band is characterized by low attenuation and is highly suitable for standard FSO operations. Its primary advantage is economic; it leverages reliable, high-performance, and cost-effective components widely used in service provider networks. Systems operating here can utilize highly sensitive silicon avalanche photodiodes (APD) alongside advanced laser technology.

• **The 1550 nm band:** Often preferred for longer distances or higher-power applications. This band offers low attenuation and compatibility with high-speed semiconductor lasers suitable for Wavelength Division Multiplexing (WDM). Crucially, this wavelength allows for the use of Erbium-Doped Fiber Amplifiers (EDFA) and Semiconductor Optical Amplifiers (SOA) to boost transmission power. These properties make the 1550 nm band ideal for high-capacity, robust FSO links [26].

2.2.1.1.c Advantages of optical frequencies

The shift from radio frequency (RF) to optical frequencies is driven by distinct physical and operational advantages. These benefits are particularly relevant when deploying infrastructure in sensitive or congested environments:

1. High Security: The highly directional nature and narrow beam width of laser communications make interception extremely difficult. This is critical for transmitting sensitive legal, financial, or military data.

2. Increased Channel Capacity: Optical carrier frequencies are significantly higher than RF, providing a vast modulation bandwidth. This supports the high data rates required by modern communication networks.

3. Electromagnetic Immunity: Photonic signals are immune to Electromagnetic Interference (EMI) and cannot be detected by standard RF meters or spectrum analyzers. This ensures electrical isolation and stealth operation

4. Environmentally Friendly: Optical systems utilize invisible, eye-safe laser beams (particularly in the 1550 nm band), offering a clean technology that poses minimal environmental risk.

5. License-Free Operation: Unlike the strictly regulated RF spectrum, optical communication does not currently require frequency allocation or licensing, which simplifies deployment and significantly reduces operational costs.

6. Reduced Multipath Propagation: The focused nature of the optical beam minimizes multipath fading, a common issue in RF where signals bounce off structures. This leads to improved communication reliability.

7. Excellent Power Efficiency: Due to low power consumption and very low beam divergence angles, optical systems deliver high energy efficiency per bit transmitted.

8. Compact and Lightweight Equipment: The equipment required for optical communication is typically lightweight and compact, facilitating easy installation on rooftops, towers, or temporary structures [36]

2.2.2 Basic Concepts of Light Propagation

2.2.2.1 Diffraction

2.2.2.1.a The Huygens-Fresnel principle

The propagation of light is best understood through Huygens' construction, which postulates that every point on a wavefront acts as the source of spherical secondary wavelets. The wavefront at any subsequent time is simply the envelope of these wavelets. Fresnel refined this concept by introducing the principle of interference between these secondary wavelets, culminating in the Huygens–Fresnel principle (see Figure 2.2). Before applying this to diffraction effects in our FSO link, we must confirm its validity for free space propagation. Let us consider a spherical monochromatic wavefront of radius r_0 originating from a point source P_0, as illustrated in Figure 2.2. Our objective is to determine the light disturbance at a specific point P. If we omit the time-periodic factor $e^{-i\omega t}$, the disturbance at a point Q on the wavefront is given by Ae^{ikr} / r_0, where A represents the amplitude at a unit distance from the source.

According to the Huygens–Fresnel principle, the total disturbance $dU(P)$ contributed by an infinitesimal element dS at point Q is :

$$\boldsymbol{dU(P) = K(\chi). A\frac{e^{ikrr^0}}{r^0}.\frac{eiks}{s}dS} \qquad \textbf{(2.3)}$$

Here, s is the distance QP, and $K(\chi)$ is the inclination factor, which describes how the amplitude of secondary waves varies with direction. χ represents the angle of diffraction between the normal at Q and the direction QP. The total disturbance at P is found by summing (integrating) these contributions across the entire wavefront, demonstrating the principle of superposition central to wave optics [37].

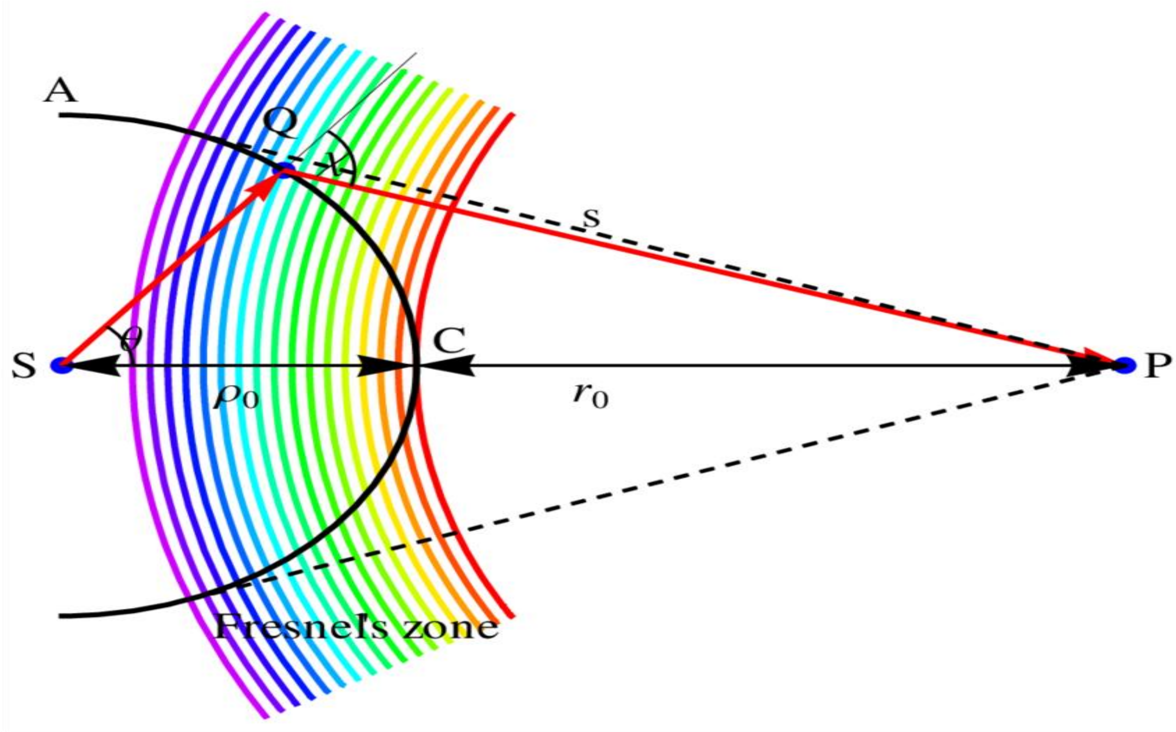

Figure 2.2: *Fresnel's zone construction [37]*

2.2.2.1.b Diffraction-limited beam divergence:

1. Beam Divergence Loss:

As an optical beam traverses the atmosphere, it naturally spreads due to diffraction. This expansion often results in the beam diameter at the receiver exceeding the receiver's aperture size (D_R), meaning a significant fraction of the transmitted energy is lost. This phenomenon, known as beam divergence loss, is depicted in Figure II.3 [28].

Mathematically, the optical power collected by the receiver (P_R) is defined by the link equation:

$$\boldsymbol{P_R = P_T\, G_T\, G.L_P} \qquad \textbf{(2.4)}$$

Where P_T is the transmitted power, L_P is the free space path loss, and G_T and G_R are the effective antenna gains for the transmitter and receiver, respectively [28]. By substituting the standard approximations for gain and path loss:

$$L_P = \left(\frac{\lambda}{4\pi R}\right)^2, \quad G_T \approx \left(\frac{\pi D_T}{\lambda}\right)^2, G_R \approx \left(\frac{\pi D_R}{\lambda}\right)^2 \qquad (2.5)$$

We can derive the received optical power as:

$$P_R \approx P_T \left(\frac{D_T D_R}{\lambda R}\right)^2 \qquad \mathbf{(2.6)}$$

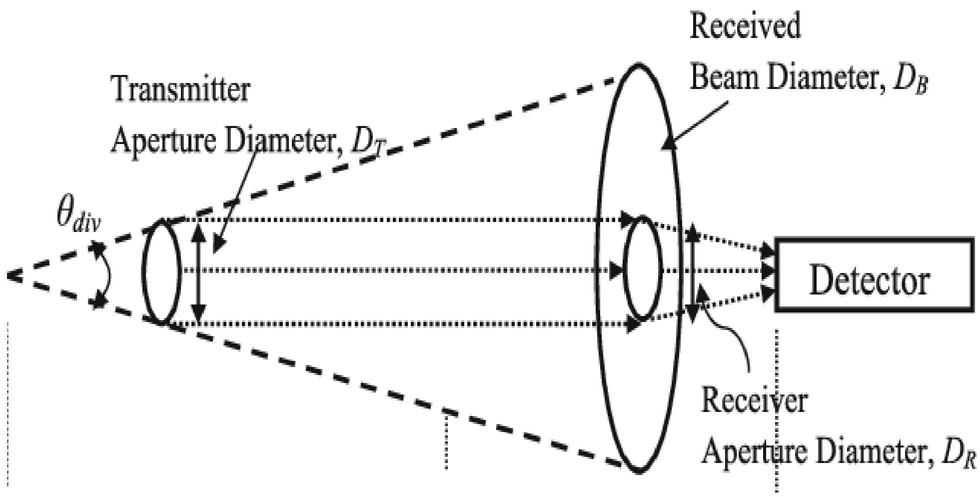

Figure 2.3: *Loss due to beam divergence [28]*

2. **Diffraction-Limited Beam Divergence Loss:**

The diffraction-limited beam divergence loss, often termed geometric loss (L_G), can be expressed in decibels as:

$$L_G = -10\left(2\log(4\pi) + \log\left(\frac{A_T\ A_R}{\lambda^2 R^2}\right)\right) \qquad (2.7)$$

(Note: The log term has been simplified for clarity, assuming circular apertures).

A narrower beam divergence is generally preferable to minimize this power loss. However, an excessively narrow beam demands extreme pointing accuracy, making the system vulnerable to misalignment caused by building sway or thermal expansion. Therefore, the design must strike a balance between power efficiency and pointing stability [28].

The diffraction-limited divergence angle (θ_{div}) is approximated by:

$$\theta_{div} \approx \frac{\lambda}{D_T} \qquad (2.8)$$

This relationship highlights a key design trade-off: increasing the transmitter aperture

(D_{T}) reduces diffraction, resulting in a more collimated beam. Conversely, a smaller aperture increases divergence, spreading the energy over a larger area and reducing the power density at the receiver. For a non-diffraction-limited source with an initial divergence angle θ_{div}, the beam diameter at distance R expands to roughly $D_T + \theta_{div}R$. The fraction of power received is then:

$$\frac{P_R}{P_T} = \frac{D_R^2}{(D_T + \theta_{div}R)^2} \qquad (2.9)$$

And the corresponding loss in decibels is:

$$L_G = -20 \log\left(\frac{D_R}{D_T+\theta_{div}R}\right) \qquad (2.10)$$

3. Beam Expanders for Divergence Control:

To mitigate diffraction-induced spreading, beam expanders are often employed. By increasing the initial beam diameter before it leaves the transmitter, the expander effectively reduces the divergence angle θ_{div}, allowing the system to deliver higher optical power densities over longer distances, as shown in Figure II.4.

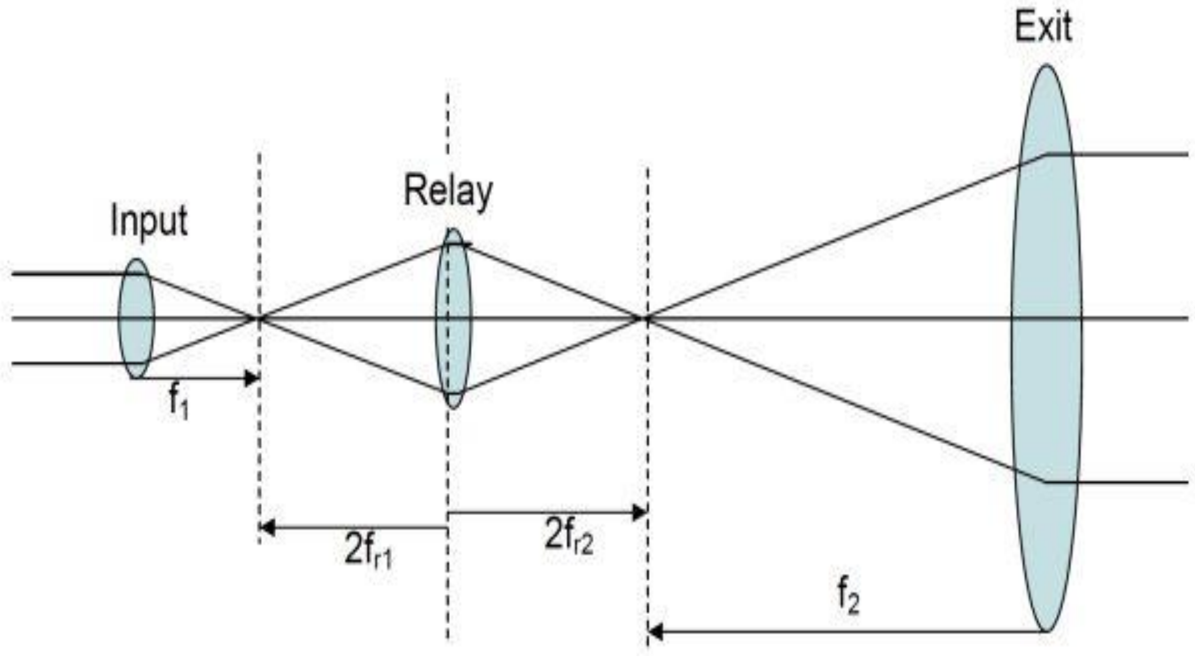

Figure 2.4: *Beam expander to increase diffraction aperture [30].*

2.2.3 Impact of Beam Divergence on Link Alignment and Pointing Losses

2.2.3.1Causes of Beam Divergence

Optical propagation in the atmosphere of El Oued is hindered by three primary phenomena: scattering, absorption, and optical turbulence. While scattering (by dust and aerosols) and absorption (by atmospheric gases) primarily reduce the total power reaching the receiver, optical turbulence introduces spatial distortions. These temperature-induced refractive index fluctuations cause the beam to broaden and wander. To quantify how much a real-world laser deviates from the ideal mathematical Gaussian model, we use the Beam Quality Factor (M^2):

$$M^2 = \frac{\pi w_0 \theta}{\lambda} \quad (2.11)$$

An M^2 value of 1 represents a perfect Gaussian beam; higher values indicate a lower-quality beam that will diverge more rapidly than predicted by ideal equations [36].

2.2.3.2 Beam Wander and Misalignment Issues

In arid regions, intense thermal gradients near the ground cause beam wander, a phenomenon where the beam's center randomly shifts position at the receiver plane. This displacement, combined with mechanical vibrations or building sway, leads to pointing errors. Even a slight misalignment can cause the narrow laser beam to partially or completely miss the receiver aperture, resulting in significant power fading.

The probability of a pointing error (P_e) can be modeled using the following exponential relationship:

$$Pe = e^{-\left(\frac{\Delta\theta}{\theta}\right)^2} \quad (2.12)$$

- P_e **:** is the probability of a pointing error.
- $\Delta\theta$ **:** represents the misalignment angle.
- θ **:** is the beam divergence angle.

2.2.3.3 Interference in wave phenomena

Interference describes the interaction of waves when they overlap. This behavior is categorized by the nature of the sources:

1. **Coherent sources:**

These generate waves with a constant phase relationship. The crests and troughs align predictably over time, meaning the waves are in phase. Such sources possess a fixed frequency (monochromaticity) and exhibit both spatial and temporal correlation. Lasers are the prime example of coherent sources, essential for maintaining a stable communication link.

2. **Incoherent sources:**

These emit waves with random, unpredictable phase relationships. The alignment of peaks and troughs fluctuates rapidly, often containing multiple frequencies and amplitudes. Common examples include sunlight and standard light bulbs, which lack the coherence required for precise interference-based applications.

3. **Constructive interference:**

This occurs when waves of identical frequency align phase to phase (peak aligns with peak). The result is a wave of increased amplitude manifesting as bright bands in optics or stronger signal strength in communications.

4. **Destructive interference:**

This occurs when waves interact in opposite phases (peak aligns with trough), leading to partial or complete cancellation. In optics, this creates dark fringes; in communications, it can cause signal fading or be utilized for noise cancellation [38].

2.3 Atmospheric Effects on Optical Signals

2.3.1 Atmospheric Attenuation

The performance and reliability of Free Space Optical (FSO) systems are intrinsically linked to the state of the transmission medium, the Earth's atmosphere. Unlike optical fiber cables, which provide a protected environment, FSO links are subject to dynamic atmospheric phenomena that result in signal attenuation, the reduction of optical beam intensity as it propagates through space. This degradation is primarily caused by three physical mechanisms: molecular absorption, aerosol scattering, and refractive index fluctuations [40].

2.3.2 Factors contributing to Atmospheric Attenuation

2.3.2.1 Absorption by Atmospheric Gases :

Absorption occurs when the energy of photons is captured by gas molecules and converted into kinetic energy (heat). In the context of FSO, the primary absorbers are water vapor (H_2O), carbon dioxide (CO_2), and ozone (O_3). These molecules possess specific resonance frequencies; if the laser wavelength coincides with these frequencies, the signal is rapidly extinguished. Consequently, FSO systems must operate within specific atmospheric windows, spectral regions where absorption is minimal [32][31].

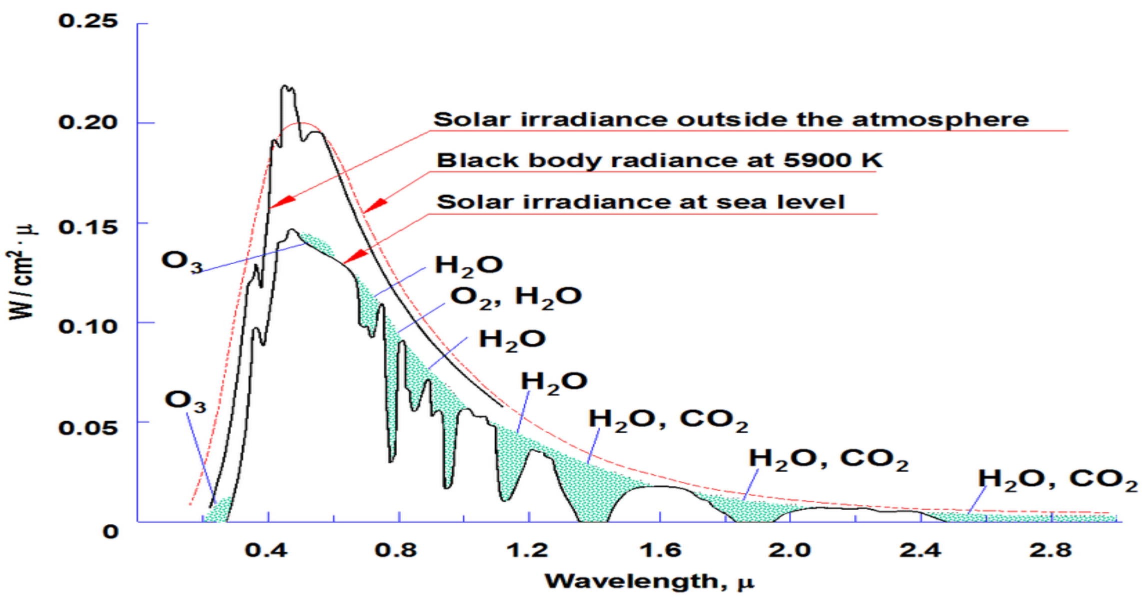

***Figure 2.5**: Solar Spectra and primary absorption bands of atmospheric gases [41].*

2.3.2.2 Scattering by Aerosols :

Scattering involves the redirection of light energy rather than its absorption. This occurs when the optical beam encounters aerosols' suspended particles, such as dust, fog, or smoke. The severity of scattering depends on the ratio of the particle size to the operating wavelength. In regions like El Oued, where dust concentrations are high, aerosol scattering is a dominant source of link degradation [42][40] [57] .

***Table 2.1:** Characteristics of atmospheric scattering particles and their associated regimes at λ = 1550 nm.*

Type	Radius (μm)	Size parameter	Scattering parameter
Air molecules	0.0001	≈ 0.0004	Rayleigh
Fog droplet	1 - 20	4.0 – 81.1	Mie Geometrical
Rain:	100 - 10000	405 – 20265	Geometrical
Snow:	1000 - 5000	4050 – 20265	Geometrical

2.3.2.3 Molecular (Rayleigh) Scattering

Rayleigh scattering occurs when light interacts with particles much smaller than its wavelength, such as nitrogen and oxygen molecules. This effect is inversely proportional to the fourth power of the wavelength (λ^{-4}), making it significantly more disruptive at shorter wavelengths (ultraviolet and visible) compared to the infrared bands typically used in FSO [31].

2.3.3 Impact of Atmospheric Conditions on FSO System

The operational efficiency of an FSO link is dictated by real-time meteorological conditions:

1. ***Weather Conditions:*** Precipitation such as heavy rain, snow, and particularly fog introduces severe attenuation. Fog is especially detrimental because its particle size is comparable to FSO wavelengths, leading to dense Mie scattering that can effectively "blind" a receiver [43].

2. ***Visibility:*** This is a macroscopic measure of atmospheric clarity. Low visibility caused by haze or smog correlates directly with higher scattering coefficients, necessitating higher power margins to maintain the link.

3. ***Optical Turbulence:*** Driven by solar heating of the Earth's surface, turbulence creates small-scale temperature and pressure variations. These fluctuations change the air's refractive index, leading to scintillation (rapid variations in signal intensity), beam wander (the random displacement of the beam's center), and spatial distortions that limit the effective transmission distance [31][36].

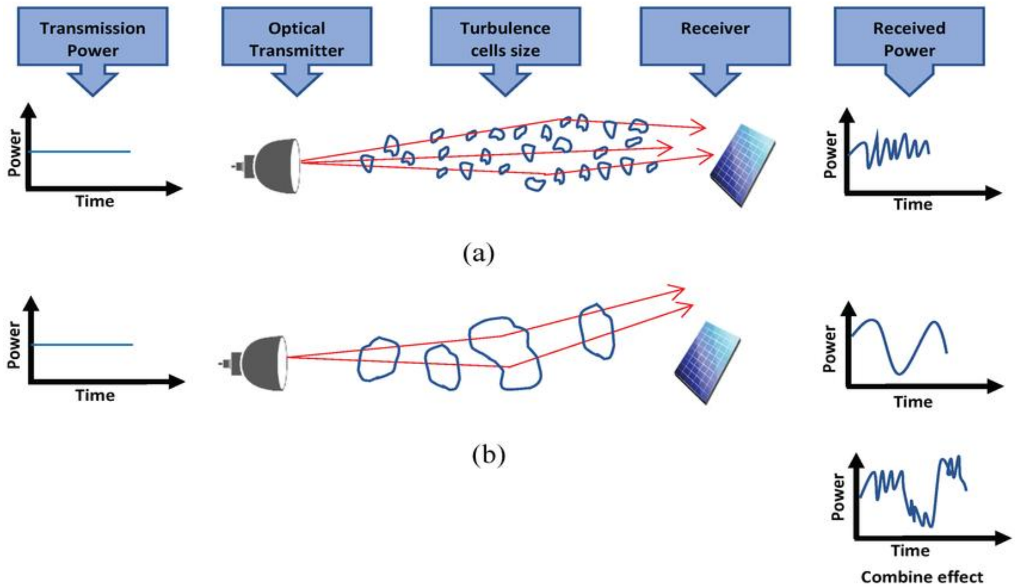

Figure 2.6: *Comparison of Turbulent Cell Size with (a) Scintillation and (b) Beam Wander. [44].*

2.3.4 Mitigation Techniques for Atmospheric Effects

To ensure high link availability, FSO designs incorporate several compensatory strategies:

1 **Wavelength Selection:** Utilizing the Near Infrared (NIR) or Short Wave Infrared (SWIR) bands helps navigate around major absorption peaks and reduces Rayleigh scattering losses **[31]**.

2 **Spatial Diversity:** Deploying multiple laser transmitters or receiver apertures reduces the impact of turbulence induced fading. By leveraging independent fading paths, spatial diversity enhances signal robustness and link availability [42].

3 **Polarization Diversity:** Transmitting data across orthogonal polarizations adds a layer of redundancy that is relatively stable against atmospheric turbulence.

4 **Adaptive Protocols:** Modern systems employ real time rate adaptive protocols that adjust the modulation scheme and transmission speed based on the current atmospheric state, maintaining connectivity even during degraded conditions [31].

2.3.5 Beer-Lambert Law

The mathematical foundation for quantifying atmospheric attenuation is the Beer-Lambert Law. It defines the transmittance (τ), *the* fraction of light that successfully traverses a path of length L:

$$\tau = \exp(-\beta L) \tag{2.13}$$

Where τ is the transmittance, β is the total attenuation coefficient, and L is the distance the light travels.

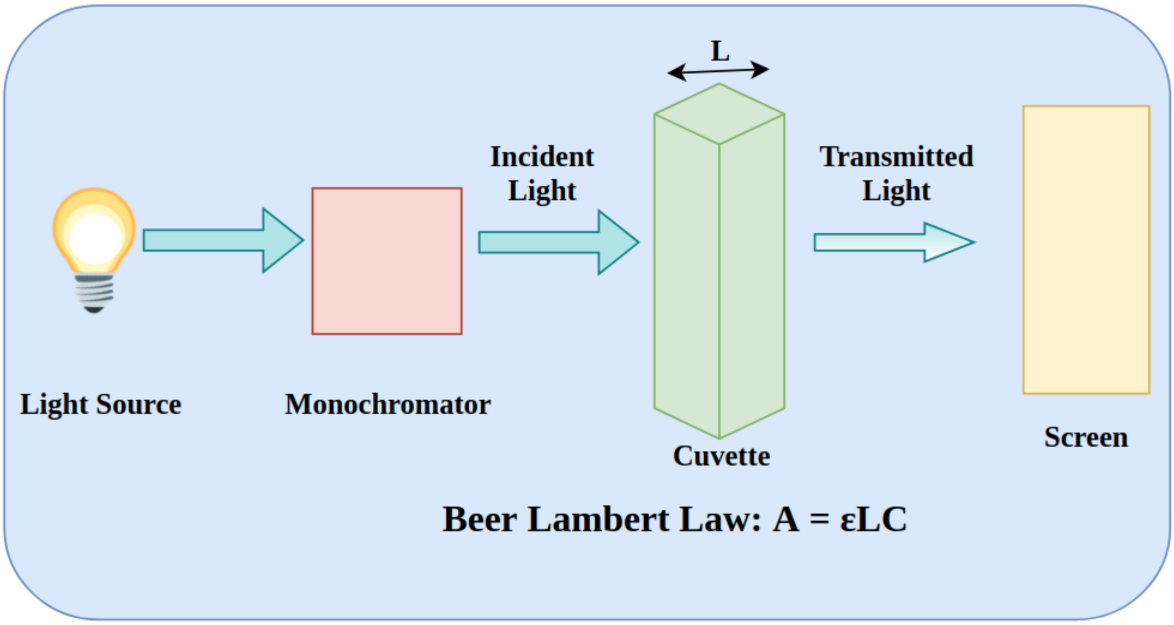

Figure 2.7: *Schematic representation of the Beer-Lambert Law for optical transmission [45]*

In complex media where both absorption and scattering are present, the transmitted light intensity (I) is expressed as :

$$I = I_0 \times e^{-\alpha l} \qquad (2.14)$$

Where:

- I is the transmitted light intensity.
- I_0 is the initial light intensity,
- α is the total attenuation coefficient (cm^{-1}), which is the sum of the absorption and scattering coefficients,
- l is the path length.

The total attenuation coefficient α can be expressed as:

$$\alpha = \alpha_{abs} + \alpha_{sca} \qquad (2.15)$$

Where:

- α_{abs} is the absorption coefficient,
- α_{sca} is the scattering coefficient.

By separating these coefficients, researchers can analyze which specific atmospheric factor (e.g., desert dust vs. humidity) is the primary contributor to signal loss in a given environment like El Oued.

2.4 Atmospheric Turbulence

The reliable deployment of Free Space Optical communication technologies is significantly hampered by atmospheric turbulence. Primarily induced by temperature gradients and pressure variations, this phenomenon stems from random, continuous alterations in the optical properties of the environment. These variations manifest as refractive index fluctuations, scintillation, and beam spreading, all of which introduce severe detrimental effects on the propagating optical signal. The design of robust FSO links [46] relies heavily on a profound understanding of these physical impacts and the statistical models employed to characterize them.

2.4.1 Refractive index fluctuations

Atmospheric turbulence originates from localized homogeneity in air temperature and pressure, compounded by wind velocity variations. These factors combine to create dynamic turbulent eddies of varying densities and sizes [31][34][46].

These eddies induce rapid, stochastic fluctuations in the refractive index of the air along the optical propagation path. Because the refractive index determines the speed of light within a medium, these spatial and temporal variations act as a series of continuously shifting lenses and prisms. Consequently, the optical beam undergoes random refraction and diffraction as it traverses the atmosphere [47].

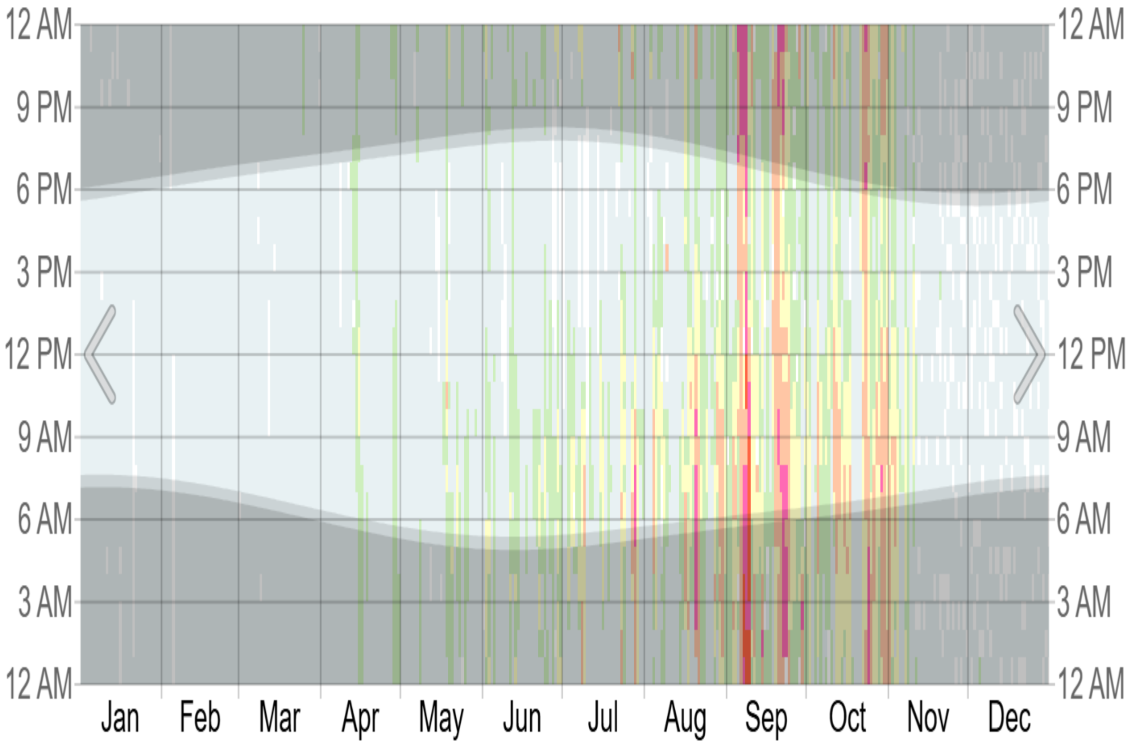

Figure 2.8: *Weather observed in 2024 at Guemar Airport for temperature [56].*

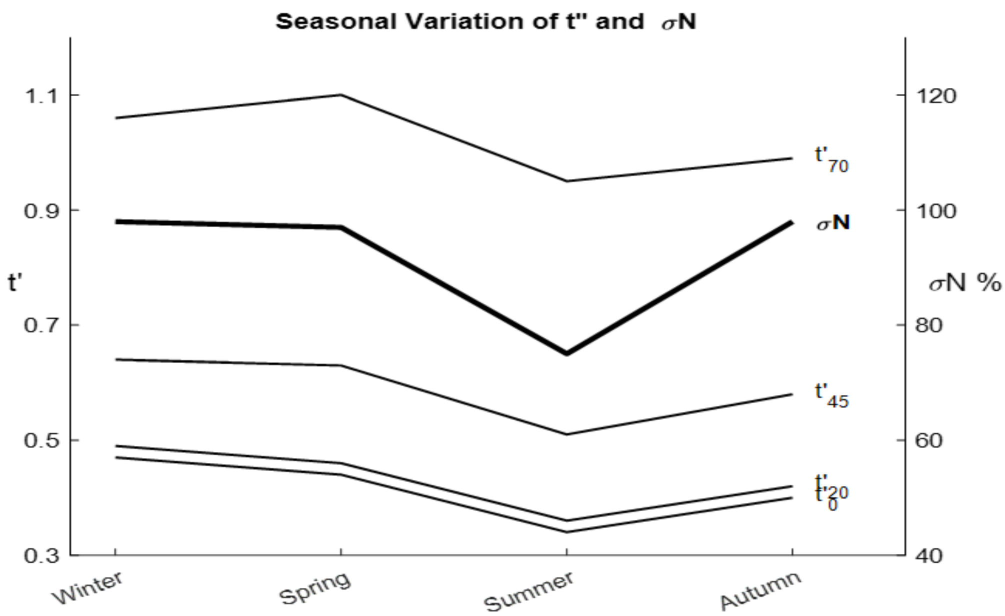

Figure 2.9: *Scheme showing the seasonal changes of refractive index fluctuations [47]*

While the relationship between the refractive index and atmospheric conditions is highly complex, it can be approximated by a simplified equation that relates the index of refraction to temperature and pressure:

$$n = 1 + 77.6 \times 10 - 6\frac{P}{T}\left(1 + \frac{7.52 \times 10^{-3}}{\lambda^2}\right) \qquad \textbf{(2.16)}$$

Where P is the atmospheric pressure in Pascals, T is the temperature in Kelvin, and λ is the optical wavelength.

This equation explicitly highlights the dependence of the refractive index on macroscopic meteorological parameters [45]. To quantify the severity of these variations, researchers use the refractive index structure parameter (C^2_n). This parameter serves as a fundamental metric for evaluating the strength of atmospheric turbulence and its consequent impact on the optical medium [48]-[49].

2.4.2 Scintillation Effects

The random variations in the refractive index along the propagation path yield two primary degradations in the optical signal: scintillation and beam spreading. Scintillation, often referred to as irradiance or intensity fluctuation, describes the rapid and random variations in the intensity of the received optical signal [31][39][50]. This phenomenon is the optical equivalent of the twinkling of stars observed at night. As the coherent laser beam propagates through the turbulent channel, it traverses air pockets with varying refractive indices. This is leading to complex scattering and interference patterns.

Both constructive and destructive interference cause significant temporal and spatial variations in light intensity at the receiver plane [31, 48]. Scintillation becomes more pronounced over longer transmission distances, leading to a drastic degradation in the system's bit error rate (BER). The severity of scintillation is dictated by factors such as temperature gradients, crosswind speeds, and the overall link distance [51]. The standard quantitative measure for this effect is the scintillation index (σ^2_I), defined as the normalized variance of the received irradiance:

$$\sigma_I^2 = \frac{\langle I^2 \rangle}{\langle I \rangle^2} - 1 \qquad \textbf{(2.17)}$$

Where I is the instantaneous received optical intensity, and $\langle \cdot \rangle$ denotes the ensemble (or time) average.

2.4.3 Beam spreading

Beyond scintillation, atmospheric turbulence induces beam spreading. As the laser beam propagates, random refractive index gradients cause it to expand radially at a rate significantly higher than natural diffraction in free space. This excessive expansion reduces the optical power density at the receiver aperture, yielding a heavily attenuated signal [27][38].

Furthermore, turbulent eddies larger than the beam's radius cause beam wander. It is a phenomenon where the entire beam's centroid randomly deviates from its intended line of sight Considering these effects, the time-averaged irradiance profile of the beam is expressed as: [51].

$$\boldsymbol{I(l,r) = \frac{2P_0}{\pi\omega_{eff}^2(l)} exp\left(-\frac{2r^2}{\omega_{eff}^2(l)}\right)} \qquad \textbf{(2.18)}$$

Where P_0 is the total transmitted beam power, and r is the radial distance from the beam's center.

Due to turbulence-induced quality deterioration, the long-term average effective beam waist, $\omega_{eff}(l)$, becomes strictly greater than the diffraction-limited waist $\omega(l)$ [27]. This effective waist is defined mathematically as

$$\boldsymbol{\omega_{eff}^2(l) = w^2(l)(1 + T)} \qquad \textbf{(2.19)}$$

Where $\omega(l)$ represents the standard beam waist after a propagation distance L in a vacuum, typically given by:

$$\boldsymbol{\omega^2(l) = \omega_0^2\left[1 + \left(\frac{2L}{K\omega_0^2}\right)^2\right]} \qquad \textbf{(2.20)}$$

Here, ω_0 denotes the initial beam waist at the transmitter (L = 0), k is the wave number, and T characterizes the additional spreading explicitly induced by turbulence.

For a horizontal FSO link, T is calculated using:

$$\boldsymbol{T = 1.33\sigma_I^2\Lambda^{5/6}} \qquad \textbf{(2.21)}$$

(Note: σ_R^2 represents the Rytov variance or turbulence strength).

The spatial parameter Λ is defined as:

$$\boldsymbol{\Lambda = \frac{2L}{K\omega^2(l)}} \qquad \textbf{(2.22)}$$

Because the effective waist $\omega_{eff}(l)$ exceeds the ideal waist $\omega(l)$, the beam experiences a severe reduction in central power concentration. This specific power loss, known as Beam

Expansion Loss (L_{BE}) is quantified in decibels as:

$$LBE = 20 \log_{10}\left(\frac{w(l)}{w_{eff}(l)}\right) \qquad (2.23)$$

2.4.4 Statistical Turbulence Models

Statistical models are essential for forecasting turbulence's effect on the optical signal because it is a naturally chaotic and stochastic process. Various Probability Density Functions (PDFs) have been proposed to model the irradiance fluctuations experienced at the receiver [46][39]. The selection of the appropriate model depends strictly on the turbulence regime (weak, moderate, or strong).

2.4.4.1 Log-normal Distribution

This model assumes that the logarithm of the received irradiance follows a standard Gaussian (normal) distribution. It is mathematically tractable and highly accurate under weak turbulence conditions, where irradiance fluctuations are minimal and single-scattering events dominate the propagation path [34][46]. The PDF (see Figure 2.10) is given by :

$$P_I(l) = \frac{1}{I\sigma\sqrt{2\pi}} exp\left(-\frac{(\ln I-\mu)^2}{2\sigma^2}\right) \qquad (2.24)$$

Where μ is the logarithmic mean, and $\sigma_I^2$is the logarithmic variance of the irradiance.

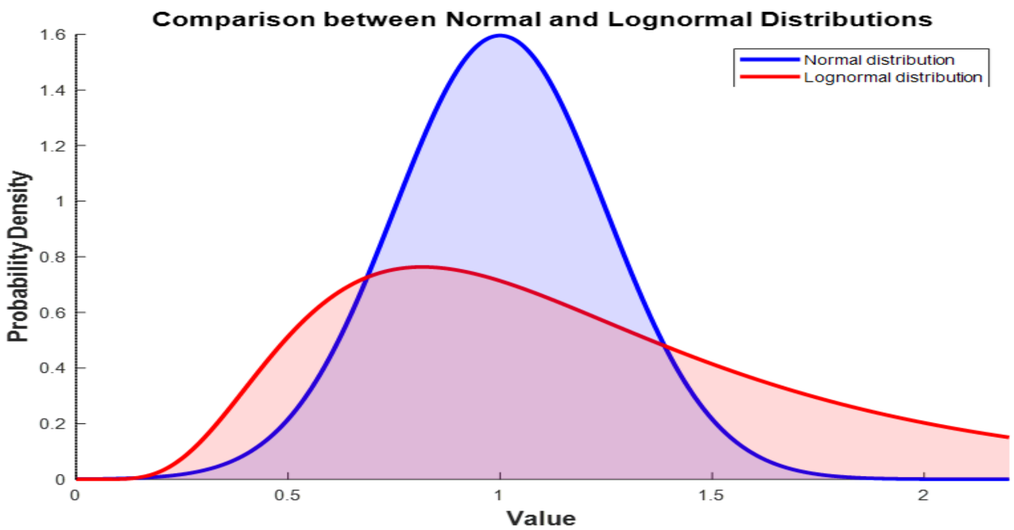

Figure 2.10: *Comparison between normal and log-normal distributions [33]*

2.4.4.2 Gamma-Gamma Distribution

The Gamma-Gamma model is a highly versatile analytical tool that factorizes the irradiance into two independent random variables representing small-scale (scintillation) and large-scale (beam wander) turbulent eddies. It provides an excellent fit for empirical data across a wide spectrum of conditions, from weak to strong turbulence, making it one of the most widely adopted models in modern FSO link analysis [45][46].

Its Probability distribution function is:

$$P(I) = \frac{2(\alpha\beta)^{(\alpha+\beta)/2}}{\Gamma(\alpha)\Gamma(\beta)} I^{\frac{(\alpha+\beta)}{2}-1} K_{\alpha-\beta}\left(2\sqrt{\alpha\beta I}\right) \qquad (2.25)$$

Where:

• $\boldsymbol{\alpha}$ and $\boldsymbol{\beta}$ are parameters related to the effective number of large-scale and small-scale eddies.

• $\boldsymbol{K_n(x)}$ is the modified Bessel function of the second kind of order $\alpha - \beta$,

and $\Gamma(x)$ is the gamma function [34]. The figure 2.11 mention the gamma distribution in different modified Bessel function.

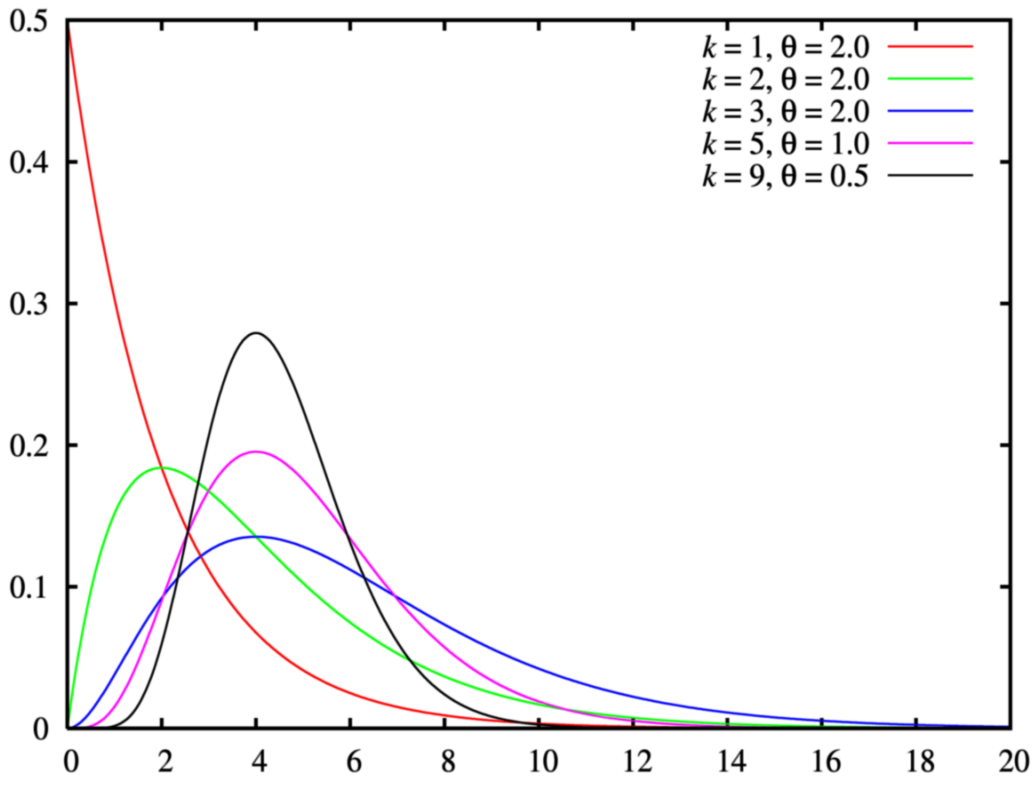

Figure 2.11: *Example profile of a gamma distribution.*

2.4.4.3 K-Distribution

The K-distribution is specifically tailored to characterize irradiance fluctuations under moderate to strong turbulence regimes [34]. By conceptualizing the received signal as a complex superposition of a randomly varying number of scattered optical waves [46], it often matches experimental data in deep turbulence better than the log-normal model. The Probability distribution function is defined as:

$$P_I(I) = \frac{2(\mu_y)^{\mu_y}}{\Gamma(\mu_y)} I^{\mu_y - 1} K_{\mu_y - 1}\left(2\sqrt{\mu_y I}\right) \qquad \textbf{(2.25)}$$

Where $K_{\mu y-1}(x)$ is the modified Bessel function of the second kind, and $\Gamma(\mu_y)$ is the Gamma function.

2.5 Weather Effects

Despite the technical advantages of Free Space Optical communication systems, specifically their wide bandwidth and license-free operation, they remain highly sensitive to local atmospheric conditions.

In a region like El Oued, the Saharan environment introduces unique challenges that extend beyond simple precipitation. In this context, winter morning fog and, more significantly, suspended dust particles play a decisive role in signal extinction and the degradation of link reliability as seen in Figure 2.12.

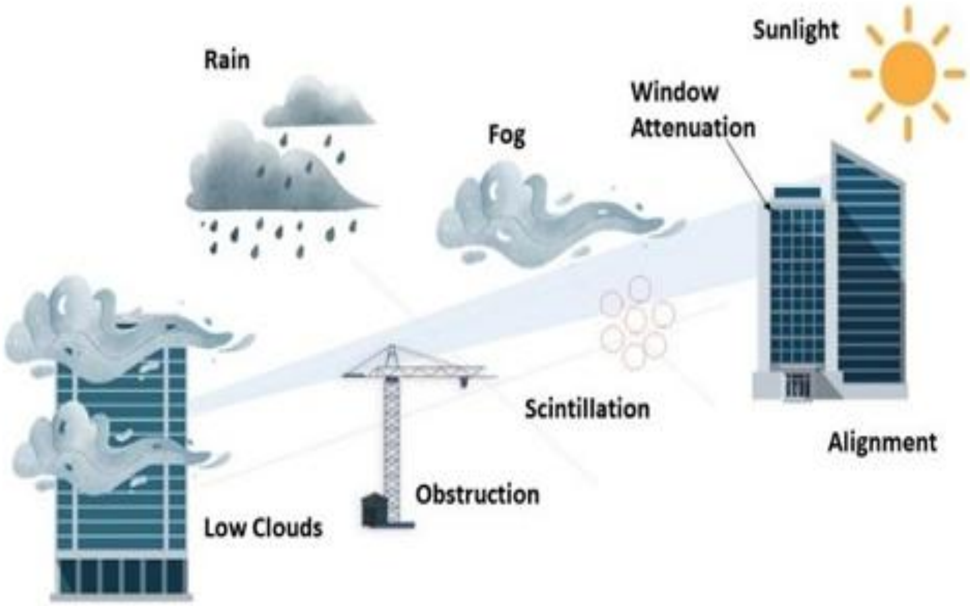

Figure 2.12: *Factors that affect the FSO communication links [55].*

2.5.1 Fog

Fog consists of suspended water droplets with diameters comparable to the wavelengths typically utilized in FSO systems (visible and near-infrared spectra). This similarity in size triggers Mie scattering [33], which causes substantial signal attenuation as photons are deflected from their intended propagation path [31].

2.5.1.1 Visibility and Attenuation

Fog density is inversely related to visibility; an increase in fog density results in diminished visibility and heightened attenuation. In cases of thick fog (visibility < 50 m), attenuation can exceed 35 dB/km. In the El Oued province, fog predominantly occurs during early winter mornings, which may lead to temporary link outages if the power margin is not sufficiently designed [36].

2.5.1.2 Empirical Models for Fog Attenuation

Kim's model is widely regarded as one of the most accurate frameworks for predicting fog attenuation based on visibility (V):

$$\boldsymbol{\beta_{fog} = \frac{3.91}{V}\left(\frac{\lambda}{\lambda_0}\right)^{-\rho}} \qquad \textbf{(2.27)}$$

Where:

- V: Visibility distance (km).
- λ: Operating wavelength (nm).
- p: Scattering size distribution coefficient.

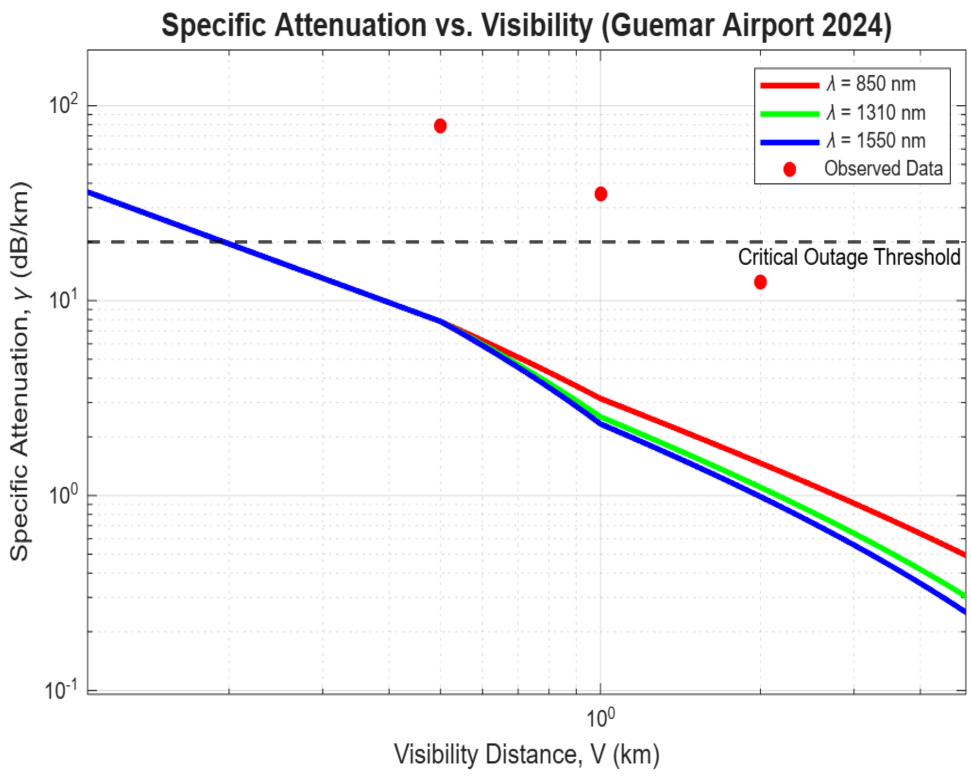

(a)

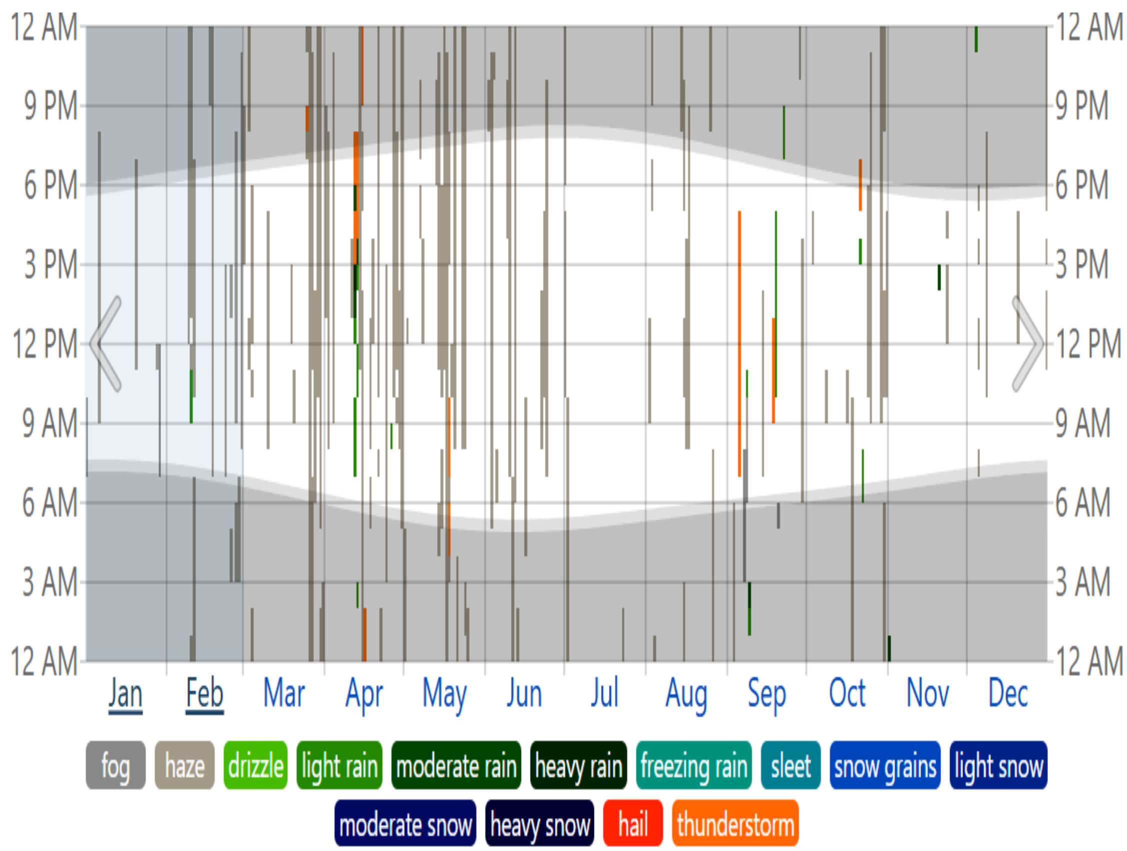

(b)

Figure 2.13: *Fog attenuation as a function of visibility distance in EL OUED (a) for different wavelengths and (b) during different months [56].*

2.5.2 Rain

Raindrops are characterized by being significantly larger than optical wavelengths, primarily causing attenuation through scattering and absorption. Due to their large size, the scattering follows the non-selective scattering regime, where attenuation is less dependent on the specific wavelength compared to fog [49].

2.5.2.1 Rain Rate and Attenuation

Attenuation is directly dependent on the rainfall rate (*R*), measured in mm/hr. Rainfall in the El Oued region is infrequent but often takes the form of sudden, heavy bursts (cloud bursts) (Figure 2.14). At a rainfall rate of 25 mm/hr, attenuation levels reach roughly 10 dB/km [31] as mentioned in Figure 2.15.

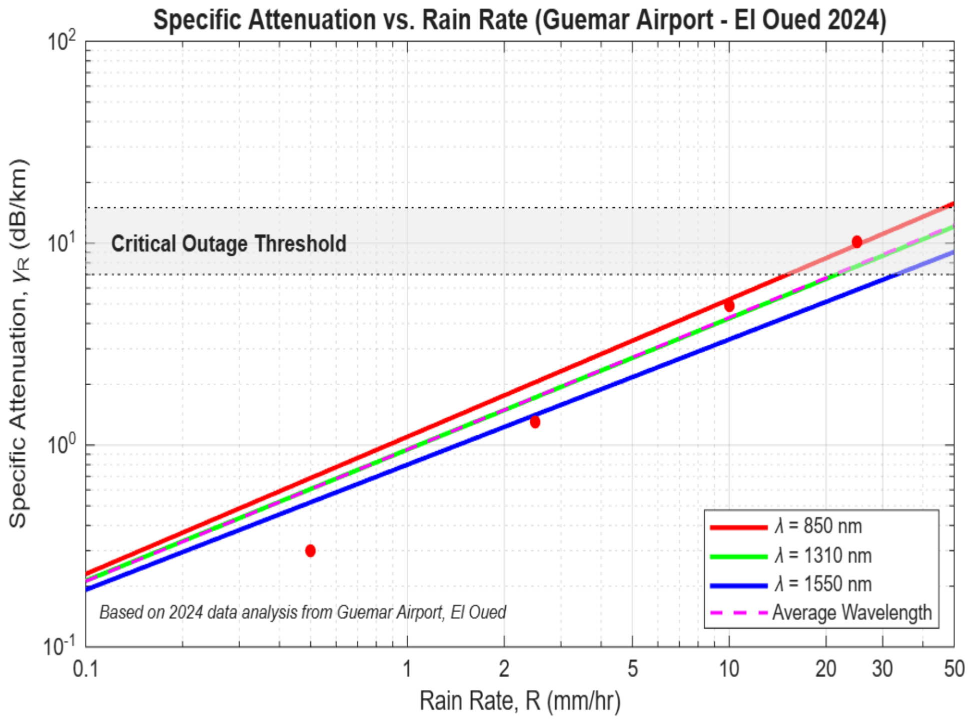

Figure 2.14: *FSO link attenuation due to rain by wavelength [56].*

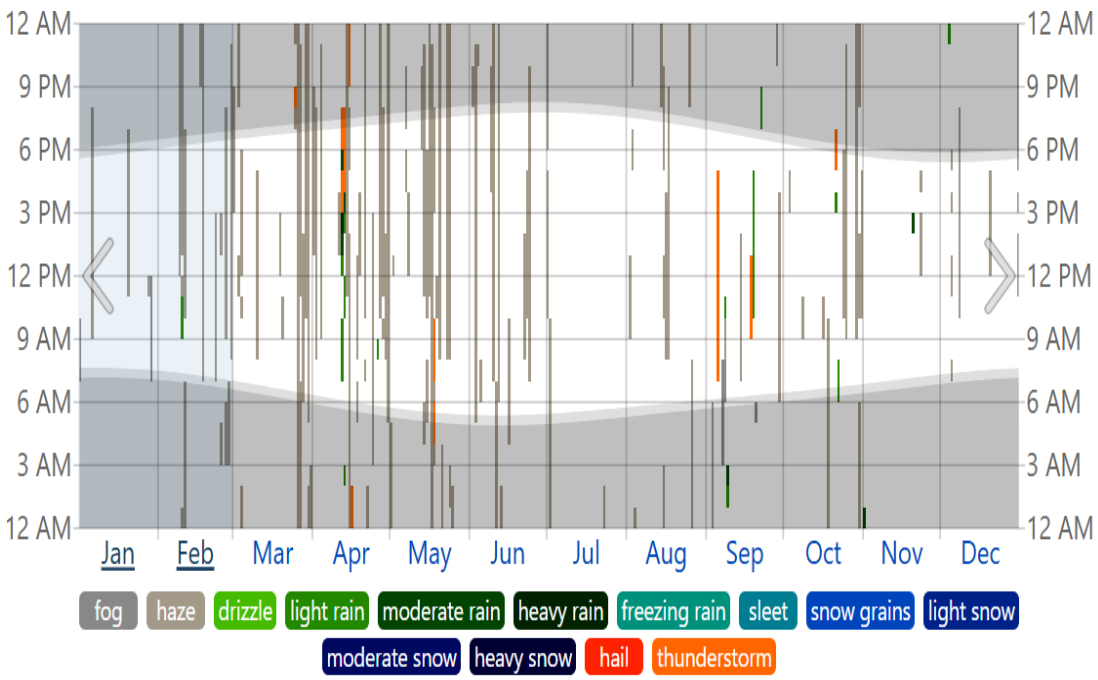

Figure 2.15: *FSO link attenuation due to rain by month [56].*

2.5.2.2 Empirical Rain Attenuation Models

Rain attenuation can be modeled using the following empirical expression:

$$Att_{rain} = k_1 R^{k_2} \tag{2.28}$$

Where Att_{rain} is the rain attenuation (dB/km), and R is the rainfall rate (mm/hr), and k_1 and k_2 are model parameters that depend on factors such as wavelength and raindrop size distribution, and may vary geographically and with rain type [35].

The value of R according to different rain conditions is shown in Table 2.2.

Table 2.2: *Rainfall rate (R) values for various precipitation conditions.*

Precipitation	Light rain	medium rain	Heavy rain	cloudburst & heavy rain
R Values (mm/hr)	1 – 2	2 – 5	5 – 15	20 – 40

The ITU-R (International Telecommunication Union - Radiocommunication Sector) provides models for rain attenuation, primarily developed for microwave and millimeter-wave frequencies.

These models use different scattering mechanisms and wavelengths than optical frequencies. However, they provide the foundation for developing specific FSO rain attenuation models. Some researchers have adopted these general principles to propose models specifically for FSO, using rainfall rate statistics or even visibility under rainy conditions as input parameters [54]-[55] [57].

2.5.2.3 Types of Snow and Attenuation

Snow can be classified into wet and dry snow, with wet snow causing higher attenuation due to liquid water on snowflakes. Dry snow impacts link more at low snowfall rates.

while wet snow impacts link more at high rates [36]. Figures 13-17 indicate an inverse relationship between snowfall visibility and attenuation, where greater visibility enables higher transmission bit rates. Snow significantly impairs FSO link connectivity, restricting viable operational distances to approximately 250 meters [49].

2.5.3 Dust and Sandstorms: The Primary Challenge in El Oued

In arid and semi-arid regions such as El Oued, dust and sandstorms represent the most significant atmospheric deterrent to free space optical communication reliability. Unlike rain or fog, which are seasonal and transient in the Sahara, dust particles are often suspended in the air year-round. These particles vary in size from a few micrometers to several hundred micrometers, leading to a complex combination of scattering and absorption that can severely extinguish the optical signal.

2.5.3.1 Physical Characteristics of Desert Dust

Dust particles in the Souf region are primarily composed of silica and various minerals. Their impact on the laser beam depends on the visibility (*V)* and the mass concentration (*C*) of the particles. During a sandstorm, the concentration of these particles increases drastically, creating a dense medium that can lead to *link outages* if the system is not designed with a high link margin.

2.5.3.2 Mathematical Modeling of Dust Attenuation

To quantify the power loss (A_{dust}) in dB/km, researchers often use empirical models designed for desert environments. One of the most widely recognized models is the Alhaider model, which relates attenuation to visibility as follows:

$$A_{dust} = a \cdot V^{-b} \quad \text{[dB/km]} \qquad (2.29)$$

Where:

- ***V*** is the visibility distance in kilometers,
- ***a*** and ***b*** are empirical coefficients that depend on the local climate and particle-size distribution.

For the Algerian Sahara, these values are often adjusted based on local meteorological data to reflect the specific silt and clay ratio of the soil.

For the original Alhaider study (often cited as a baseline for sandstorms), the values are typically: **a=0.52, b=1.07.**

Another approach used to estimate the attenuation coefficient (α_{dust}) based on the concentration of particles is given by:

$$\alpha_{dust} = \frac{3 \cdot Q_{ext} \cdot C}{4 \cdot \rho \cdot r_e} \quad \textbf{(2.30)}$$

Where:

• Q_{ext} is the extinction efficiency factor.

• C is the dust concentration (mg/m^3),

• ρ is the density of the dust particles,

• r_e is the effective radius of the particles.

2.5.3.3 Impact on FSO Infrastructure in El Oued

Beyond signal attenuation, the environment of El Oued poses significant mechanical and thermal challenges:

• **Particle Accumulation:** Dust settles on the optical transceiver lenses (the protective domes of the FSO units), creating a permanent fixed loss that increases over time unless periodic cleaning is performed.

• **Thermal Gradients:** The intense heating of dunes during the day generates strong atmospheric turbulence and scintillation (see Section II.1.2). When combined with dust scattering, this results in a doubly stochastic propagation channel that is particularly difficult to model.

2.5.4 Snow

Although snowfall is an extremely rare occurrence in El Oued, it physically causes attenuation that falls between the levels of rain and fog. Snow is categorized as dry or wet. Wet snow causes higher attenuation because its liquid water layer increases both absorption and scattering [35].

Dry snow impacts link more at low snowfall rates, while wet snow impacts link more at high rates [36]. Figure 2.16 indicates an inverse relationship between snowfall visibility and attenuation, where greater visibility enables higher transmission bit rates. Snow significantly impairs FSO link connectivity, restricting viable operational distances to approximately 250 m [49].

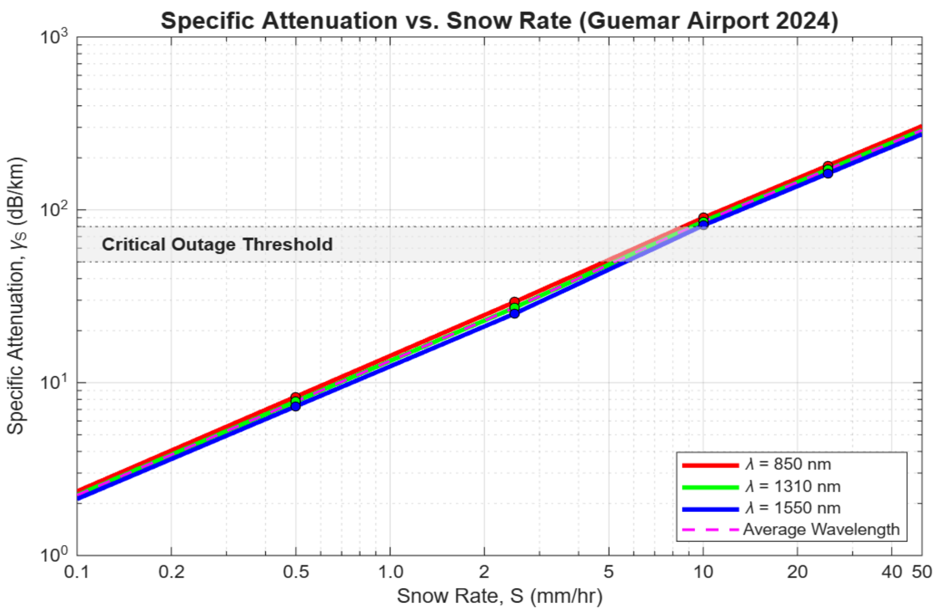

Figure 2.16: *Received signal power in relation to medium visibility in Dry Snow [56].*

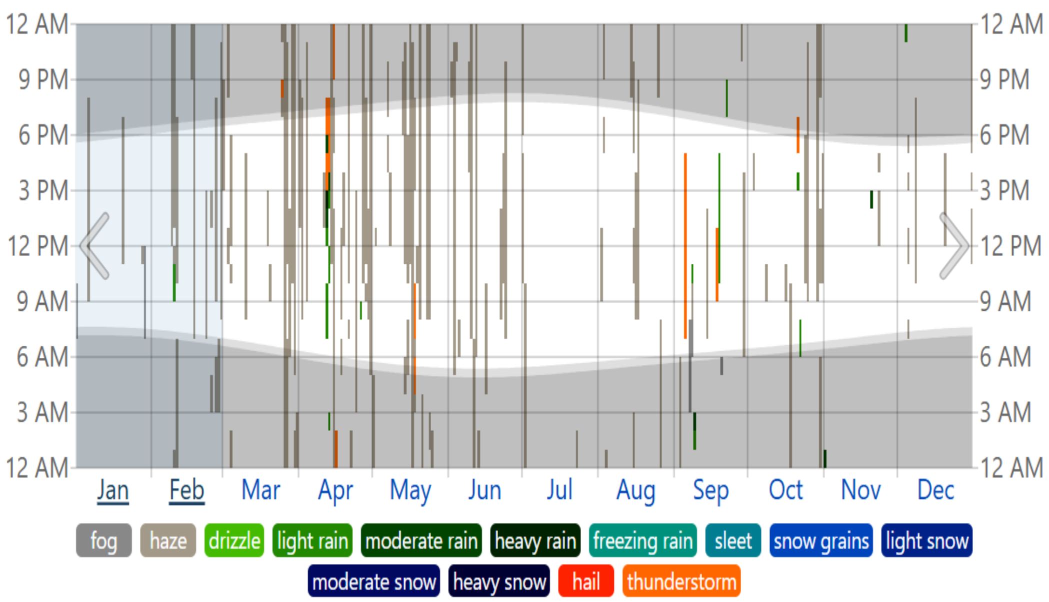

Figure 2.17: *Observed Weather in 2024 at Guemar Airport for Dry Snow [56].*

2.6 Conclusion

This chapter has established the fundamental principles governing Free-Space Optical (FSO) propagation, ranging from the strategic selection of transmission wavelengths within the NIR and SWIR bands to the complex behavior of Gaussian beams under diffraction and coherence constraints.

A significant portion of this analysis was dedicated to the environmental challenges inherent to the transmission medium, with a specialized focus on the climatic conditions of the El Oued region. We analyzed how absorption, scattering, and turbulence interact with fog, rain, and dust. These interactions induce critical attenuation, scintillation, and beam wander. In addition, it is detailed in the application of the Beer-Lambert law and robust statistical structures (log-normal, gamma-gamma, and K-distribution) in quantifying these impairments.

Finally, we evaluate a suite of countermeasures, including beam-expander optics and polarization diversity. These insights provide a rigorous scientific foundation for designing robust, high-speed FSO systems in arid environments.

Chapter 3

Performance Analysis of FSO Network

3.1 Introduction

Free-Space Optical communication systems are among the leading technological solutions in modern wireless networks, owing to their ability to provide ultra-high data rates, broad bandwidth, and a high level of information security. Despite these advantages, the efficiency of these systems remains highly dependent on volatile atmospheric conditions; environmental factors such as fog, dust, and rain cause severe signal attenuation, thereby limiting the operational range of the optical link. These challenges are particularly evident in regions with harsh desert climates, such as the El Oued region in Algeria. Consequently, the accurate characterization of these atmospheric phenomena and their impact on FSO links is a fundamental pillar for ensuring service continuity and reliability.

Recent academic studies have focused on evaluating the resilience of high-speed FSO systems employing complex and dense modulation formats such as 16-QAM. In this context, Sliti and Mrabet (2023) [60] presented advanced modeling setup using OptiSystem software and desert climatic data, proving that the bit error rate increases steadily when visibility drops below 100 m. These findings were further supported by the experimental results of Fathallah et al. (2019) [61], which showed a sharp degradation in system performance at a visibility range of 50 m due to heavy dust. Regarding efficiency enhancement, Huang et al. (2021) [62] achieved a transmission rate of 12 Gbps under moderate turbulence conditions, while Ali et al. (2023) [63] confirmed a significant collapse in the quality factor when horizontal visibility levels declined.

Building upon these studies, this work seeks to push performance boundaries by investigating and analyzing a Dual-Polarization Quadrature Amplitude Modulation (DP-16QAM) system capable of supporting speeds up to 112 Gbps. This architecture exploits polarization division multiplexing to double the spectral efficiency without increasing the required bandwidth.

This chapter provides a comprehensive performance evaluation of the 112 Gbps DP-16QAM FSO system through a series of rigorous numerical simulations, with a focus on analyzing the atmospheric interference and turbulence characteristic of the El Oued climate. Furthermore, the impact of atmospheric attenuation on key performance indicators including BER, Q-factor, and Eye Diagram integrity will be examined to provide a clear perspective on the feasibility of deploying such systems in desert environments.

3.2 Simulation Setup and Analysis

This section details the simulation framework for the DP-16QAM free-space optical system, operating at a high-speed data rate of 112 Gb/s. The simulation incorporates the specific atmospheric conditions of El Oued, Algeria, ensuring an accurate depiction of the system's performance in a real-world desert context. The analysis is conducted using OptiSystem 23, an advanced and extensive software platform for the design and evaluation of optical communication systems, enabling precise modeling of polarization division multiplexing and coherent detection components. This system model has the following essential components as shown in *Figure 3.1*.

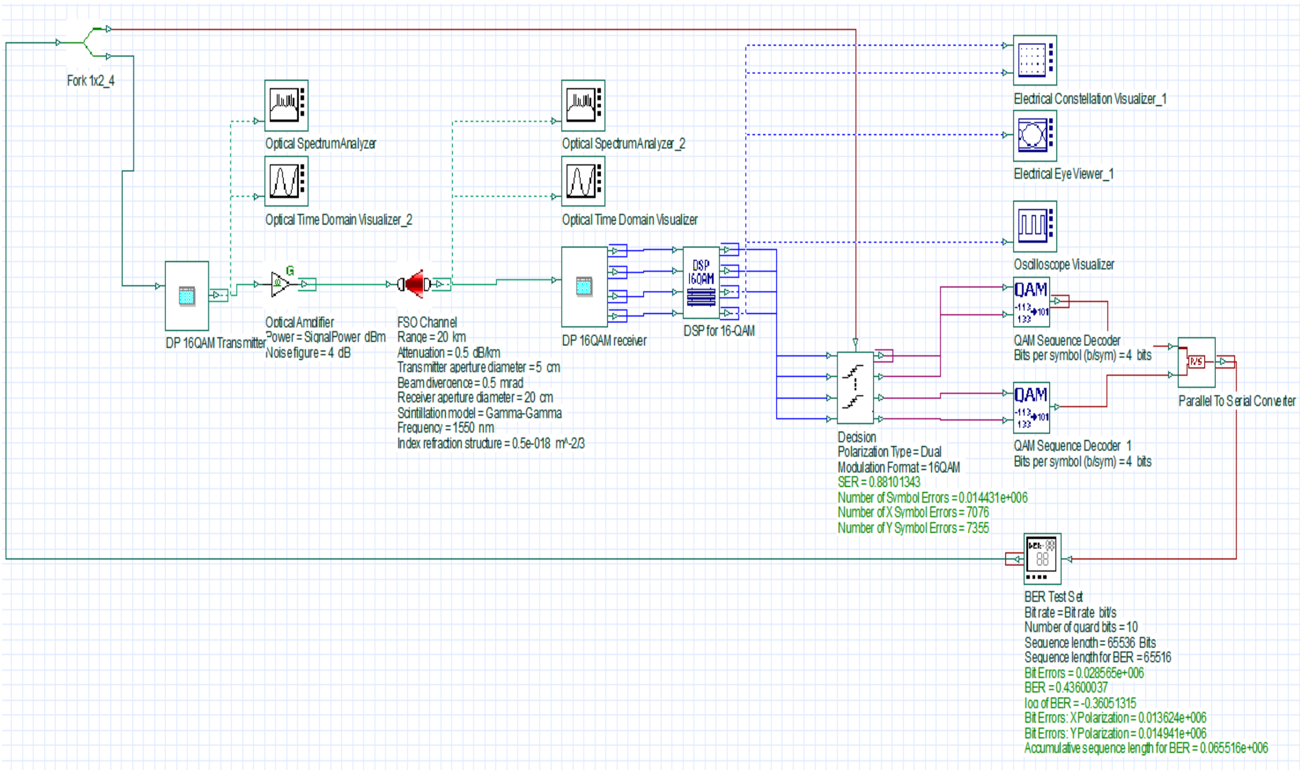

Figure 3.1: *DP-16-QAM FSO configuration.*

3.2.1 Transmitter (Tx Subsystem)

The DP-16QAM Transmitter functions as a high-capacity engine for modern optical communication systems. It maximize the data throughput over a single optical channel by combining two advanced multiplexing techniques. First, it utilizes 16-QAM modulation, which encodes 4 bits per symbol by manipulating both the amplitude and the phase of the light wave. Second, it employs polarization division multiplexing, which splits the laser carrier into two orthogonal states (X and Y polarizations), effectively doubling the data rate by transmitting independent signals simultaneously on each state.

3.2.2 16-QAM sequence generator

The transmitter architecture employs a 16-QAM sequence generator operating at a specified symbol rate, mapping 4 bits per symbol onto a complex constellation. The digital symbols are converted to analog waveforms through matched M-ary pulse generators utilizing root-raised cosine filters with controlled roll-off factors, generating precisely synchronized in-phase (I) and quadrature (Q) electrical components.

3.2.3 Mach-Zehnder modulators (MZMs)

Optical modulation is achieved using dual lithium niobate ($LiNbO_3$) Mach-Zehnder modulators characterized by well-defined $V\pi$ voltages for the target modulation format. The I and Q optical signals are combined through a high-performance 90° hybrid coupler with minimal phase error, generating a complex optical field that preserves both amplitude and phase information. This configuration produces a polarization-multiplexed 16-QAM optical signal as depicted in Figure 3.2.

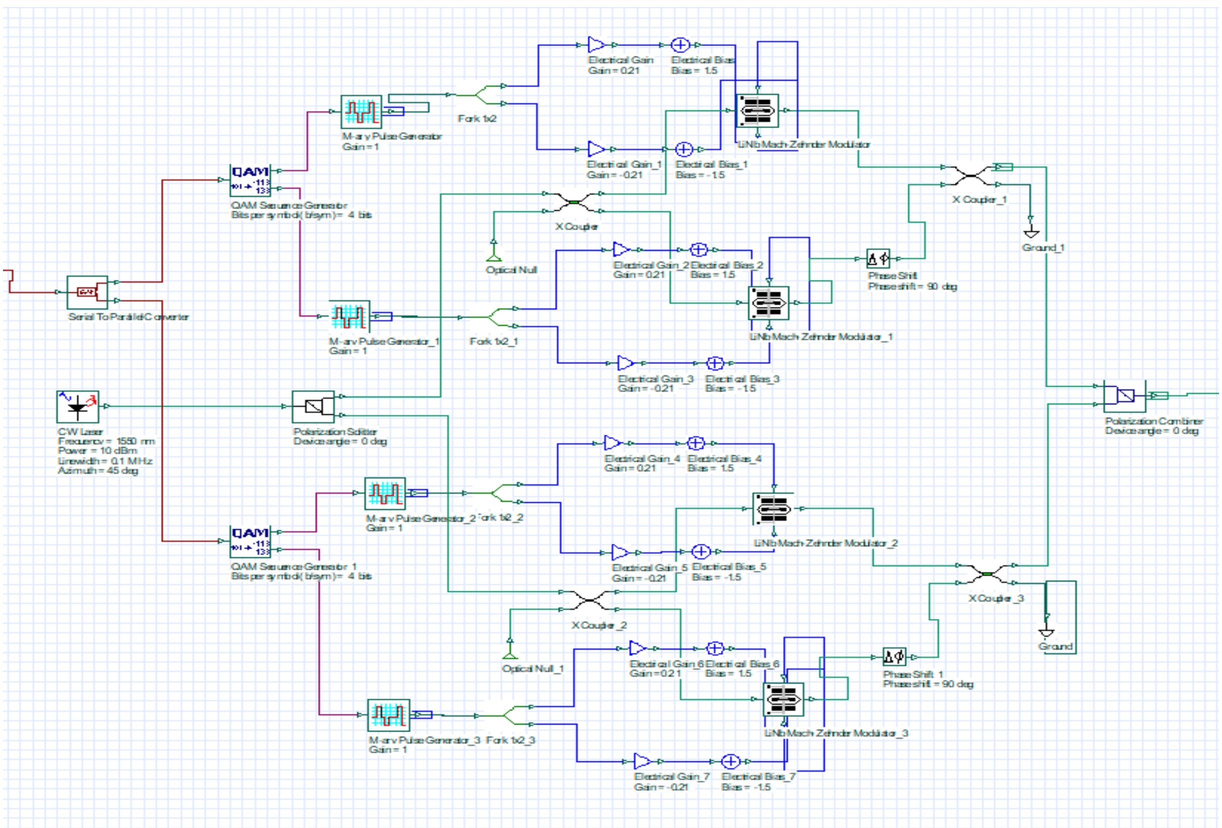

Figure 3.2: *Optical DP 16-QAM transmitter layout.*

3.2.4 FSO Channel

The FSO Channel is modeled as a line-of-sight (LoS) optical link with a variable transmission range R. Atmospheric attenuation is implemented using the Beer-Lambert law. With the attenuation coefficient α varying according to seven distinct weather conditions as seen in Figure 3.3:

Very Clear, Clear, Light Rain, Dust Haze, Light Fog, Dust Storm, and Severe Dust Storm.

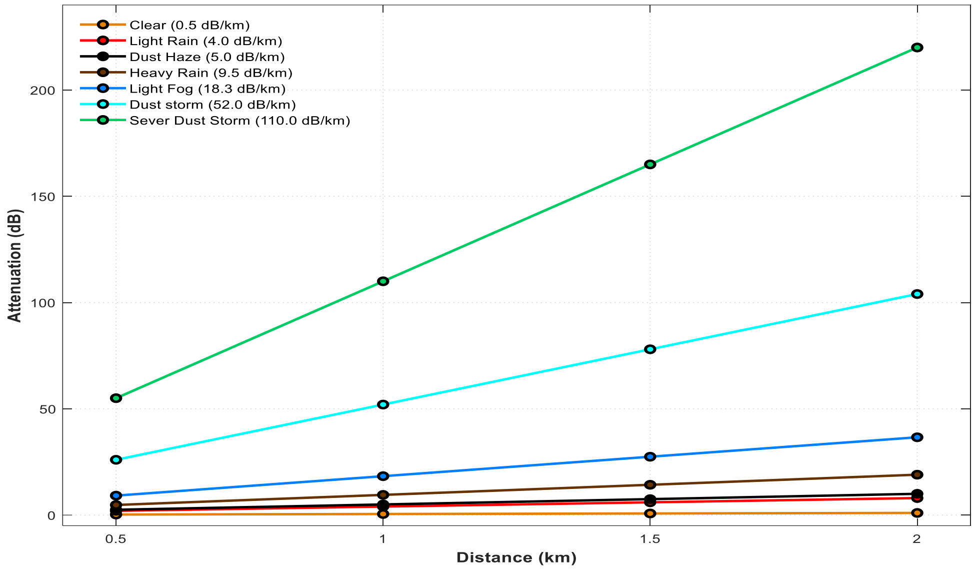

Figure 3.3: *Attenuation vs Distance under Different Weather Conditions.*

The illustrated data provides a quantitative assessment of atmospheric-induced signal degradation, demonstrating how different weather scenarios influence the propagation efficiency over a defined distance. The transmitted signal before and after propagation in the free space is mentioned in Figure 3.4.

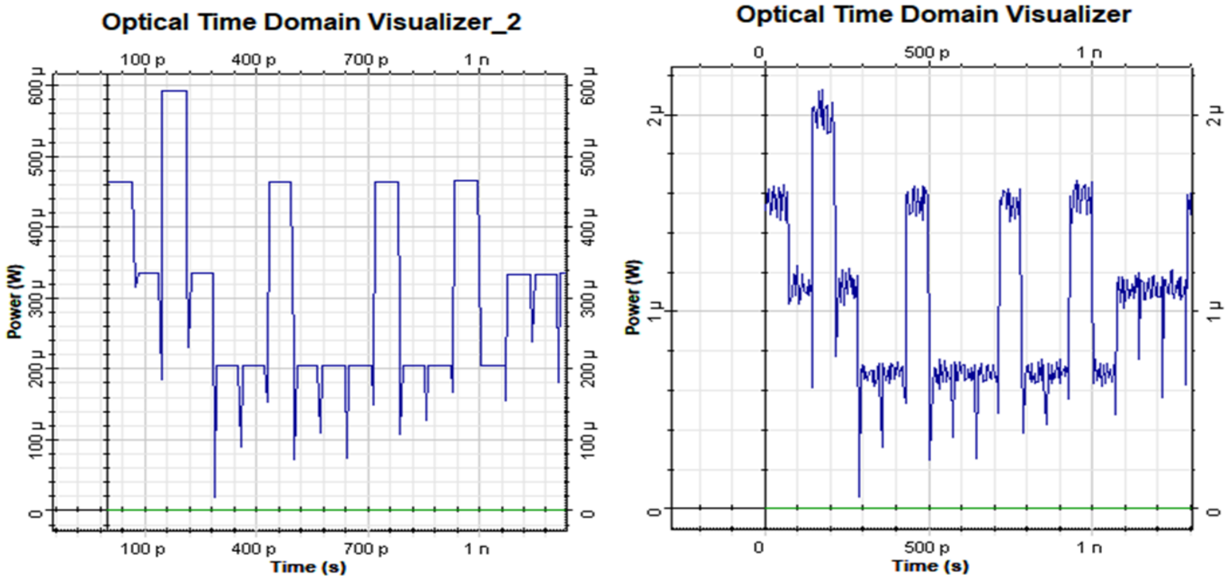

Figure 3.4: *Transmitted signal before and after free space Channel Optical DP 16-QAM transmitter layout*

3.2.5 Receiver (Rx subsystem)

The receiver unit (Rx Subsystem) is the fundamental component responsible for data recovery from modulated optical signals and their effective conversion from the optical domain to the electrical domain. This unit employs coherent detection technology, a refined architecture specifically designed to handle complex modulation formats such as DP-16QAM, as it allows for the complete restoration of the optical wave characteristics, including amplitude, phase, and polarization. The process begins with a Local Oscillator (LO) laser operating at a wavelength of 1550 nm, featuring a narrow spectral linewidth of 0.1 MHz. This specific linewidth value is critical for ensuring phase stability and mitigating random phase noise that could compromise the accuracy of QAM symbol recovery. Both the LO signal and the received signal are passed through polarization splitters to distribute the processing into two symmetrical branches representing the horizontal and vertical polarizations (X and Y).

Within each polarization branch, the signals are integrated via a 90° optical hybrid, consisting of optical couplers (X Couplers) and precision phase shifters, to extract the In-phase (I) and Quadrature (Q) components. These components are subsequently directed to eight PIN Photodetectors organized in balanced Configurations. This technical setup is specifically designed to suppress common-mode noise and eliminate unwanted DC terms, significantly enhancing the receiver's sensitivity and Signal-to-Noise Ratio (SNR). In the final stage, the optical currents are converted into electrical voltage signals through differential subtractors, followed by an amplification stage using electrical amplifiers with a gain of 20 dB.

This process ensures the signal levels are boosted to the range required for subsequent digital signal processing, enabling accurate recovery of the signal constellation and evaluation of the optical link performance under various atmospheric conditions, as illustrated in the system's structural schematic.

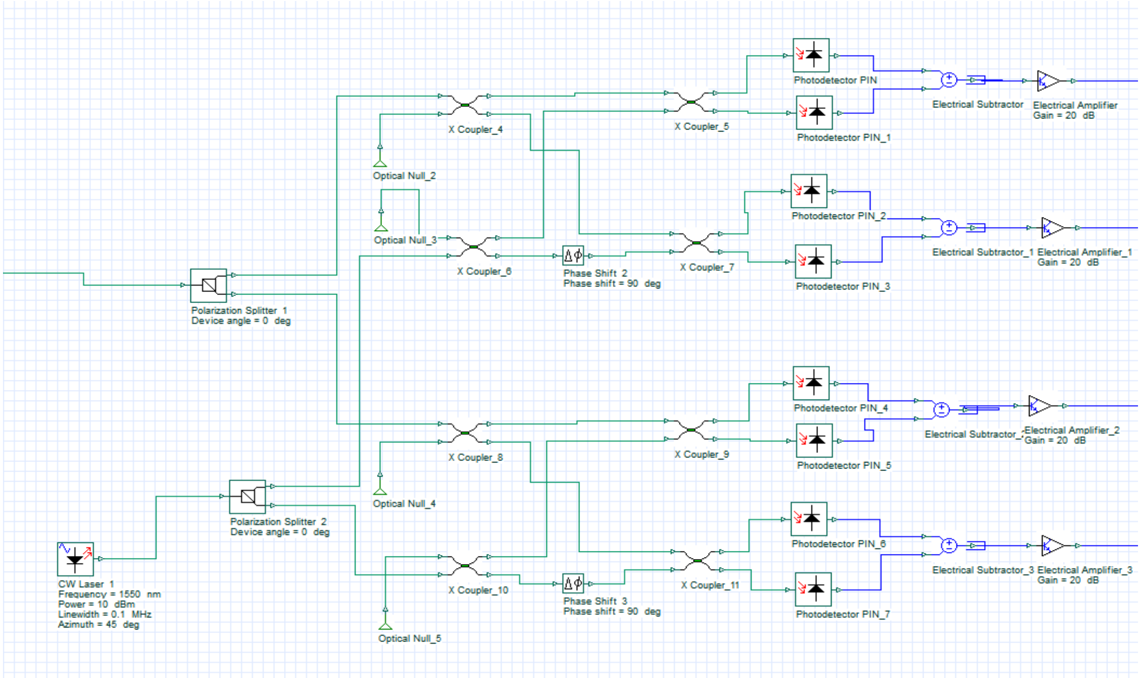

Figure 3.5: *Optical DP 16-QAM receiver layout.*

3.2.6 Additional Supporting Components

- **Optical amplifiers** are essential for long-distance transmissions, using pre-amplifiers and post-amplifiers to boost and strengthen attenuated signals. These amplifiers are defined by their output power (around 0 dBm) and noise figure (e.g., 4 dB).
- **The digital signal processing unit** in a 16-QAM system acts as the brain of the receiver, responsible for recovering data from an transmitted signal that has been severely distorted by harsh atmospheric conditions. The process begins with normalization and resampling to stabilize the electrical signal levels. This is followed by polarization demultiplexing, a critical step in DP systems to decouple the interference between the horizontal and vertical paths.

  Next, the unit performs clock and frequency recovery to ensure precise timing synchronization and to correct frequency offsets between the transmitter and receiver lasers. The DSP also handles channel equalization to compensate for atmospheric attenuation and dispersion, followed by carrier phase recovery to stabilize the points of the constellation diagram into their correct positions. Finally, the algorithms perform decision-making and demapping, assigning each received symbol to its corresponding original bits (4 bits per symbol), which enables the system to achieve a low bit error rate even in the presence of intense sandstorms or thermal turbulence.
- **The QAM Sequence Decoder** is the component responsible for the final stage of data recovery, where it converts processed digital symbols back into logical bits. Its scientific mechanism is based

on the demapping process, where it receives the coordinates of points in the constellation diagram from the DSP or decision unit and compares each point to its ideal position within the 16-QAM grid. Since each symbol in this system carries a specific amplitude and phase representing 4 bits, the decoder translates each location into its corresponding binary string (e.g., 0110 or 1101). Its importance lies in bridging the gap between the physical properties of the wave and the original digital information, ensuring that the data flows in the correct serial sequence before reaching the BER analyzer for final evaluation.

- **Eye Diagram Visualizer** is employed to evaluate the temporal quality of the signal. It illustrates the timing of signal transitions and detects problems like jitter and inter-symbol interference.
- **The Electrical Constellation Visualizer** is a pivotal visual diagnostic tool in digital communication systems, representing the modulated signal in a two-dimensional plane by plotting the In-phase (I) component on the horizontal axis and the Quadrature (Q) component on the vertical axis. In a 16-QAM system, an ideal signal appears as a uniform 4 x 4 grid of 16 points, each representing a unique symbol carrying 4 bits. Its scientific value lies in its ability to instantly reveal physical channel impairments; for instance, scattered or circular patterns indicate phase noise, while compressed points signify attenuation or interference. Consequently, it serves as the primary means for evaluating DSP algorithm efficiency before conducting the final BER statistical measurement.
- **The Electrical Eye Viewer** is a visual tool for time-domain signal analysis that uses pulse superimposition to evaluate ISI and noise. An open eye indicates a clear signal, while eye closure signals severe distortion.
- **BER Test Set** is a statistical tool that compares received bits to original transmitted bits to calculate the error ratio. It serves as the ultimate benchmark for overall system performance and data integrity.

3.3 Weather Conditions and Atmospheric Attenuation

The research take into account of major weather conditions in El-Oued region as mentioned in table 3.1, which attenuation coefficients are extracted from DAUO local meteorological statistics cite in Annex data that transit to Visibility and Sky Conditions, and with apply of Alhaider Law cite in section 2.5.3.1.

Table 3.1: *Attenuation at different atmospheric phenomena.*

Atmospheric phenomena	Attenuation (dB/km)	Index refraction C_n^2 ($m^{-2/3}$)
Clear	0.5	10^{-17}
Light Rain	4	10^{-16}
Dust Haze	5	$5*10^{-15}$
Heavy Rain	9.5	10^{-14}
Light Fog	18.3	$5*10^{-16}$
Dust storm	52	10^{-13}
Severe Dust Storm	110	10^{-12}

Table 3.2: *Simulation parameters*

Simulation parameters	Value
Wave length	1550 nm
Power	10 dBm
Bit rate per channel	112 Gbps
Transmitter aperture diameter	5 cm
Receiver aperture diameter	20 cm
Beam divergence	0.5 mrad
Scintillation model	Gamma-Gamma
Linewidth	0.1 MHz
Modulation	DP-16QAM
responsivity	1 A/W
Refractive index structure constant (C_n^2)	weather - related
PIN photodiode responsivity	1 A/W
Dark current	10 nA

3.4 Results simulation and discussion

This study examines seven prevailing weather conditions in the El Oued region , with attenuation and refraction coefficients derived from ITU recommendations and local meteorological studies of Guemar Abdelkader Al-Amoudi Airport.

3.4.1 Comparative Analysis of Q-Factor and Log (BER) Performances under Atmospheric Phenomena

- **Clear scenario**

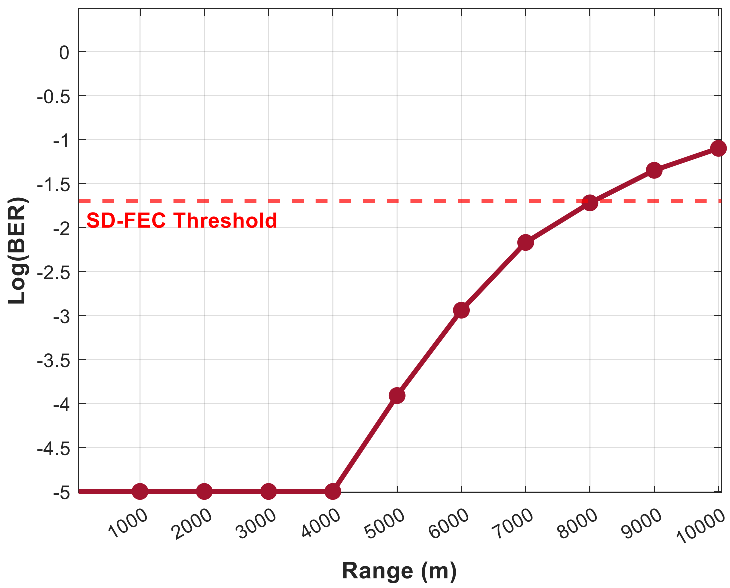

Figure 3.6: *Log (BER) vs Distance for clear scenario.*

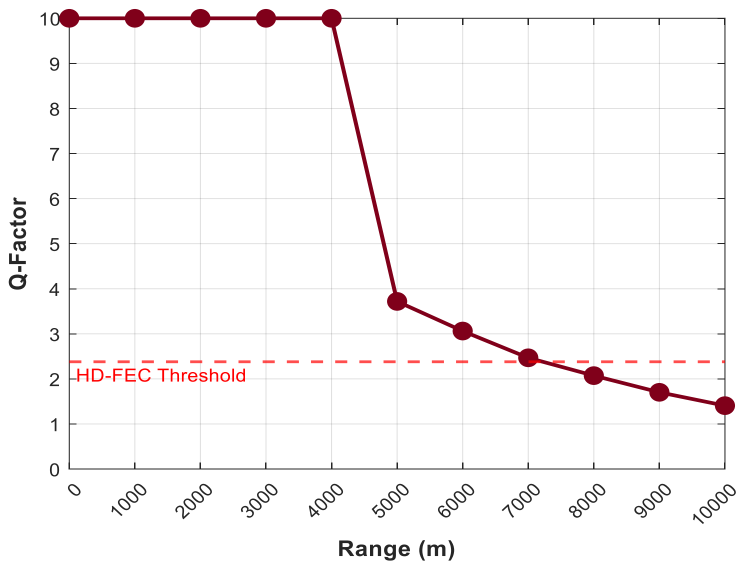

Figure 3.7: *Q-Factor vs. Distance for clear scenario.*

The simulation results depicted in Figures 3.6 and 3.7 demonstrate the performance of the proposed FSO communication system utilizing DP-16QAM coherent modulation at an aggregate data rate of 112 Gbps. The study was conducted under a clear atmospheric scenario characterized by a constant attenuation coefficient of 0.5 dB/km. Quantitative analysis of the curves reveals that the system achieves optimal signal quality and stability at propagation distances up to 4000 m, where the Q-factor remains saturated at its maximum value (Q > 10) alongside a negligible bit error rate (< -5) This superior performance is directly attributed to the effectiveness of the DSP algorithms and the fold capacity without generating significant Inter-Symbol Interference (ISI) within this range. However, as the link distance increases, a gradual performance degradation is observed due to the cumulative path loss of 0.5 dB/km, leading to a continuous reduction in the Optical Signal-to-Noise Ratio (OSNR). Consequently, the system performance intersects the Forward Error Correction thresholds specifically the Hard-Decision (HD-FEC) and Soft-Decision (SD-FEC) limits at a maximum transmission range of approximately 8000 m.

These findings confirm that the proposed design can reliably sustain ultra-high-capacity links up to 8 km in clear desert environments, serving as a robust baseline for evaluating system resilience under severe atmospheric impairments.

- **Light Rain scenario**

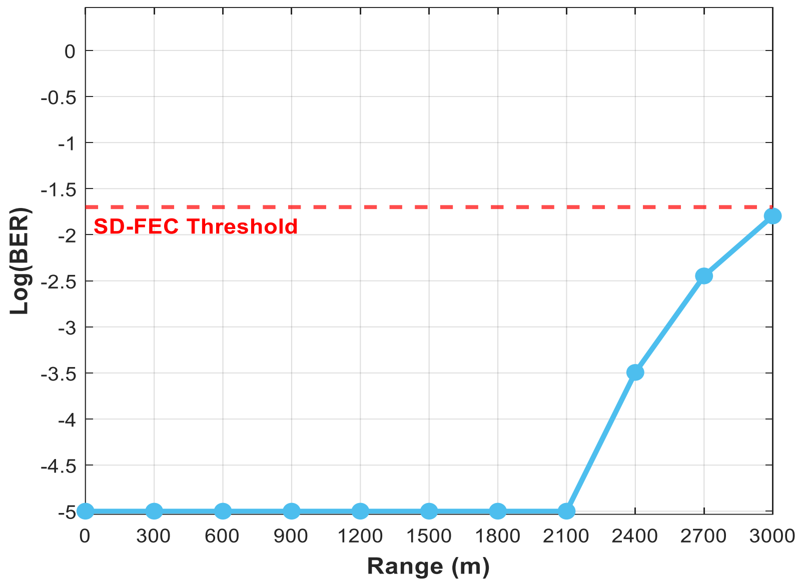

Figure 3.8: *Log (BER) vs Distance for Light Rain scenario.*

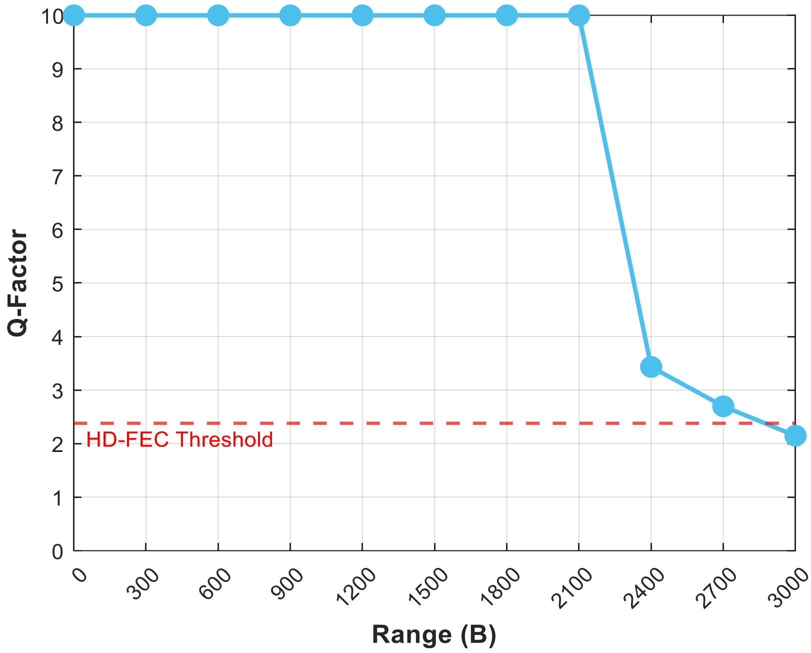

Figure 3.9: *Q-Factor vs Distance for Light Rain scenario.*

The simulation results depicted in Figures 3.8 and 3.9 illustrate the performance of the 112 Gbps DP-16QAM FSO system under a light rain scenario. A significant reduction in the operational range is observed compared to the clear-weather baseline, driven by an atmospheric attenuation coefficient of 4 dB/km. The system maintains optimal signal integrity, with a Q-factor exceeding 10 and a Log(BER) below -5, for distances up to only 2100 m. Beyond this point, a sharp degradation in signal quality occurs due to the enhanced scattering and absorption effects induced by raindrops. This atmospheric attenuation forces the system performance to intersect the Forward Error Correction thresholds specifically the SD-FEC and HD-FEC limits at a transmission distance of approximately 3000 m, representing a reduction in the effective link range of over 60%.

These results highlight the high vulnerability of multi-level modulation schemes and ultra-high data rates to climatic fluctuations; the available OSNR margin depletes rapidly, restricting reliable communication to a maximum radius of 3 km under such precipitation conditions.

➢ **Dust Haze scenario**

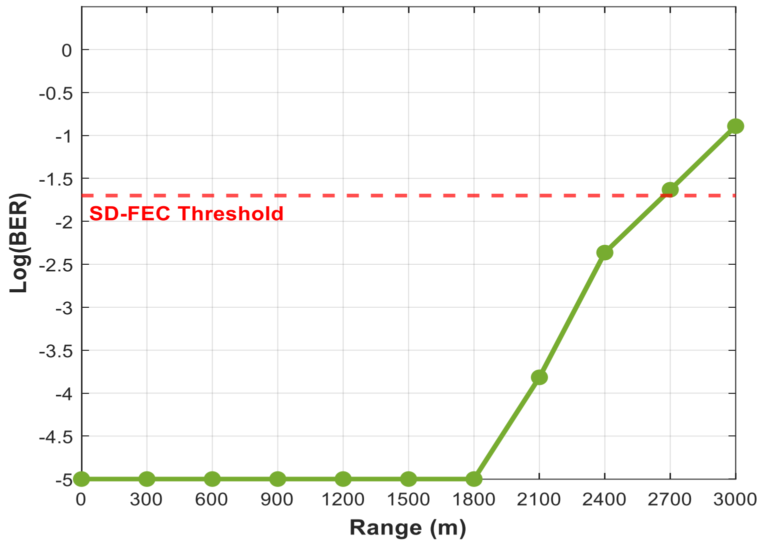

Figure 3.10: *Log (BER) vs. Distance for Dust Haze scenario.*

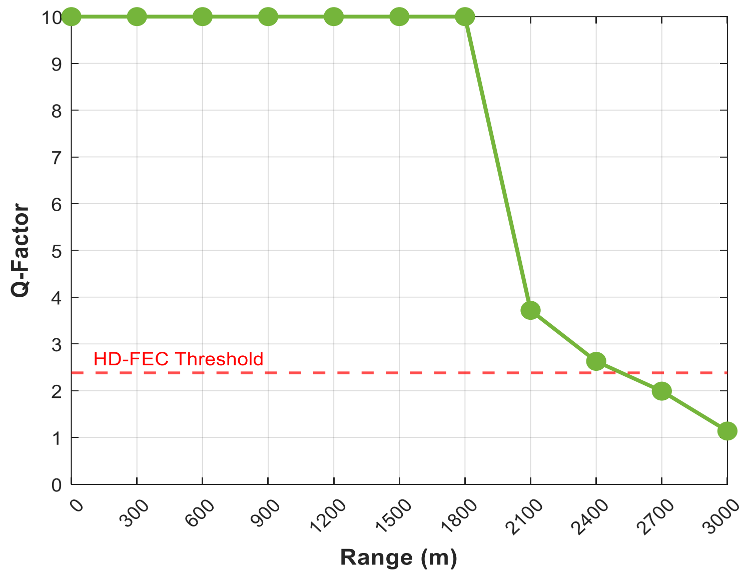

Figure 3.11: *Q-Factor vs. Distance for Dust Haze scenario.*

The simulation results depicted in Figures 3.10 and 3.11 illustrate the performance of the 112 Gbps DP-16QAM FSO system under a dust haze scenario. The outcomes indicate a severe degradation in signal quality compared to the clear-weather baseline, driven by a substantial atmospheric attenuation coefficient of 5 dB/km. The system maintains stable performance with optimal levels (Q >10) over a limited distance of up to 1800 m, followed by a rapid collapse in link characteristics. This decline is primarily driven by Mie scattering and strong absorption caused by suspended dust particles. Due to this high atmospheric attenuation, the Q-factor intersects the HD-FEC threshold at approximately 2500 m, while the bit error rate exceeds the SD-FEC limit at 2700m. These findings confirm that dust haze conditions represent a major physical obstacle to the continuity of ultra-high-capacity optical wireless links in desert environments. In this scenario, the effective communication range is reduced by more than 70% compared to clear weather, emphasizing the necessity of implementing advanced power control techniques or enhancing receiver sensitivity to ensure link reliability.

- **Heavy Rain scenario**

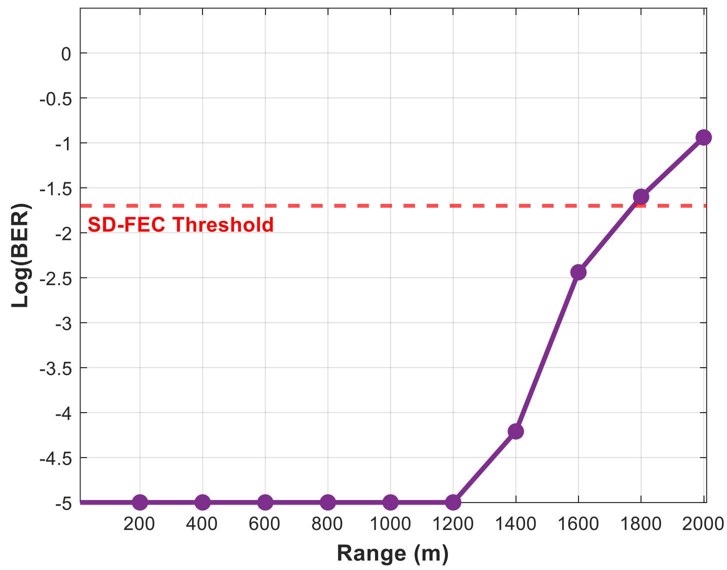

Figure 3.12: *Log (BER) vs. Distance for Heavy Rain scenario.*

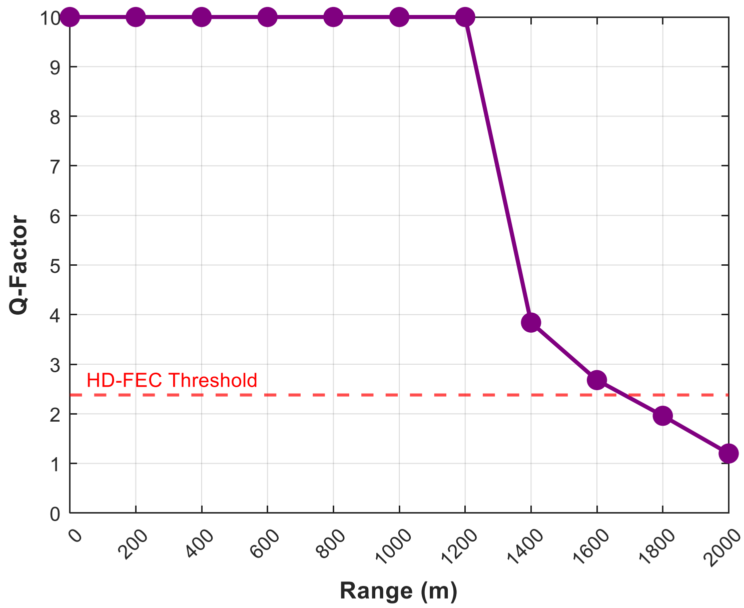

Figure 3.13: *Q-Factor vs. Distance for Heavy Rain scenario.*

The simulation results depicted in Figures 3.12 and 3.13 illustrate the performance of the system under a heavy rain scenario. The results reveal a severe degradation in the optical link's operational range compared to the clear-weather baseline, driven by a marked atmospheric attenuation coefficient of 9.5 dB/km. The system maintains stable signal integrity at its optimal levels (Q > 10 and Log(BER)

< -5) for a distance not exceeding 1200 m. This represents a significant reduction from the 4000 m stable range observed under clear conditions, reflecting the intense scattering and absorption of the optical beam caused by the high density of large raindrops. Beyond this threshold, the performance drops sharply, with the Q-factor intersecting the HD-FEC threshold at approximately 1700 m, while the bit error rate exceeds the SD-FEC limit at 1800 m.

These findings demonstrate that heavy rain reduces the effective system range by approximately 78% relative to clear weather. Consequently, maintaining a 112 Gbps FSO link under such conditions becomes extremely challenging without the implementation of advanced mitigation techniques or dynamic data rate reduction to ensure connection availability.

- **Light Fog scenario**

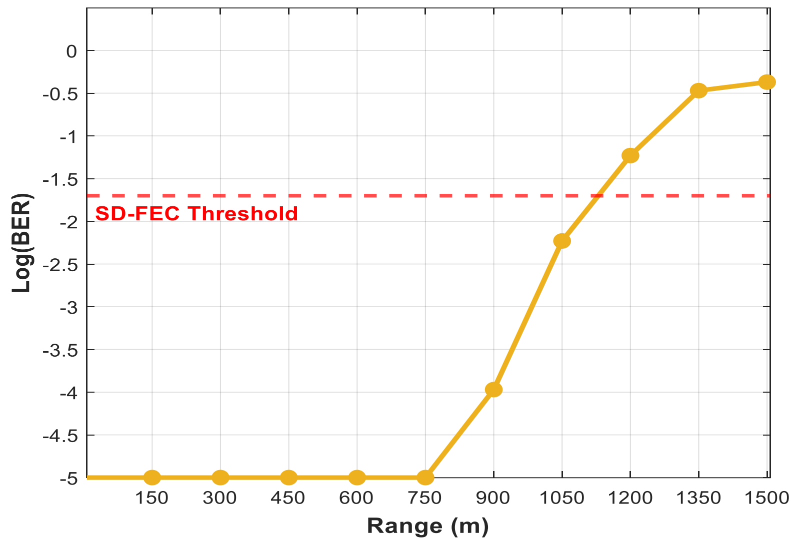

Figure 3.14: *Log (BER) vs. Distance for Light Fog scenario.*

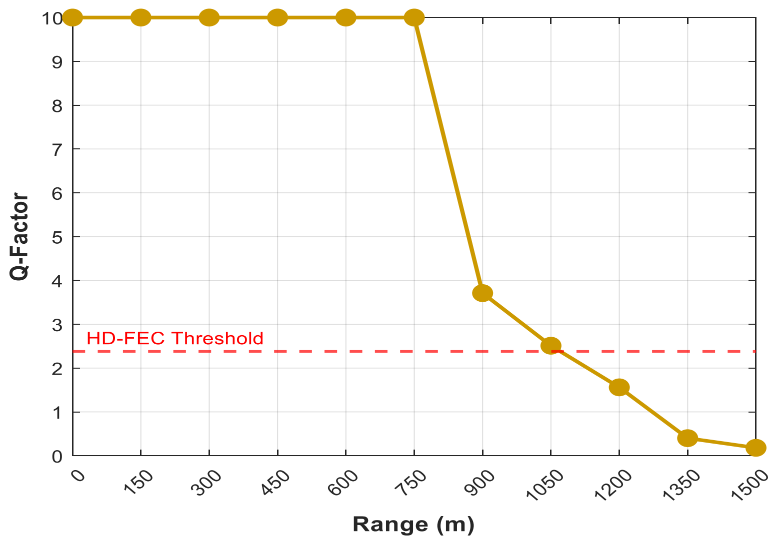

Figure 3.15: *Q-Factor vs. Distance for Light Fog scenario*

The simulation results depicted in Figures 3.14 and 3.15 illustrate the performance of the 112 Gbps DP-16QAM FSO system under a light fog scenario. The outcomes indicate that fog presents a more substantial challenge to link stability than the previously analyzed rain conditions, driven by a severe atmospheric attenuation coefficient of 18.3 dB/km. The system maintains stable performance (Q > 10) over a highly restricted distance of only 750 m. Beyond this point, a sharp and immediate degradation occurs due to the size of fog droplets being comparable to the operating laser wavelength, which triggers intense Mie scattering.

This severe atmospheric attenuation forces the Q-factor to intersect the HD-FEC threshold at approximately 1050 m, while the BER exceeds the SD-FEC limit at 1150 m. These findings confirm that light fog reduces the effective communication range by over 85% compared to the clear-weather baseline. Consequently, high-speed FSO links under fog conditions are strictly range-limited, necessitating the integration of hybrid topologies or advanced amplification techniques to maintain service availability.

- **Dust storm scenario**

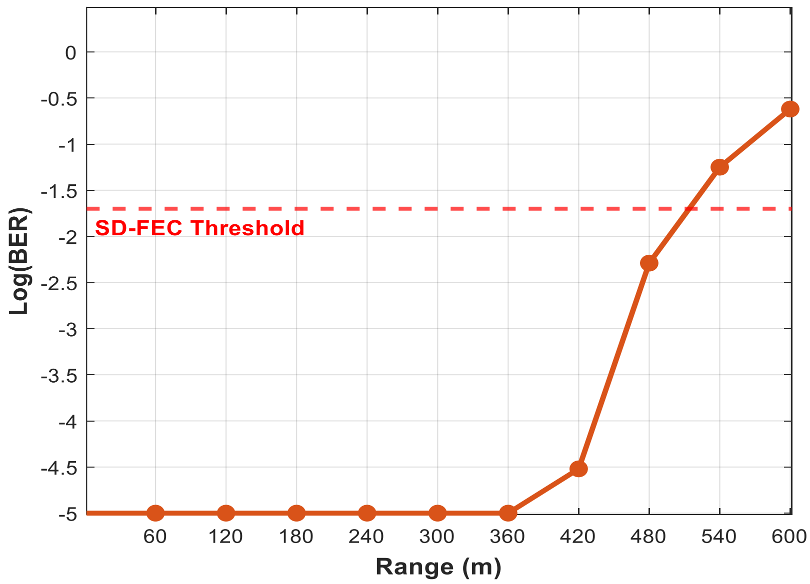

Figure 3.16: *Log (BER) vs. Distance for Dust storm scenario.*

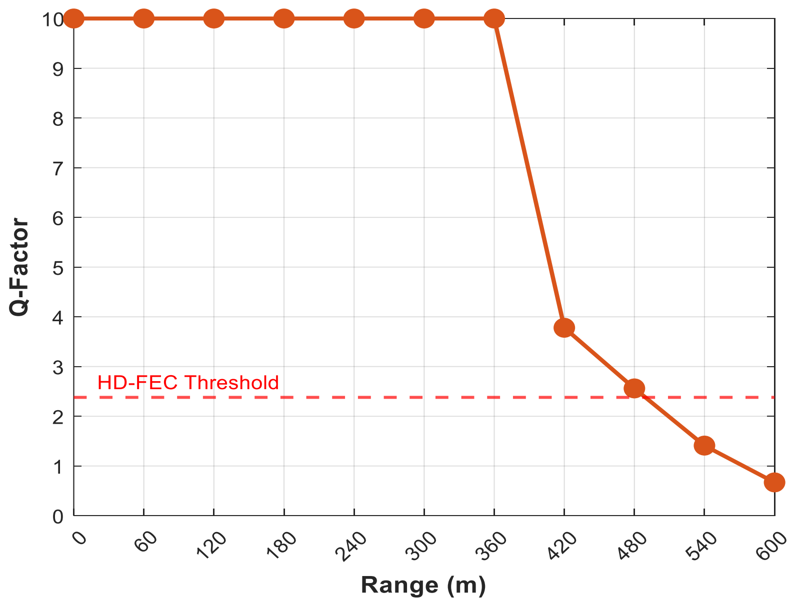

Figure 3.17: *Q-Factor vs. Distance for Dust storm scenario.*

The simulation results depicted in Figures 3.16 and 3.17 illustrate the performance of the system under a dust storm scenario. The outcomes indicate that this specific environment represents the most critical and detrimental condition for the optical link among all studied cases, characterized by a severe atmospheric attenuation coefficient of 52 dB/km. The system maintains stable signal integrity ($Q > 10$) over a highly restricted range of only 360 m, followed by a sharp degradation in performance due to the extreme density of suspended dust particles, which induces total scattering and severe absorption of the optical beam.

This intense atmospheric attenuation forces the Q-factor to intersect the HD-FEC threshold at a distance of 480 m, while the BER exceeds the SD-FEC limit at approximately 520 m. These findings confirm that dust storms pose the ultimate physical barrier to high-capacity FSO links, reducing the effective communication range by more than 93% compared to clear-weather operation. Consequently, high-speed optical wireless transmission under such severe conditions is impractical for extended distances without deploying hybrid topologies, such as a combined FSO/RF system, to ensure absolute service continuity.

➢ **Severe Dust Storm scenario**

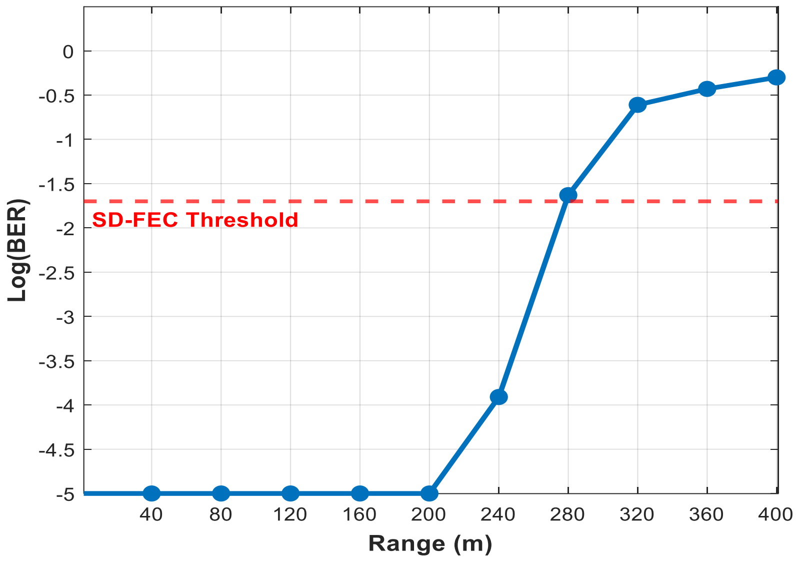

Figure 3.18: *Log (BER) vs. Distance for Severe Dust Storm scenario*

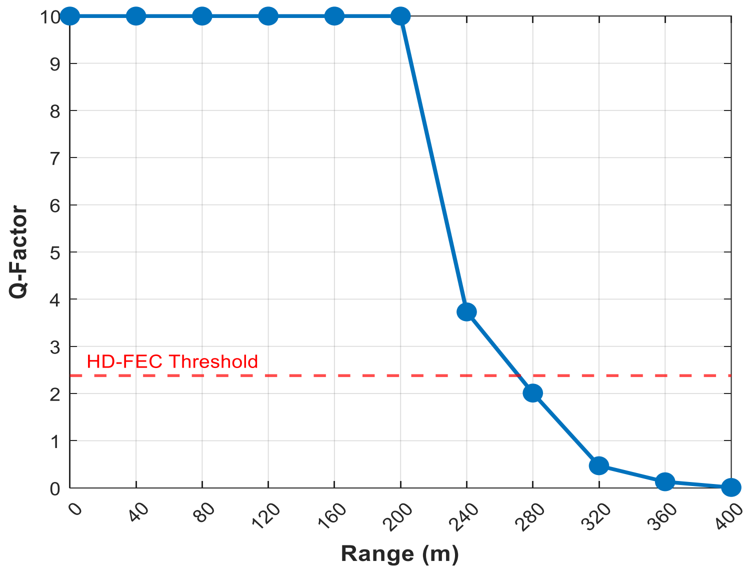

Figure 3.19: *Q-Factor vs. Distance for Severe Dust Storm scenario.*

The simulation results depicted in Figures 3.18 and 3.19 show the performance of the 112 Gbps DP-16QAM FSO system under a severe dust storm scenario. The data reveals a complete breakdown in the optical link performance at extremely short propagation distances, driven by a catastrophic atmospheric attenuation coefficient of 110 dB/km. The system maintains stable signal integrity maintained for only 200 m. This is followed by a sharp degradation in link characteristics due to the extreme density of suspended dust particles, forcing the Q-factor to intersect the HD-FEC threshold at approximately 270 m. These findings confirm that severe dust storms reduce the effective system range by over 96% compared to the clear-weather baseline, making standalone FSO architectures technically impractical.

To mitigate these physical limitations, implementing advanced engineering solutions is essential, such as MIMO techniques to counteract scattering-induced fading, or deploying a hybrid FSO/RF topology. By dynamically switching traffic to RF channels which are significantly less susceptible to dust attenuation during optical link degradation service continuity and link availability can be guaranteed even under the harshest desert climatic fluctuations.

Quantitative analysis of the data compiled in *Table III.3* reveals a systematic, non-linear correlation between the atmospheric attenuation coefficient and the operational boundaries of the proposed 112 Gbps DP-16QAM FSO system across the diverse climatic conditions of the El Oued region.

Table 3.3*: Performance Comparison of 112 Gbps DP-16QAM FSO Link Under Various Atmospheric Conditions.*

Atmospheric Scenario	Attenuation Coefficient (dB/km)	Stable Range (Q>10) (m)	HD-FEC Threshold Intersection (m)	SD-FEC Limit Intersection (m)	Range Reduction vs. Baseline (%)
Clear Weather	0.5	4000	~7000	~8000	Baseline (0%)
Light Rain	4.0	2100	~2800	~ 3000	47.5%
Dust Haze	5.0	1800	~2500	~2700	55.0%
Heavy Rain	9.5	1200	~1700	~1800	70.0%
Light Fog	18.3	750	~1050	~1150	81.25%
Dust Storm	52.0	360	~480	~520	91.0%
Severe Dust Storm	110.0	200	~270	~280	95.0%

3.4.2. Constellation diagram performance

Table 3.4: *Constellation diagrams at different weather conditions.*

Constellation diagram	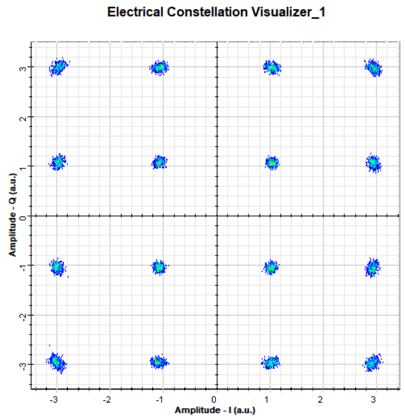 (a)	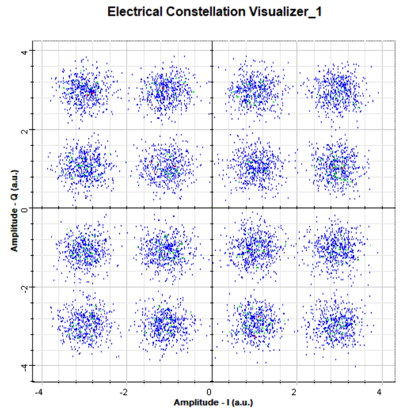 (b)	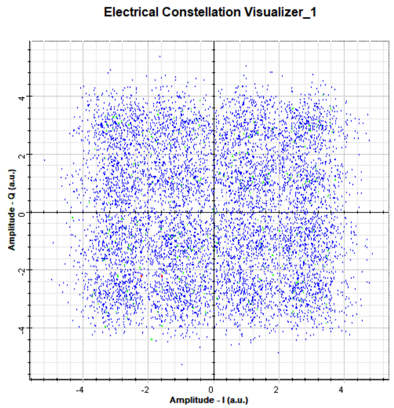 (c)
Weather conditions	**Range**	**Range**	**Range**
Clear scenario	1 km	4 km	8 km
Light Rain scenario	300 m	2.1 km	3 km
Dust Haze scenario	300 m	1.8 km	3 km
Heavy Rain scenario	200 m	1.2 km	2 km
Light Fog scenario	150 m	750 m	1500 m
Dust storm scenario	60 m	360 m	600 m
Severe Dust Storm scenario	40 m	200 m	400 m

The analysis reveals that the performance of the advanced FSO wireless communication system, which utilizes DP-16QAM modulation to transmit an ultra-high data capacity of 112 Gbps, is intrinsically linked to the level of attenuation and scattering caused by suspended particles in the atmosphere a behavior accurately reflected across the three constellation diagrams.

In the clear-weather scenario, the optical beam experiences minimal attenuation, resulting solely from geometric divergence and minor thermal scintillation, which allows the system to maintain an ideal signal with sharp, completely isolated symbol clusters, as shown in (Diagram (a)) at a propagation distance of 1 km. It continues to deliver an engineered acceptable performance with distinct points, as shown in (Diagram (b)), up to a distance of 4 km at a critical quality threshold of 2.38, where FEC algorithms are fully relied upon to recover the degradation of the high-speed digital signal, before the link completely breaks down into a state of total randomness, as shown in (Diagram (c)), at a distance of 8 km due to the severe degradation of the optical signal-to-noise ratio.

As meteorological conditions vary and water molecules or solid particles enter the link path, the operational ranges contract progressively. The light rain and dust haze scenarios exhibit closely matched effects, reducing the acceptable distance (Diagram (b)) to approximately 2.1 km and 1.8 km, respectively, since attenuation in these regimes depends on moderately intense geometric and Mie scattering mechanisms. This degradation accelerates under the Heavy Rain scenario, pulling the acceptable distance back to 1.2 km due to the high density of droplets absorbing and scattering the energy of the photons carrying the ultra-high digital traffic.

Critical impairments reach their peak when transitioning to the light fog scenario, which stands as a primary adversary for such optical systems due to resonant Mie scattering; here, the diameters of the fog droplets are strictly comparable to the operating laser wavelength (1550 nm), leading to a sharp drop in the acceptable distance to just 750 m. Finally, the dust storm and severe dust storm scenarios record the harshest performance of all, where the massive mass concentration of solid particles inflicts near-total blockage and severe absorption of the optical beam alongside deep fading. This causes the safe distance for (Diagram B) to shrink to 360 m, and then to a mere 200 m under severe conditions, with the system completely collapsing into total randomness (Diagram (c)) at a distance of 400 m.

This scientifically proves that dense dust storms and fog induce a reduction in the transmission efficiency and coverage of the optical link exceeding 95% compared to clear weather a physical limitation that structurally demands the implementation of spatial diversity techniques, such as MIMO architectures, to ensure service continuity at such massive capacities.

3.4.3.Eye diagram

Table 3.5: *Eye diagram degradation for different FSO weather conditions.*

Eye diagram	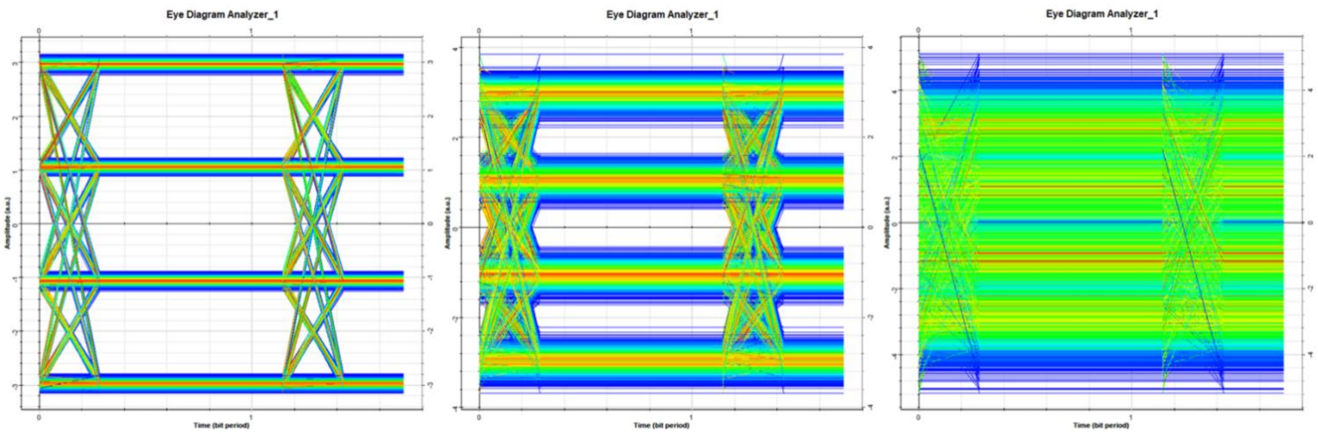 (a)	(b)	(c)
Weather conditions	**Range**	**Range**	**Range**
Clear scenario	**1 km**	**4 km**	**8 km**
Light Rain scenario	**300 m**	**2.1 k m**	**3 km**
Dust Haze scenario	**300 m**	**1.8 km**	**3 km**
Heavy Rain scenario	**200 m**	**1.2 km**	**2 km**
Light Fog scenario	**150 m**	**750 m**	**1500 m**
Dust storm scenario	**60 m**	**360 m**	**600 m**
Severe Dust Storm scenario	**40 m**	**200 m**	**400 m**

The analysis of the eye diagram shows that the performance of the FSO system is strictly governed by the level of inter-symbol interference and atmospheric noise, both of which directly determine the opening dimensions of the three parallel eyes.

In the clear-weather scenario, the optical beam encounters minimal attenuation, maintaining wide and optimum eye openings, as shown in (Diagram (a)) at a propagation distance of 1 km. The link continues to operate with an engineered acceptable partial eye closure, as shown in (Diagram (b)), up to 4 km where the system reaches its critical quality thresholds. At this range, the signal approaches the HD-FEC limit and fully relies on the ultimate SD-FEC limit to overcome high-speed signal degradation, before the eyes completely close into total randomness, as shown in (Diagram (c)) at a distance of 8 km, causing a total service outage.

As atmospheric conditions fluctuate, these eye openings contract progressively. The light rain and dust haze scenarios exhibit closely matched effects, reducing the acceptable eye distance (Diagram (b)) to 2.1 km and 1.8 km, respectively, due to moderate geometric and Mie scattering mechanisms, while this closure accelerates under heavy rain, pulling the distance back to 1.2 km. critical degradation reaches its peak during the light fog scenario, which severely suffocates the link and closes the eye openings at just 750 m due to resonant Mie Scattering, as the fog droplets closely match the operating laser wavelength (1550 nm).

Ultimately, the severe dust storm scenario records the harshest performance, where the massive mass concentration of dust induces near-total beam blockage and rapid fading, shrinking the safe eye margin (Diagram (b)) to a mere 200 m, with the link completely collapsing (Diagram (c)) at 400 m. This scientifically demonstrates that fog and dense dust storms reduce the link's penetration efficiency by more than 95% compared to clear weather a physical limitation that structurally demands the implementation of spatial diversity techniques, as MIMO method, to maintain stable eye openings and ensure service continuity under massive transmission capacities.

3.4.4 Signal Spectrum

Table 3.6: *Signal Spectrum degradation table for different FSO weather conditions.*

<table>
<tr><td>Signal Spectrum</td><td>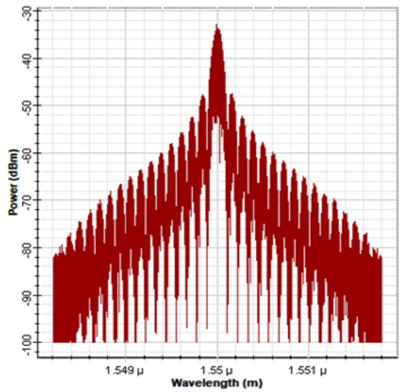

A</td><td>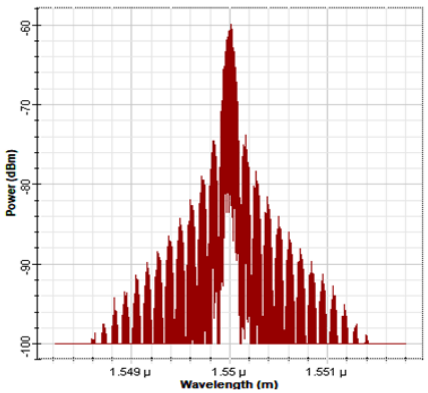

B</td><td>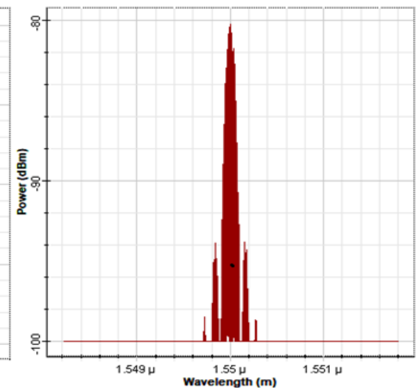

C</td></tr>
<tr><td>Weather conditions</td><td>Range</td><td>Range</td><td>Range</td></tr>
<tr><td>Clear scenario</td><td>1 km</td><td>4 km</td><td>8 km</td></tr>
<tr><td>Light Rain scenario</td><td>300 m</td><td>2.1 k m</td><td>3 km</td></tr>
<tr><td>Dust Haze scenario</td><td>300 m</td><td>1.8 km</td><td>3 km</td></tr>
<tr><td>Heavy Rain scenario</td><td>200 m</td><td>1.2 km</td><td>2 km</td></tr>
<tr><td>Light Fog scenario</td><td>150 m</td><td>750 m</td><td>1500 m</td></tr>
<tr><td>Dust storm scenario</td><td>60 m</td><td>360 m</td><td>600 m</td></tr>
<tr><td>Severe Dust Storm scenario</td><td>40 m</td><td>200 m</td><td>400 m</td></tr>
</table>

The analysis of the optical signal spectrum reveals how the high-speed data-bearing laser beam battles atmospheric impairments across varying propagation distances and volatile weather conditions. The transmission profile begins with (Spectrum A), where the signal demonstrates its peak performance characterized by a broad, fully resolved coherent modulated spectrum reaching a towering peak power of -30 dBm. This optimal behavior is observed in scenarios where the optical path introduces minimal attenuation, such as traveling through a clear atmosphere at 1 km. Crucially, the system maintains this robust spectral profile even when cutting through the most hostile environments like severe dust storms or dense fog, provided the transmission ranges are highly restricted (between 40 m and 300 m), leaving the suspended particulates insufficient interaction length to scatter or absorb the photons' energy.

However, as the propagation distance extends or meteorological impairments intensify, cumulative atmospheric factors continuously deplete the optical power margin, a phenomenon clearly reflected in (Spectrum B). In this intermediate regime, a severe attenuation of the optical carrier is observed, forcing the peak power down to approximately -60 dBm. This overall power drop causes the weaker, high-frequency modulation sidebands to systematically fade away as they sink beneath the receiver's noise floor due to continuous scattering mechanisms.

Ultimately, the signal's journey reaches its physical boundary in (Spectrum C), where the optical link undergoes extreme spectral degradation. In this critical state, the distinctive multi-carrier sideband features completely vanish, leaving nothing but a frail, narrow optical spike whose peak power plunges toward -80 dBm. This fragile scenario represents the absolute operational limit of the FSO link corresponding to 8 km in clear weather or a meager 400 m under the catastrophic attenuation of severe dust storms. It serves as a definitive engineering baseline proving that the system has entirely exhausted its power margin, rendering the channel highly vulnerable to total service outage without the deployment of space-diversity MIMO configurations or hybrid FSO/RF topologies

3.5 MIMO Performance

3.5.1 System design

Performance evaluation and comparative analysis between different transmission systems are essential steps in identifying the optimal architecture capable of meeting the stringent requirements of modern networks, particularly given the challenges posed by hostile desert environments. In this context, this study focuses on conducting a comprehensive comparison between the conventional SISO-FSO communication system and the 4 x 4 MIMO configuration, while maintaining a 112 Gbps total transmission capacity for both systems.

This comparison aims to highlight the fundamental role of spatial diversity in enhancing the reliability of the optical link, where the 112 Gbps data flow is transmitted through four parallel, spatially separated physical paths. This spatial distribution serves as a robust statistical mitigation technique that counteracts the impact of deep signal fading caused by severe dust storms and intense atmospheric turbulence modeled by the Gamma-Gamma distribution. Through the analysis of key quality metrics, specifically the bit error rate and the Q-Factor, we seek to demonstrate the operational limits of each system and the extent to which the MIMO architecture can ensure service continuity under the high-attenuation conditions characteristic of the El Oued region.

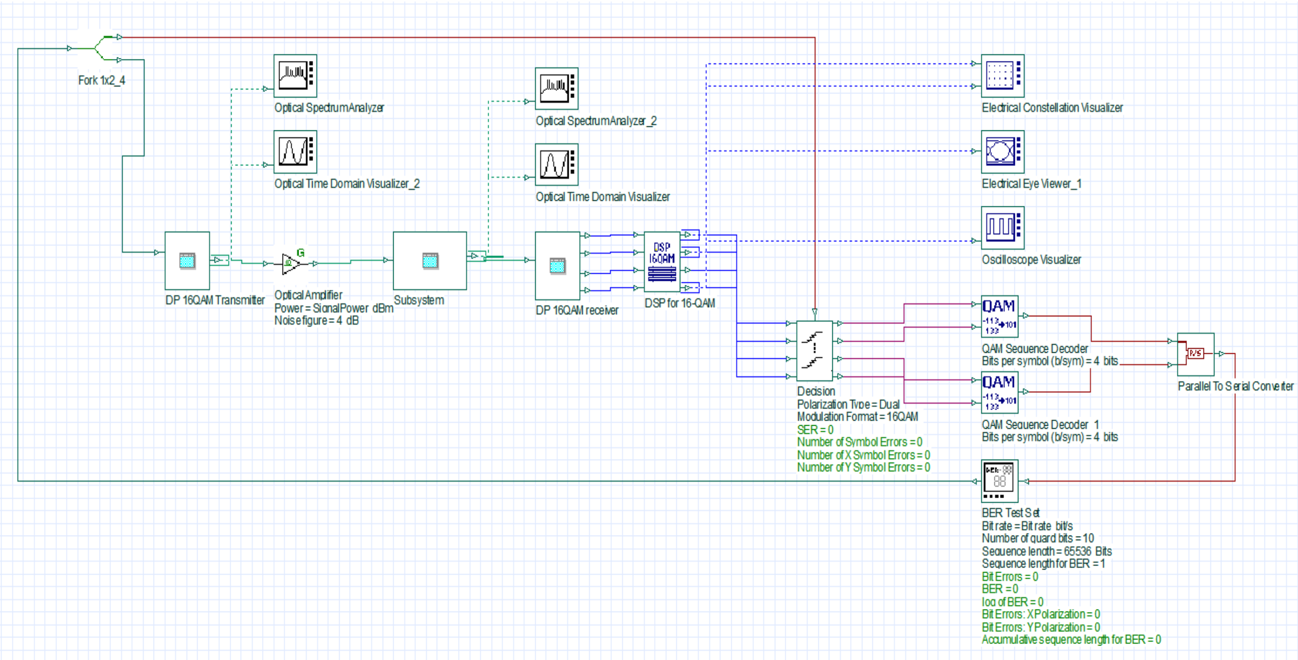

Figure 3.20: *FSO MIMO 4x4 DP-16-QAM Modulation System.*

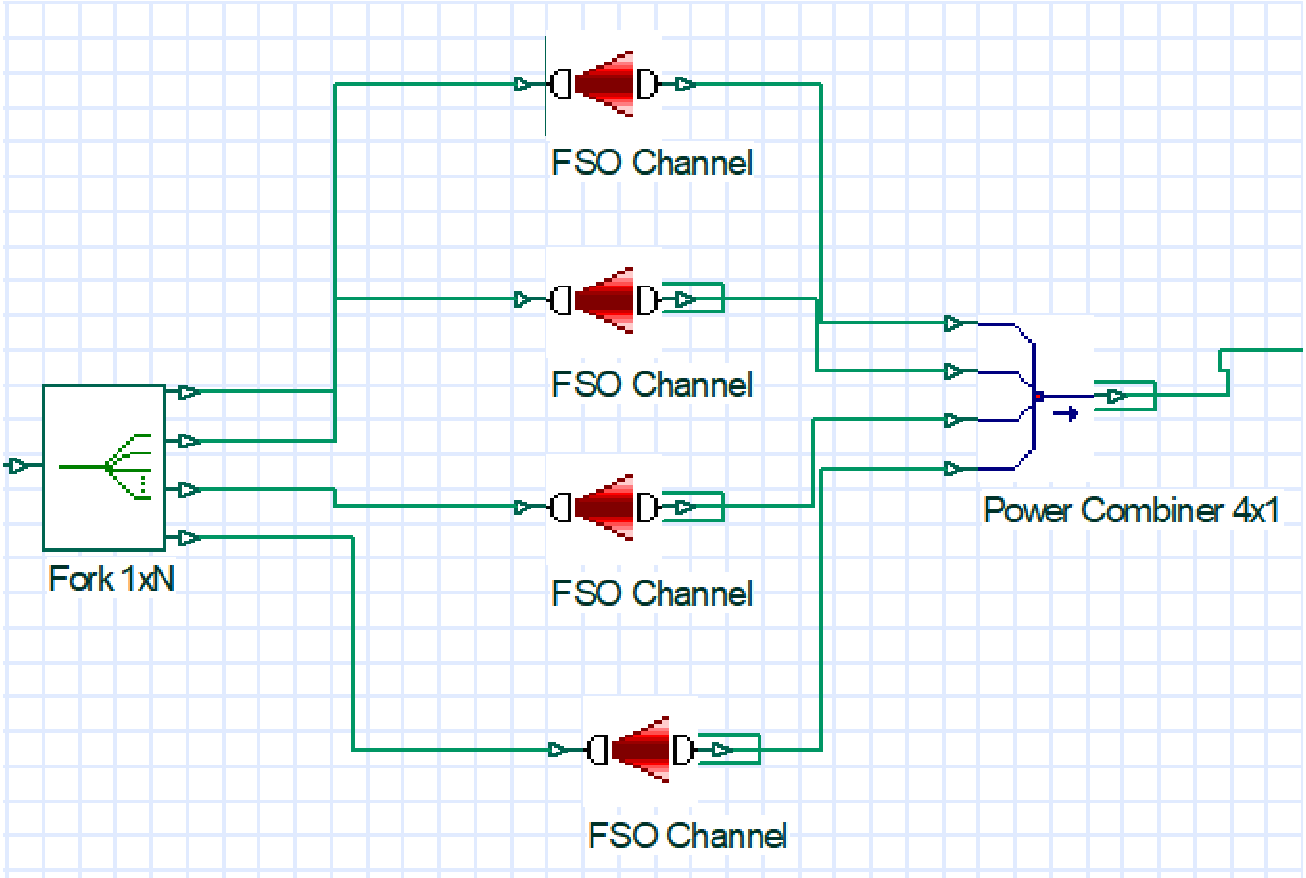

Figure 3.21: *Block diagram of the 4x4 MIMO FSO channel configuration*

This schematic illustrates the architectural design of an high-speed FSO communication system, leveraging a 4x4 MIMO configuration integrated with DP-16QAM modulation to achieve an aggregate data capacity of 112 Gbps. Operating under a spatial diversity framework to combat harsh desert conditions, the system transmits the 112 Gbps data flow simultaneously through four parallel, spatially separated physical paths. At the transmitter stage, each optical path utilizes dual-polarization technology to modulate both the amplitude and phase of the carrier signal using the 16-QAM format. These four redundant beams propagate through the free-space optical channel, modeled by a custom Subsystem unit that simulates severe environmental impairments such as heavy dust storm attenuation and atmospheric scintillation.

At the receiver side, a coherent optical receiver and an advanced digital signal processing unit work to aggregate the signals, dynamically compensating for polarization crosstalk and environmental noise while mitigating power loss during peak atmospheric disturbances. Finally, the system incorporates precise performance monitoring tools, including a BER Analyzer and an Electrical Constellation Visualizer, to validate the resilience and high reliability of this MIMO FSO topology against meteorological fluctuations in next-generation networks.

3.5.2 Comparative Performance Analysis

3.5.2.1 Clear scenario (0.5 dB/km)

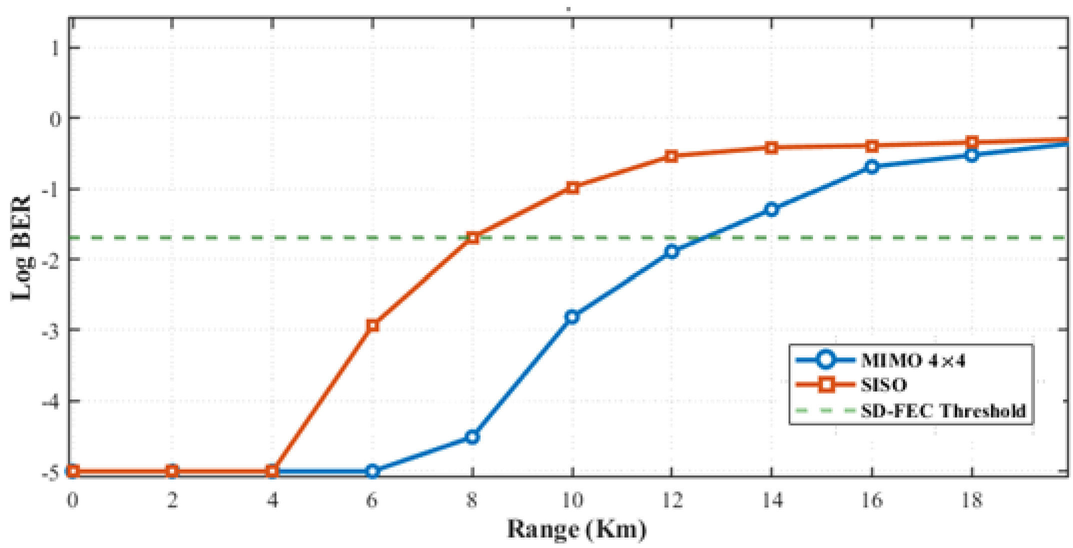

Figure 3.22: *Log (BER) vs. Distance for Clear scenario.*

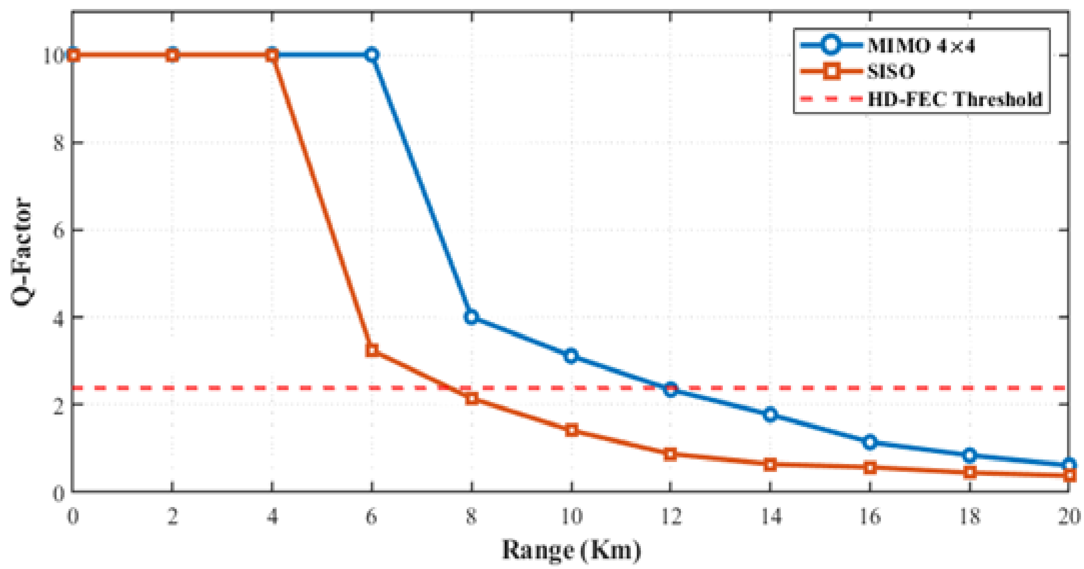

Figure 3.23: *Q-Factor vs. Distance for Clear scenario.*

The simulation results the qualitative superiority of the 4x4 MIMO architecture compared to the conventional SISO system under clear sky conditions (0.5 dB/km), where low atmospheric attenuation allows for significant kilometer-scale communication reaches for the 112 Gbps system based on DP-16QAM technology. By analyzing the BER curves, it is observed that the SISO system begins to experience performance degradation after a propagation distance of 4 km and officially exceeds the SD-FEC threshold at approximately 8 km. In contrast, the MIMO configuration, utilizing spatial diversity, succeeds in maintaining total signal stability up to 6 km and does not cross this forward error correction threshold until approximately 12.5 km, yielding a substantial range extension of 4.5 km.

This performance disparity is further reinforced by the corresponding Q-Factor analysis. The SISO system falls below the critical reference threshold at a distance of 7.5 km, while the 4x4 MIMO system exhibits enhanced structural resilience, remaining operationally viable up to 12 km.

These graphical findings prove that even under optimal meteorological conditions, geometric path loss and distance-related power dissipation remain key limiting constraints for ultra-high-speed optical links.

3.5.2.2 Light Rain scenario (4 dB/km)

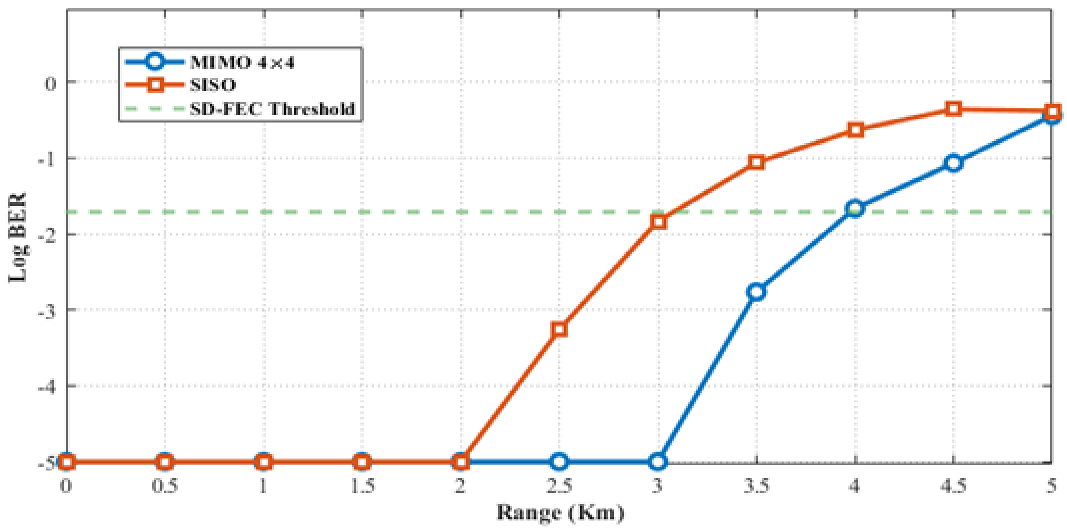

Figure 3.24: *Log (BER) vs. Distance for Light Rain scenario.*

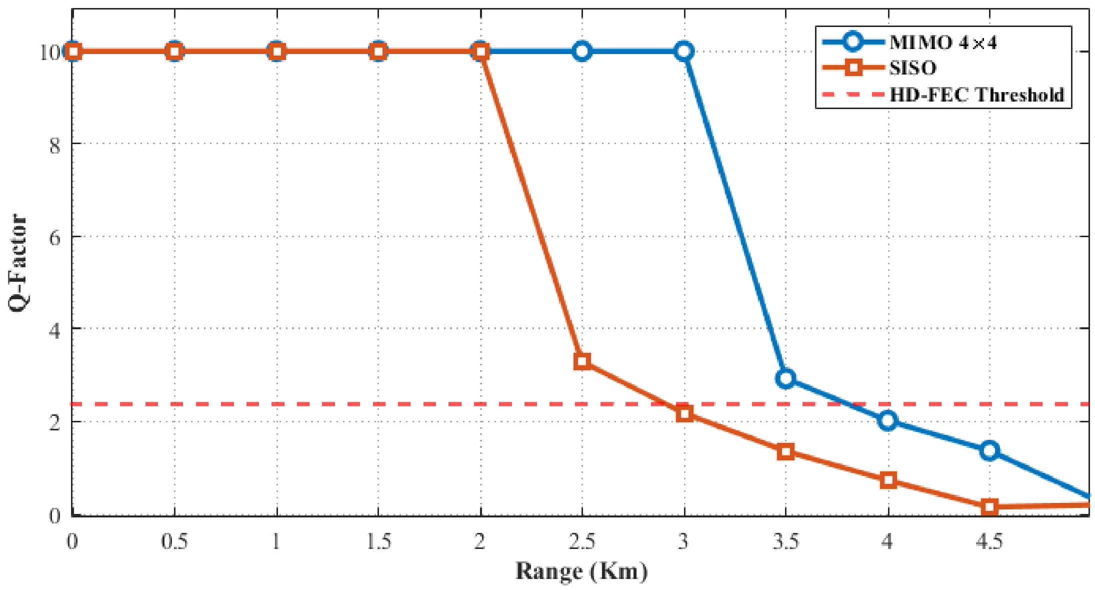

Figure 3.25: *Q-Factor vs. Distance for Light Rain scenario.*

The simulation results obtained under light rain conditions (4 dB/km) hold particular significance when applied to a desert environment, where rainfall represents a critical meteorological event that interacts with the region's suspended sandy particles.

By evaluating the BER curves in Figure 3.24, it is evident that the conventional SISO system experiences rapid performance collapse, crossing the critical SD-FEC threshold at a propagation distance of only 3 km. Conversely, the 4x4 MIMO topology, leveraging spatial diversity, succeeds in extending the link's viability up to approximately 4.1 km, offering a vital coverage extension under localized attenuation.

This superiority is further validated by the Q-Factor performance shown in Figure 3.25. The SISO link drops below the reference threshold at a distance of 2.8 km, whereas the resilient MIMO architecture maintains an acceptable Q-factor up to 3.8 km. From a physical perspective, raindrops interacting with airborne dust in arid regions heavily exacerbate Mie scattering and severe optical signal attenuation. However, by distributing the DP-16QAM signal across four independent physical channels, the spatial diversity framework averages out the uncorrelated fading fluctuations. This significantly reduces the probability of catastrophic burst errors, ensuring robust connection stability and high throughput even during abrupt atmospheric transitions that deviate from clear-sky baselines.

3.5.2.3 Light Fog scenario (18.3 dB/km)

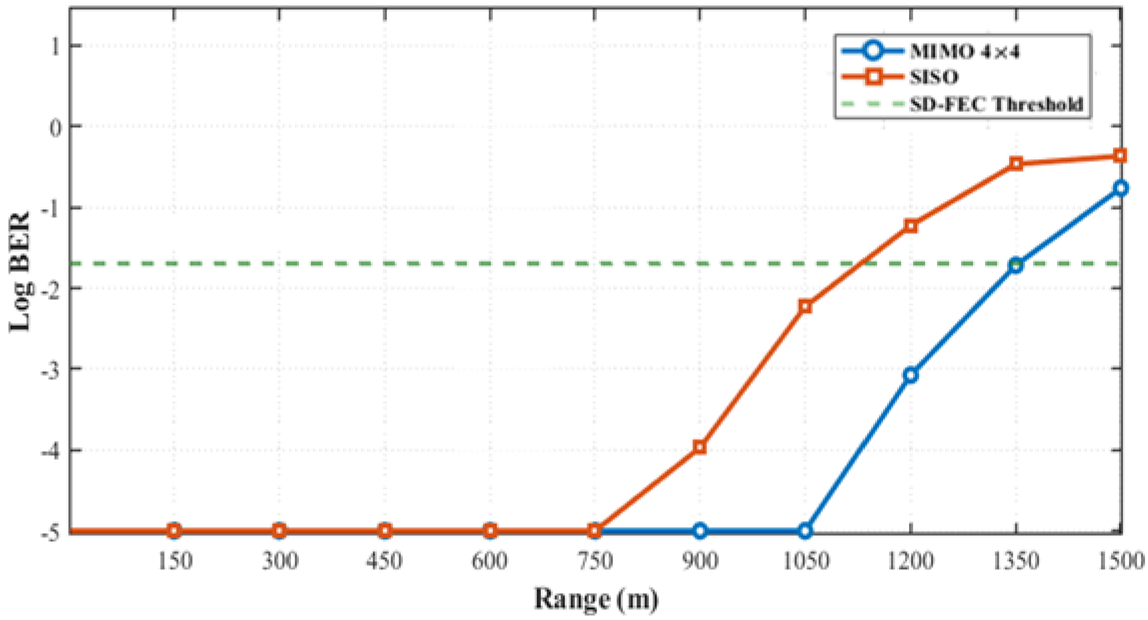

Figure 3.26: *Log (BER) vs. Distance Light Fog scenario*

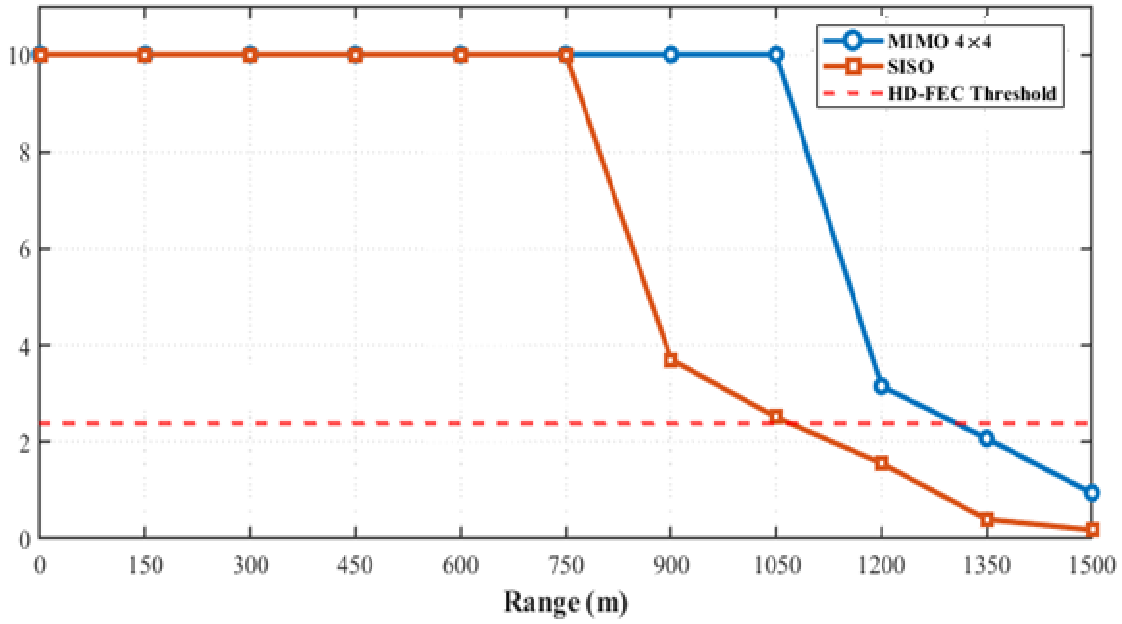

Figure 3.27: *Q-Factor vs. Distance for Light Fog scenario.*

The simulation results reveal a critical contraction in the FSO system's operational reach as the atmospheric attenuation coefficient escalates to 18.3 dB/km, characterizing light fog conditions that induce severe optical beam scattering.

Observing the BER curves in Figure 3.26, the conventional SISO system experiences an abrupt performance collapse, exceeding the critical SD-FEC threshold at a propagation distance of only 1150 m. Conversely, the 4x4 MIMO configuration proves exceptionally efficient under these restricted visibility conditions, successfully leveraging spatial diversity to delay signal failure up to exactly 1350 m, which yields a critical 250 m link margin extension.

This performance disparity is further verified by the corresponding Q-Factor analysis presented in Figure 3.27. The SISO link falls below the reference threshold at approximately 1050 m, whereas the resilient 4x4 MIMO topology remains operationally viable up to 1300 meters.

Scientifically, fog particles whose dimensions are highly comparable to the optical transmission wavelength (1550 nm) exert intense Mie scattering that severely dissipates optical power. Under such harsh conditions, deploying multiple physical paths via a MIMO framework becomes an indispensable necessity.

3.5.2.4 Severe Dust Storm scenario (110 dB/km)

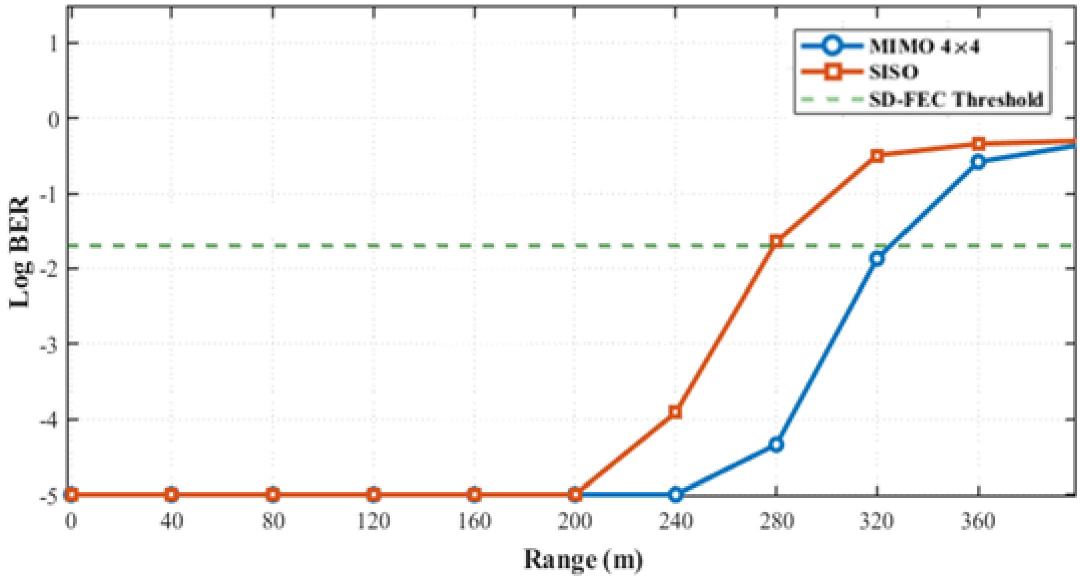

Figure 3.28: *Log (BER) vs. Distance for Severe Dust Storm scenario.*

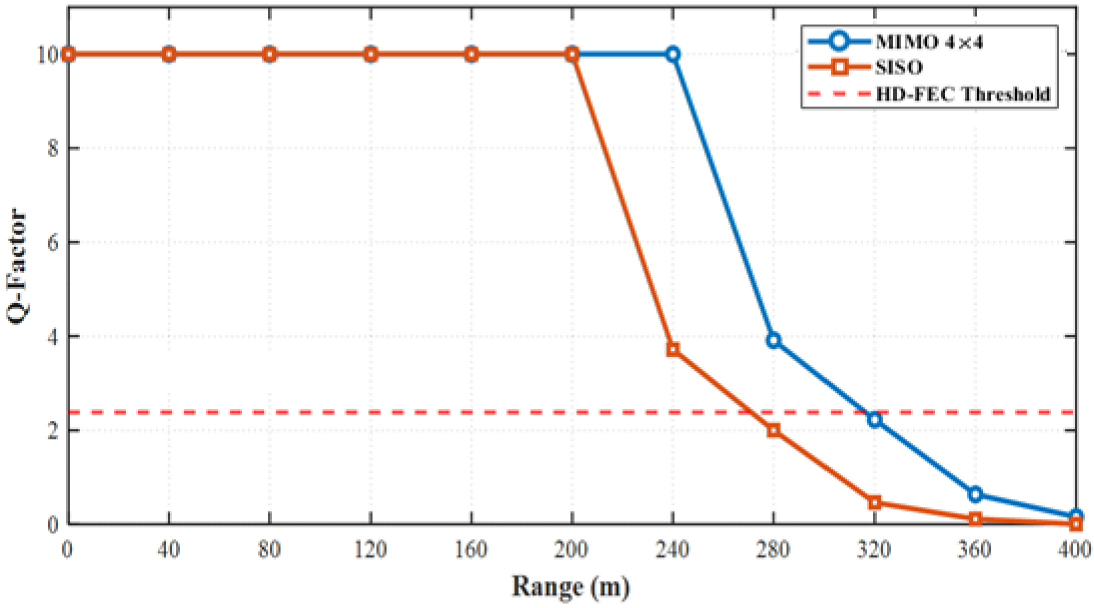

Figure 3.29: *Q-Factor vs. Distance for Severe Dust Storm scenario.*

The simulation results highlight a dramatic collapse in the FSO system's operational range when exposed to a severe dust storm (110 dB/km), where the communication distance shrinks to be measured in only tens of meters. By analyzing the BER curve, we find that the SISO system loses its ability to correct errors and exceeds the SD-FEC threshold at a critical distance estimated at 280 m. In contrast, the 4x4 MIMO system demonstrates a notable superior capability despite the atmospheric harshness, successfully delaying the reach of this threshold up to 320 m through the use of Spatial Diversity. This conclusion is further reinforced by the Q-Factor analysis, where the SISO system falls below the confidence threshold at a distance of 275 m, while the MIMO system maintains an acceptable signal quality up to 315 m.

These results prove that in a desert environment suffering from dense dust storms, dust particles cause a near-total blockage of the optical path. This makes MIMO technology an extreme technical necessity to provide a few dozen extra meters that could be decisive in ensuring a minimum level of high-speed digital connectivity and preventing total service disruption.

Table 3. 7: *Comparison of the range of SISO and 4x4 MIMO systems under different FSO conditions*

Atmospheric Scenario	Attenuation Coefficient	Maximum Range (SISO)	Maximum Range (4×4 MIMO)	Range Improvement (%)
Clear Scenario	0.5 dB/km	~ 8 km	~ 12.5 km	56.25
Light Rain	4 dB/km	~ 3 km	~ 4 km	33.33
Light Fog	18.3 dB/km	~ 1150 m	~ 1350 m	17.39
Severe Dust Storm	110 dB/km	~ 280 m	~ 320 m	14.29

The table provides a comparative study and a quantitative measure demonstrating the superiority of the 4 x 4 MIMO system over the SISO configuration in Free Space Optics (FSO) links under various climatic conditions. The data clearly indicates a sharp inverse relationship between the atmospheric attenuation coefficient and the maximum link range. While the transmission reach extends up to 12.5 km in clear weather achieving a significant performance leap with a range improvement of +56.25 % it severely contracts to just a few hundred meters (320 m) during severe dust storms due to the intense signal scattering caused by dense dust particles. Although the percentage of range improvement gradually declines as weather conditions worsen, reaching +14.29 % at the highest attenuation level (110 dB/km), the MIMO technology remains engineeringly critical to ensure link availability, providing a vital diversity gain that maintains connection reliability in harsh desert environments

3.5.2.5 Constellation diagram

Table 3.8: *Constellation diagram comparison under various FSO weather conditions and ranges*

Constellation diagram	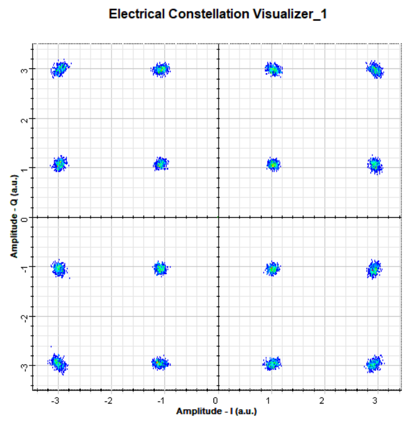 A		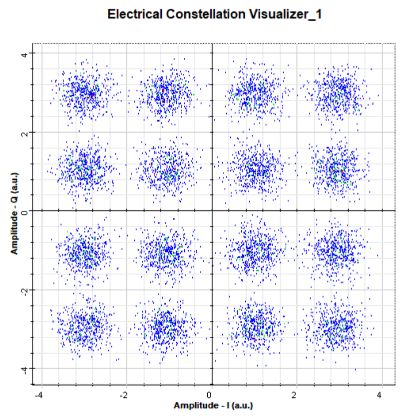 B		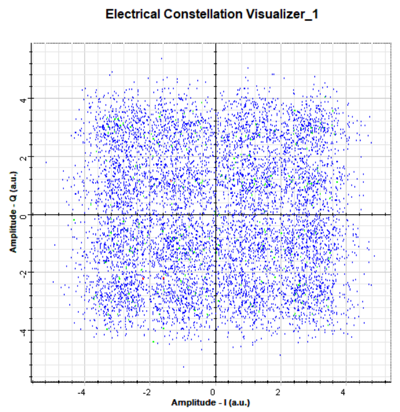 C	
Weather conditions	**SISO**	**MIMO**	**SISO**	**MIMO**	**SISO**	**MIMO**
Clear scenario	**1 km**	**1 km**	**8 km**	**12 km**	**16 km**	**18 km**
Light Rain scenario	**1 km**	**1km**	**3 km**	**4 km**	**5 km**	**5 km**
Light Fog scenario	**150 m**	**150 m**	**1000 m**	**1300 m**	**1500 m**	**1500 m**
Severe Dust Storm scenario	**40 m**	**40 m**	**280 m**	**320**	**400 m**	**400 m**

Based on our analysis of the constellation diagrams and the numerical data provided in the table, the performance of the DP-16QAM system across different weather scenarios can be summarized as follows: Clear skies represent the ideal environment, providing unique spectral stability that enables the MIMO system to achieve a maximum operational range of 18 km, outperforming the SISO system which stops at 16 km before complete signal degradation. Meanwhile, light rain exerts a limited and uniform attenuation effect, dropping the maximum distance for both systems to 5 km without causing severe disruption to the phase angles.

On the other hand, light fog acts as a critical physical barrier, shrinking the ideal transmission range to just 150 m and causing the constellation to reach its threshold of random interference and fading at 1500 m due to severe scattering from microscopic water droplets that match the optical wavelength. Finally, severe dust storms present the harshest environmental scenario for the optical link in desert regions; the dense absorption and path obstruction caused by airborne dust particles trigger a total collapse of cross-polarization isolation and severe signal fading, accelerating the transformation of the constellation into an undecidable block of random noise at a highly critical distance of just 400 m for both systems.

3.5.3 Eye diagram

Table 3.9: *Eye diagram comparison under various FSO weather conditions and ranges*

Eye diagram	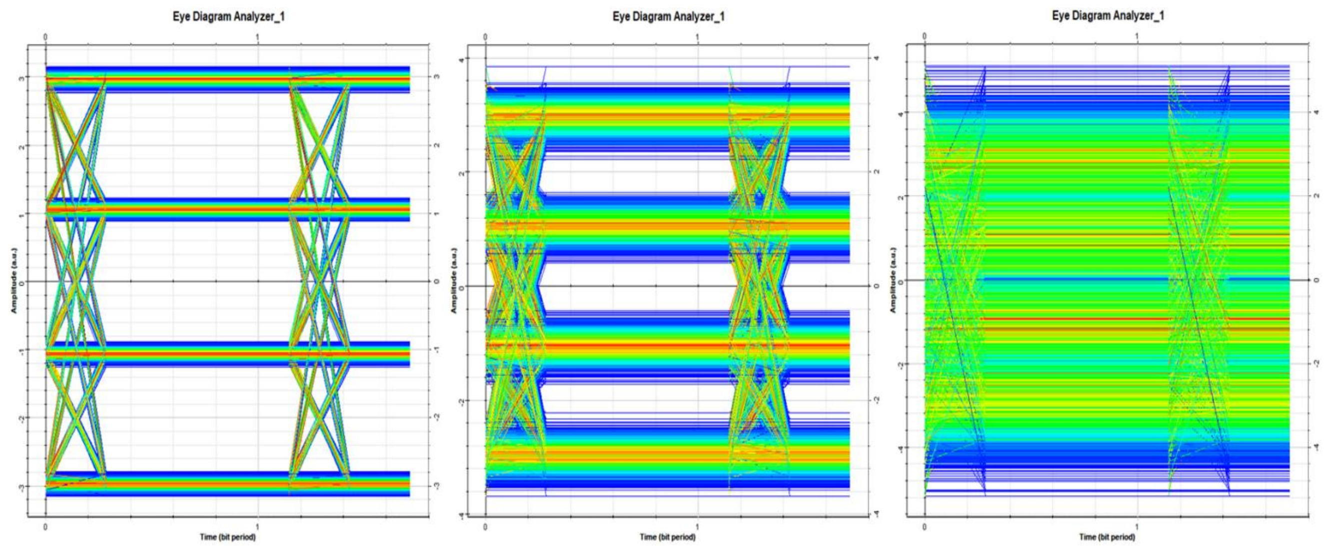 (a)		(b)		(c)	
Weather conditions	**SISO**	**MIMO**	**SISO**	**MIMO**	**SISO**	**MIMO**
Clear scenario	**1 km**	**1 km**	**8 km**	**12 km**	**16 km**	**18 km**
Light Rain scenario	**1 km**	**1km**	**3 km**	**4 km**	**5 km**	**5 km**
Light Fog scenario	**150 m**	**150 m**	**1000 m**	**1300 m**	**1500 m**	**1500 m**
Severe Dust Storm scenario	**40 m**	**40 m**	**280 m**	**320**	**400 m**	**400 m**

Based on our analysis of the eye diagrams of the DP-16QAM FSO system, the structural behavior of the digital pulses across the three stages can be clearly evaluated when projected onto the adopted FEC thresholds, where the first represents the HD-FEC limit for Q Factor, and the second represents the SD-FEC limit for BER value.

In Stage (a), the three eye openings exhibit maximum vertical and horizontal width with an absolute absence of time jitter, resulting from the high efficiency of the DSP algorithms in isolating the four distinct amplitude levels (4-PAM mapping per polarization) at short transmission ranges (e.g., 1 km under clear skies or 40 m during severe dust storms); at this phase, the error rate remains within a highly secure margin and the quality factor significantly exceeds the baseline, guaranteeing completely error-free transmission.

As the link distance and atmospheric attenuation increase, the system transitions into Stage (b), where the pulse traces suffer from noticeable thickening and increased jitter, while the eye openings narrow vertically and horizontally as a direct physical manifestation of atmospheric scintillation fading. Nevertheless, the digital system metrics remain resilient and strictly confined within the fully correctable zone above the HD-FEC threshold. Here, the engineering superiority of the MIMO configuration over SISO becomes highly pronounced, as spatial diversity successfully stabilizes the eye opening and maintains its readability over longer distances (such as extending the operational range from 8 km to 12 km under clear skies).

Finally, in Stage (c), the signal structure undergoes total degradation, leading to complete eye closure of all three levels due to severe Inter-Symbol Interference and the complete failure of the receiver to decode the overlapping pulses under extreme path loss. This simultaneous violation entirely disables the error-correction capability of the system, forcing the high-capacity optical link into a total link outage a catastrophic breakdown that is rapidly accelerated to very short ranges under the harsh influence of light fog at 1500 m and severe dust storms at a critical boundary of just 400 m, where the heavy concentration of airborne particles induces severe scattering and path absorption that simultaneously destroy the pulse geometry and its optical power.

3.6 Conclusion

This thesis explores FSO communication as a strategic infrastructure solution for digital transformation in geographically unique regions, with a specific focus on the province of El Oued, Algeria. While FSO technology offers a high-capacity (up to 112 Gbps) and cost-effective alternative to traditional optical fiber cables, its operational reliability in arid desert environments is critically challenged by harsh climatic conditions.

The study identifies the complex meteorological profile of the El Oued region as a primary bottleneck for FSO deployment. This profile is characterized by intense thermal scintillation (exceeding 45°C), severe sandstorms (Sirocco winds), and aerosol complexity resulting from the interaction between airborne dust and agricultural moisture. These phenomena induce significant optical signal scattering, absorption, and phase instability factors that traditional propagation models often fail to address. To mitigate these limitations, this research proposes and evaluates a 4x4 MIMO architecture integrated with DP-16QAM modulation.

Through rigorous simulation across four distinct atmospheric scenarios clear sky, light rain, light fog, and severe dust storms. The study demonstrates that the MIMO spatial diversity architecture significantly mitigates channel fading and prevents premature signal failure. Performance metrics, evaluated against Bit Error Rate and Q-Factor thresholds relative to FEC limits, confirm that the proposed MIMO-FSO architecture maintains signal integrity where conventional SISO links fail. Notably, in extreme dust storm conditions (110 dB/km), the MIMO system provides a decisive link margin, effectively bridging the connectivity gap and ensuring service continuity.

These findings establish the MIMO-FSO architecture as a definitive engineering solution for resilient, high-speed communication in arid desert regions, providing a robust framework that accounts for the unique climatic variables of the Algerian Sahara.

General Conclusion

General Conclusion

In conclusion, this study confirms that free space optics technology represents a major milestone and a highly promising engineering solution for meeting the growing demand for high-capacity, broadband wireless communication networks in desert environments. This is particularly evident when deployed as an efficient, cost-effective alternative to traditional optical fiber cables in remote and topographically challenging areas. However, despite the massive advantages this system offers such as ultra-high data rates and robust physical security its operational deployment in arid, desert regions faces harsh climatic challenges that strictly limit its transmission range. Severe dust storms, extreme temperature spikes leading to intense thermal scintillation, and light fog scenarios act as aggressive physical barriers. These phenomena induce heavy optical attenuation and scattering, ultimately causing severe inter-symbol interference, degradation of signal quality, and the breakdown of polarization multiplexing isolation.

To mitigate these critical limitations, the strategic integration of multiple-input multiple-output technology proves to be an indispensable engineering solution. The results demonstrate that leveraging spatial diversity within MIMO-configured links significantly suppresses the adverse effects of atmospheric fading and prevents premature eye diagram closure. By introducing a substantial fade margin gain, the MIMO architecture effectively preserves the system's quality factor and bit error rate well within the correctable bounds of the critical forward error correction limits (HD-FEC / SD-FEC). Consequently, it is established that the advanced MIMO-FSO system using high-order modulation schemes like DP-16QAM is not merely an optional upgrade, but rather one of the most viable and definitive solutions to guarantee link availability, stability, and reliability for next-generation wireless infrastructures under extreme desert conditions.

Future Work

To expand upon the findings and contributions of this thesis, several promising directions for future research are recommended. First, investigating the integration of a hybrid FSO/RF framework could provide a robust fail-safe mechanism during severe dust storms or total optical path blockages. Second, incorporating machine learning-based Adaptive Modulation and Coding (AMC) techniques would allow the MIMO-FSO system to dynamically optimize data rates in real-time response to rapid desert turbulence variations. Finally, future efforts will focus on validating the simulated bit error rate (BER) and quality factor (Q-factor) performance through experimental hardware-in-the-loop (HIL) testing under controlled environments that mimic arid climatic conditions.

References

References

[1] A. K. Majumdar and J. C. Ricklin, Free-Space Laser Communications: Principles and Advances. Springer, 2015.

[2] H. Willebrand and B. S. Ghuman, Free Space Optics: Enabling Optical Connectivity in Today's Networks. Sams Publishing, 2002.

[3] L. C. Andrews and R. L. Phillips, Laser Beam Propagation through Random Media, 2nd ed. SPIE Press, 2005.

[4] Transparency Market Research, "Free Space Optics Market," [Online]. Available: https://www.transparencymarketresearch.com/free-space-optics-market.html. Accessed: Mar. 03, 2026.

[5] H. Kaushal, V. K. Jain, and S. Kar, Free Space Optical Communication. Springer India, 2017.

[6] A. K. Majumdar and J. C. Ricklin, Free-Space Laser Communications: Principles and Advances. Springer, 2015.

[7] H. Willebrand and B. S. Ghuman, Free Space Optics: Enabling Optical Connectivity in Today's Networks. Sams Publishing, 2002.

[8] A. K. Majumdar and J. C. Ricklin, Free-Space Laser Communications: Principles and Advances. Springer, 2015.

[9] W. Stallings, Data and Computer Communications, 10th ed. Pearson, 2013.

[10] G. Maral and M. Bousquet, Satellite Communications Systems, 5th ed. Wiley, 2009.

[11] T. S. Rappaport, Wireless Communications: Principles and Practice, 2nd ed. Prentice Hall, 2002.

[12] GeeksforGeeks, "Advantages and disadvantages of wireless communication," [Online]. Accessed: Feb. 26, 2026.

[13] M. Cao, H. Wang, Y. Yao, and S. Hou, "Performance Evaluation of FSO Communications under Sand Dust Conditions," International Journal of Antennas and Propagation, vol. 2019, Art. ID 2046896, 2019. DOI: 10.1155/2019/2046896.

[14] Brewminate, "Picturing a voice: Margaret Watts-Hughes and the Eidophone," [Online]. Available:https://brewminate.com/picturing-a-voice-margaret-watts-hughes-and-the-eidophone. Accessed: Mar. 10, 2026.

[15] H. Henniger and O. Wilfert, "An introduction to free-space optical communications," Journal of Radio Engineering, vol. 19, no. 2, pp. 203–212, 2010.

[16] A. Abisayo, "Optically amplified free-space optical communication systems," Jul. 2013.

[17] S. B. Alexander, Optical communication receiver design. Bellingham, WA: SPIE Optical Engineering Press, vol. TT22, 1997.

[18] R. Ramaswami and K. N. Sivarajan, Optical Networks – A Practical Perspective, 2nd ed. London: Academic Press, 2002.

[19] A. Aladeloba, "Optically Amplified Free-space Optical Communication Systems," Ph.D. dissertation, Dept. Elect. Electron. Eng., Univ. Nottingham, Nottingham, UK, 2013.

[20] ResearchGate, "FSO Backhaul Connectivity for Cellular Networks," [Online].

[21] H. Kaushal, V. K. Jain, and S. Kar, "Applications of FSO Communication Systems," in Free Space Optical Communication, Springer, 2017, pp. 34–37.

[22] V. Foucal, "Design of high-speed short-distance optical interconnections in free space. Prototyping of communication modules for embedded applications," Thesis.

[23] D. Killinger, "Free Space Optics For Laser Communication Through the Air," Optics & Photonics News, Optical Society of America, Oct. 2002.

[24] P. Tjondronegoro, "Free-Space Optics for Fixed Wireless Broadband," Thesis, Munich University of Technology, Dec. 2004.

[25] Y. Harichane and I. Benkraouda, "Étude et évaluation des performances d'un système de communication," Chlef: Université Hassiba Benbouali, 2019.

[26] F. Nadeem, V. Kvicera, M. S. Awan, E. Leitgeb, S. S. Muhammad, and G. Kandus, "Weather effects on hybrid FSO/RF communication link," IEEE Journal on Selected Areas in Communications, vol. 27, no. 9, pp. 1687–1697, 2009.

[27] A. G. Alkholidi and K. S. Altowij, Free space optical communications theory and practices. IntechOpen, Nov. 2014.

[28] M. Singh and S. Gupta, "Multi-level pseudo-random sequence generation for coherent optical transmission systems," Sep. 2014.

[29] N. Hadjadji, "Contribution à l'étude des techniques et dispositifs dédiés aux réseaux de télécommunications optiques reconfigurables," 2019.

[30] N. Hadjadji, "Contribution à l'étude des techniques et dispositifs dédiés aux réseaux de télécommunications optiques reconfigurables," Université des Sciences et de la Technologie d'Oran Mohamed Boudiaf (USTOMB), Oran, Algérie, Jul. 2021.

[31] M. H. A. Jahid, M. H. Alsharif, and T. J. Hall, "A contemporary survey on free space optical communication: potentials, technical challenges, recent advances, and research direction," Apr. 2022.

[32] A. Abisayo, "Optically amplified free-space optical communication systems," Jul. 2013.

[33] L. Chaudhary, S. Yadav, and R. Mathur, "Next generation free space optics system in wireless communication technology," International Journal of Advances in Electrical and Electronics Engineering, p. 255.

[34] H. Singh, R. Miglani, N. Mittal, S. Gupta, F. Tubbal, R. Raad, and E. M. Amhoud, "Designing an optimized free space optical (FSO) link for terrestrial commercial applications under turbulent channel conditions," Apr. 2023.

[35] H. Khalil, F. Qamar, R. Shahzadi, M. Ali, M. F. Nadeem, N. Qamar, and I. A. Sajjad, "FSO communication: Benefits, challenges, and its analysis in DWDM communication system," Sir Syed University Research Journal of Engineering and Technology, Apr. 2020.

[36] J. G. Chalil, S. Kadam, C. Joseph, K. J. Kulkarni, and A. A. B. Raj, "Characterization of Free-space Gaussian Beam Propagation and Recent Developments of FSO Communication Technology: A Review," Int. J. Eng. Res. Rev., vol. 12, no. 3, pp. 1–24, 2024.

[37] M. Born and E. Wolf, Principles of Optics, 7th ed. Cambridge, UK: Cambridge University Press, 1999.

[38] GeeksforGeeks, "Coherent and incoherent Addition of Waves," [Online]. Available: https://www.geeksforgeeks.org/coherent-and-incoherent-addition-of-waves/. May 2024.

[39] R. Paschotta, "Coherence," RP Photonics Encyclopedia, [Online]. Available: https://www.rp-photonics.com/coherence.html. Feb. 2025.

[40] A. K. Rahman, N. Julai, C. B. M. Rashidi, et al., "Impact of rain weather over free space optic communication transmission," Indonesian Journal of Electrical Engineering and Computer Science, vol. 14, no. 1, pp. 303–310, 2019.

[41] ResearchGate, "Ozone: Space Vision (Space monitoring of Earth Atmospheric Ozone)," [Online].

[42] G. Yang, "Space-diversity free-space optical systems: performance analysis under correlated fading conditions," May 2020.

[43] S. Kaur and A. Kakati, "Analysis of Free Space Optics link performance considering the effect of different weather conditions and modulation formats for terrestrial communication," Apr. 2018.

[44] A. Tou, S. Driz, B. Fassi, et al., "Harnessing polarization diversity for enhanced reliability in free space optical communications," Progress In Electromagnetics Research C, vol. 142, pp. 27–35, 2024.

[45] A. O. Aladeloba, "Optically amplified free-space optical communication systems," University of Nottingham, [Online]. Available: http://eprints.nottingham.ac.uk/13304/. Jul. 2013.

[46] D. Kone, A. S. Penétjiligué, and A. Kamagaté, "Evaluation of free space optical (FSO) link under weather conditions in Abidjan," International Journal of Physics, Nov. 2024.

[47] E. El-desoky El-sayed Ebrahim and E. Bakery, "Design and analysis of DWDM transmission system for free space optical communications," Faculty of Engineering, Mansoura University, 2018.

[48] A. El-Qady and M. Abaza, "Performance analysis of the effects of atmospheric turbulence on free space optical communication using multi-hop decode and forward relay in north and south of Egypt," Aug. 2024.

[49] S. Chaudhary and A. Amphawan, "The role and challenges of free-space optical systems," Journal of Optical Communications, 2014.

[50] F. T. Mahmood, A. H. Ali, and A. H. A. Haeder, "Weathers effect on the free space optics communication system," Indonesian Journal of Electrical Engineering and Computer Science, vol. 31, no. 1, pp. 222–228, Jul. 2023.

[51] A. Tou, S. Driz, B. Fassi, and I. S. K. Mahadjoubi, "Harnessing polarization diversity for enhanced reliability in free space optical communications," Mar. 2024.

[52] N. A. Olsson, "Lightwave systems with optical amplifiers," Journal of Lightwave Technology, vol. 7, no. 7, pp. 1071–1082, Jul. 1989.

[53] C.-H. Liu, Y.-C. Chang, T. B. Norris, and Z. Zhong, "Graphene photodetectors with ultra-broadband and high responsivity at room temperature," Nature Nanotechnology, vol. 9, no. 4, pp. 273–278, Mar. 2014.

[54] E. Verdugo, L. d. S. Mello, C. P. Colvero, and R. Nebuloni, "Estimation of rain attenuation in FSO links based on visibility measurements," Mar. 2023.

[55] S. Magidi and T. Pondani, "Estimating the performance of free space optical communication in rain weather conditions using various models and modified duobinary return to zero technique," Sep. 2020.

[56] S. A. Al-Gailani et al., "A Survey of Free Space Optics (FSO) Communication Systems, Links, and Networks," IEEE Access, vol. 9, pp. 7353–7373, 2021. DOI: 10.1109/ACCESS.2020.3048049.

[57] WeatherSpark, "Average Weather in El Oued Algeria," [Online]. Available: https://weatherspark.com/, 2024. Accessed: 2026.

[58] J. Goldhirsh, "A parameter review and assessment of attenuation and backscatter properties associated with dust storms over desert regions in the frequency range of 1 to 100 GHz," IEEE Transactions on Antennas and Propagation, vol. 49, pp. 1447–1462, 2001.

[59] A. S. Goudie and N. J. Middleton, Desert dust in the global system. Springer Science & Business Media, 2006.

[60] M. Sliti and N. Mrabet, "Modeling and performance evaluation of FSO communication systems under desert environmental conditions using OptiSystem," Journal of Optical Communications, vol. 44, no. 3, pp. 315–322, 2023.

[61] H. Fathallah, W. G. Alheadary, and M. S. Alouini, "Experimental evaluation of free-space optical (FSO) links under heavy dust and low visibility desert conditions," IEEE Photonics Journal, vol. 11, no. 4, pp. 1–12, 2019.

[62] X. Huang, L. Zhang, and Y. Wang, "High-speed 12 Gbps FSO transmission system under moderate atmospheric turbulence conditions," Optics & Laser Technology, vol. 138, p. 106850, 2021.

[63] M. A. Ali, S. M. Ahmed, and Z. Khan, "Impact of reduced horizontal visibility on the quality factor (Q-factor) of next-generation FSO communication links," Optical and Quantum Electronics, vol. 55, no. 6, p. 524, 2023.

Annex

METAR/SPECI from DAUO, El-Oued (Algeria).

SA 17/05/2025 00:00->	METAR DAUO 170000Z 22005KT CAVOK 20/08 Q1016=
SA 17/05/2025 01:00->	METAR DAUO 170100Z 22004KT CAVOK 19/08 Q1015=
SA 17/05/2025 02:00->	METAR DAUO 170200Z 21002KT CAVOK 18/07 Q1015=
SA 17/05/2025 03:00->	METAR DAUO 170300Z 24002KT CAVOK 18/07 Q1015=
SA 17/05/2025 04:00->	METAR DAUO 170400Z 23004KT CAVOK 16/08 Q1015=
SA 17/05/2025 05:00->	METAR DAUO 170500Z 24003KT 220V280 CAVOK 17/08 Q1016=
SA 17/05/2025 06:00->	METAR DAUO 170600Z 24001KT CAVOK 20/09 Q1016=
SA 17/05/2025 07:00->	METAR DAUO 170700Z 23003KT 190V270 CAVOK 22/08 Q1017=
SA 17/05/2025 08:00->	METAR DAUO 170800Z 25002KT CAVOK 25/08 Q1018=
SA 17/05/2025 09:00->	METAR DAUO 170900Z 25002KT CAVOK 27/08 Q1018=
SA 17/05/2025 10:00->	METAR DAUO 171000Z 27003KT CAVOK 28/08 Q1018=
SA 17/05/2025 11:00->	METAR DAUO 171100Z 34003KT 9999 FEW030 29/07 Q1018=
SA 17/05/2025 12:00->	METAR DAUO 171200Z 27005KT 9999 SCT030 29/07 Q1017=
SA 17/05/2025 13:00->	METAR DAUO 171300Z 29007KT 240V350 9999 FEW030 29/06 Q101
SA 17/05/2025 14:00->	METAR DAUO 171400Z 18003KT 9999 FEW030 30/05 Q1016=
SA 17/05/2025 15:00->	METAR DAUO 171500Z 29005KT 230V330 9999 FEW030 31/04 Q101
SA 17/05/2025 16:00->	METAR DAUO 171600Z 31004KT 250V030 CAVOK 30/04 Q1016=
SA 17/05/2025 17:00->	METAR DAUO 171700Z 31005KT 270V360 CAVOK 30/03 Q1016=
SA 17/05/2025 18:00->	METAR DAUO 171800Z 30004KT 260V350 CAVOK 29/03 Q1016=
SA 17/05/2025 19:00->	METAR DAUO 171900Z 02003KT CAVOK 28/03 Q1016=
SA 17/05/2025 20:00->	METAR DAUO 172000Z 07003KT CAVOK 27/03 Q1017=
SA 17/05/2025 21:00->	METAR DAUO 172100Z 10004KT CAVOK 26/04 Q1017=
SA 17/05/2025 22:00->	METAR DAUO 172200Z 11003KT 070V140 CAVOK 26/04 Q1018=
SA 17/05/2025 23:00->	METAR DAUO 172300Z 14005KT 110V170 CAVOK 25/03 Q1018=
SA 18/05/2025 00:00->	METAR DAUO 180000Z 15005KT 120V180 CAVOK 24/05 Q1017=
SA 18/05/2025 01:00->	METAR DAUO 180100Z 17003KT 140V200 CAVOK 23/05 Q1017=
SA 18/05/2025 02:00->	METAR DAUO 180200Z 17003KT CAVOK 23/06 Q1017=
SA 18/05/2025 03:00->	METAR DAUO 180300Z 17003KT CAVOK 22/05 Q1017=
SA 18/05/2025 04:00->	METAR DAUO 180400Z 21003KT CAVOK 20/05 Q1017=
SA 18/05/2025 05:00->	METAR DAUO 180500Z 22003KT CAVOK 20/06 Q1018=
SA 18/05/2025 06:00->	METAR DAUO 180600Z 16003KT 130V200 CAVOK 23/07 Q1018=
SA 18/05/2025 07:00->	METAR DAUO 180700Z 17006KT 130V190 CAVOK 25/08 Q1019=
SA 18/05/2025 08:00->	METAR DAUO 180800Z 16009KT 110V200 CAVOK 27/08 Q1019=
SA 18/05/2025 09:00->	METAR DAUO 180900Z 15006KT 120V210 CAVOK 29/07 Q1019=
SA 18/05/2025 10:00->	METAR DAUO 181000Z 15005KT 100V220 CAVOK 31/07 Q1019=
SA 18/05/2025 11:00->	METAR DAUO 181100Z 16005KT 070V220 CAVOK 33/06 Q1019=
SA 18/05/2025 12:00->	METAR DAUO 181200Z 17004KT CAVOK 33/06 Q1018=
SA 18/05/2025 13:00->	METAR DAUO 181300Z 23003KT CAVOK 35/05 Q1017=
SA 18/05/2025 14:00->	METAR DAUO 181400Z 18004KT 120V250 CAVOK 35/05 Q1016=
SA 18/05/2025 15:00->	METAR DAUO 181500Z 28003KT 200V360 CAVOK 35/04 Q1016=
SA 18/05/2025 16:00->	METAR DAUO 181600Z 23004KT 170V280 CAVOK 35/05 Q1016=
SA 18/05/2025 17:00->	METAR DAUO 181700Z 14002KT CAVOK 34/05 Q1015=
SA 18/05/2025 18:00->	METAR DAUO 181800Z 00000KT CAVOK 34/04 Q1016=
SA 18/05/2025 19:00->	METAR DAUO 181900Z 11003KT CAVOK 32/04 Q1016=
SA 18/05/2025 20:00->	METAR DAUO 182000Z 14003KT CAVOK 31/05 Q1016=
SA 18/05/2025 21:00->	METAR DAUO 182100Z 14005KT CAVOK 30/05 Q1017=
SA 18/05/2025 22:00->	METAR DAUO 182200Z 15004KT CAVOK 29/05 Q1017=
SA 18/05/2025 23:00->	METAR DAUO 182300Z 15004KT 120V180 CAVOK 28/05 Q1017=
SA 19/05/2025 00:00->	METAR DAUO 190000Z 15005KT CAVOK 27/05 Q1017=
SA 19/05/2025 01:00->	METAR DAUO 190100Z 15005KT CAVOK 27/05 Q1016=
SA 19/05/2025 02:00->	METAR DAUO 190200Z 16004KT CAVOK 26/06 Q1016=
SA 19/05/2025 03:00->	METAR DAUO 190300Z 15003KT CAVOK 25/06 Q1016=
SA 19/05/2025 04:00->	METAR DAUO 190400Z 00000KT CAVOK 24/06 Q1017=
SA 19/05/2025 05:00->	METAR DAUO NIL=
SA 19/05/2025 06:00->	METAR DAUO 190600Z 16002KT CAVOK 26/06 Q1017=
SA 19/05/2025 07:00->	METAR DAUO 190700Z 15005KT 120V200 CAVOK 28/06 Q1018=
SA 19/05/2025 08:00->	METAR DAUO 190800Z 30003KT CAVOK 30/07 Q1018=
SA 19/05/2025 09:00->	METAR DAUO 190900Z 29004KT CAVOK 32/06 Q1018=
SA 19/05/2025 10:00->	METAR DAUO 191000Z 22002KT CAVOK 35/06 Q1018=
SA 19/05/2025 11:00->	METAR DAUO 191100Z 33004KT CAVOK 35/06 Q1017=
SA 19/05/2025 12:00->	METAR DAUO 191200Z 34004KT CAVOK 37/05 Q1016=
SA 19/05/2025 13:00->	METAR DAUO 191300Z 01005KT CAVOK 37/04 Q1016=
SA 19/05/2025 14:00->	METAR DAUO 191400Z 01005KT CAVOK 37/04 Q1016=
SA 19/05/2025 15:00->	METAR DAUO 191500Z 12003KT CAVOK 37/03 Q1014=
SA 19/05/2025 16:00->	METAR DAUO 191600Z 02006KT CAVOK 37/03 Q1014=
SA 19/05/2025 17:00->	METAR DAUO 191700Z 34003KT CAVOK 37/06 Q1014=
SA 19/05/2025 18:00->	METAR DAUO 191800Z 05003KT CAVOK 36/03 Q1014=